University of Potsdam
Applied Condensed-Matter Physics

---

# Coupling of the electrical, mechanical and optical response in polymer/liquid-crystal composites

Dissertation
in partial fulifillment of the
requirements of the degree of
Doctor of Natural Sciences
(Dr.rer.nat.)
in Applied Materials Physics

submitted to the
Faculty of Mathematics and Natural Sciences
of the University of Potsdam

presented by
**Lakshmi Meena Ganesan**

Potsdam, March 4, 2010

*to my mother Mangaleswari and brother Saravanan*

அன்பு தாய்க்கும், அண்ணனுக்கும்

# Statement

Lakshmi Meena Ganesan,
student matric. no. 733464

**I, Lakshmi Meena Ganesan,** formally submit my thesis **"Coupling of the electrical, mechanical and optical response in polymer/liquid-crystal composites"** in fulfillment of the requirements set forth by the Regulations for awarding the title "doctor rerum naturalium" (Dr. rer. nat.) in the Mathematics-Natural Science Faculty of the University of Potsdam.

I declare that the work presented in this thesis has not been submitted as an exercise for a degree to any other university.

The work described herein is entirely my own, except for the assistance mentioned in the acknowledgments and collaborative work mentioned in the list of publications. The present thesis work was completed within the "Applied Condensed-Matter Physics" (ACMP) group at the Department of Physics in University of Potsdam.

*Lakshmi Meena Ganesan*
Potsdam, March 4, 2010

# Abstract

Micrometer-sized liquid-crystal (LC) droplets embedded in a polymer matrix may enable optical switching in the composite film through the alignment of the LC director along an external electric field. When a ferroelectric material is used as host polymer, the electric field generated by the piezoelectric effect can orient the director of the LC under an applied mechanical stress, making these materials interesting candidates for piezo-optical devices. In this work, polymer-dispersed liquid crystals (PDLCs) are prepared from poly(vinylidene fluoride-trifluoroethylene) (P(VDF-TrFE)) and a nematic liquid crystal (LC). The anchoring effect is studied by means of dielectric relaxation spectroscopy. Two dispersion regions are observed in the dielectric spectra of the pure P(VDF-TrFE) film. They are related to the glass transition and to a charge-carrier relaxation, respectively. In PDLC films containing 10 and 60 wt% LC, an additional, bias-field-dependent relaxation peak is found that can be attributed to the motion of LC molecules. Due to the anchoring effect of the LC molecules, this relaxation process is slowed down considerably, when compared with the related process in the pure LC. The electro-optical and piezo-optical behavior of PDLC films containing 10 and 60 wt% LCs is investigated. In addition to the refractive-index mismatch between the polymer matrix and the LC molecules, the interaction between the polymer dipoles and the LC molecules at the droplet interface influences the light-scattering behavior of the PDLC films. For the first time, it was shown that the electric field generated by the application of a mechanical stress may lead to changes in the transmittance of a PDLC film. Such a piezo-optical PDLC material may be useful e.g. in sensing and visualization applications. Compared to a non-polar matrix polymer, the polar matrix polymer exhibits a strong interaction with the LC molecules at the polymer/LC interface which affects the electro-optical effect of the PDLC films and prevents a larger increase in optical transmission.

# Kurzfassung

Mikrometer-große, in eine Polymermatrix eingebettete Flüssigkristall-Tröpfchen können als elektro-optische Lichtventile fungieren, da die Ausrichtung der Flüssigkristalle durch ein externes elektrisches Feld verändert werden kann. Wird nun ein ferroelektrisches Polymer als Matrix verwendet, so kann das durch den piezoelektrischen Effekt erzeugte und von der äußeren mechanischen Spannung abhängige elektrische Feld den Flüssigkristall ausrichten. Solche Materialien können daher als piezo-optische Lichtventile eingesetzt werden. Im Rahmen dieser Arbeit wurden PDLCs (polymer-dispersed liquid crystals) durch Einbettung von nematischen Flüssigkristallen in Poly(Vinylidenfluoride-Trifluorethylene) (P(VDF-TrFE)) erzeugt. Die Wechselwirkungen an der Grenzfläche zwischen Flüssigkristall und Polymer wurden mittels dielektrischer Spektroskopie untersucht. Im dielektrischen Spektrum des reinen P(VDF-TrFE) wurden zwei Dispersions-Regionen beobachtet, welche vom Glasübergang und einer Ladungsträgerrelaxation des Polymers herrühren. PDLC-Folien mit unterschiedlichen Anteilen von Flüssigkristall-Tröpfchen (10 bzw. 60 Gewichtsprozente) zeigten beim Anlegen eines elektrischen Wechselfelds zusätzliche Relaxationseffekte, welche der Bewegung der eingebetteten Flüssigkristall-Moleküle zugeordnet werden konnten. Durch die Einlagerung der Flüssigkristall-Moleküle weist die Struktur eine Relaxation auf, die gegenüber vergleichbaren Prozessen im reinen Flüssigkristall deutlich verlangsamt ist. Des weiteren wurde das elektrooptische und piezo-optische Verhalten der mit 10 und 60 Gewichtsprozent Flüssigkristall geladenen Folien untersucht. Die Lichtstreuung hängt dabei ab von der Fehlanpassung der Brechungsindizes von Polymermatrix und Flüssigkristallen sowie von den Wechselwirkungen der Polymerdipole mit den Flüssigkristall-Molekülen an der Tröpfchenoberfläche. Es konnte erstmalig gezeigt werden, dass die Lichtdurchlässigkeit der PDLC-Folien durch eine externe mechanische Spannung gesteuert werden kann. Dieser Effekt macht das piezo-optische PDLC-Material für die Verwendung in Optik- und Sensoranwendungen interessant. Im Vergleich mit unpolaren Wirtspolymeren zeigen polare Wirtsmaterialien eine deutlich stärkere Wechselwirkung zwischen den Flüssigkristall-Molekülen an der Polymer/Flüssigkristall-Grenzfläche, welche den elektrooptischen Effekt beeinflusst und so die maximale Transmissionsänderung reduziert.

# Acknowledgements

# Contents

# Glossary

| Notation | Description |
|---|---|
| $A$ | Area |
| $C$ | Capacitance |
| $C_P$ | Heat capacity of the sample |
| $E/\vec{E}$ | External field |
| $E_A$ | Activation energy |
| $F$ | Force applied |
| $I$ | Current |
| $I_0$ | Incident light intensity |
| $I_t$ | Transmitted light intensity |
| $K$ | Elastic constant of the LC |
| $L$ | Sample thickness |
| $Q$ | Electric charge stored |
| $R$ | Resistance |
| $R_d$ | LC droplet radius |
| $R_m$ | Mean droplet radius |
| $T$ | Transmission of the PDLC film |
| $T_\mathbf{p}$ | Polarization temperature |
| $T_0$ | Vogel temperature |
| $T_A$ | Activation temperature |
| $T_R$ | Reference sample temperature |
| $T_S$ | Sample temperature |
| $T_\mathbf{c}$ | Crystallization temperature |
| $T_\mathbf{g}$ | Glass transition temperature |
| $T_\mathbf{m}$ | Melting temperature |
| $V$ | Voltage |
| $V_{on}$ | Switch on voltage of the PDLC film |
| $Y$ | Admittance |
| $Z$ | Impedance |
| $\Delta P$ | Electrical power difference between the sample and the reference sample |
| $\Delta T$ | Temperature difference between the sample and the reference sample |

| Notation | Description |
|---|---|
| $\Delta\epsilon$ | Dielectric anisotropy |
| $\Delta n$ | Birefringence |
| $\Gamma$ | Relative phase difference |
| $\Phi_R$ | Heat flow rate to the reference sample |
| $\Phi_S$ | Heat flow rate to the sample |
| $\alpha_{cr}$ | $\alpha$ crystalline phase |
| $\beta$ | Symmetric shape parameter |
| $\beta_{cr}$ | $\beta$ crystalline phase |
| $\boldsymbol{\alpha}$ | Alpha relaxation |
| $\boldsymbol{\beta}$ | Secondary relaxation |
| $\boldsymbol{\delta}$ | Relaxation due to isolated molecules |
| $\boldsymbol{\gamma}$ | Relaxation due to smaller molecular units |
| $\chi$ | Electric susceptibility |
| $\epsilon^{''}$ | Dielectric loss |
| $\epsilon^{'}$ | Permittivity |
| $\epsilon^*$ | Material's complex permittivity |
| $\epsilon^*_{CC}$ | Cole-Cole function |
| $\epsilon^*_{CD}$ | Cole-Davidson function |
| $\epsilon^*_{HN}$ | Havriliak-Negami function |
| $\epsilon_0$ | Free space permittivity |
| $\epsilon_{LC}$ | Dielectric constant of the liquid crystal |
| $\epsilon_P$ | Dielectric constant of the polymer |
| $\epsilon_\perp$ | Permittivity perpendicular to the director |
| $\epsilon_\infty$ | Unrelaxed permittivity |
| $\epsilon_\parallel$ | Permittivity parallel to the director |
| $\epsilon_m$ | Dielectric constant of the composite film |
| $\epsilon_r$ | Relative permittivity |
| $\epsilon_s$ | Static permittivity |
| $\gamma$ | Asymmetric shape parameter |
| $\gamma_{cr}$ | $\gamma$ crystalline phase |
| $\lambda$ | Light wavelength |
| $\nu_{LC}$ | Volume fraction of the liquid crystal |
| $\omega$ | Angular frequency |
| $\sigma^{''}$ | Imaginary part of electric conductivity |
| $\sigma^{'}$ | Real part of electric conductivity |
| $\sigma^*$ | Complex electric conductivity |
| $\sigma_{dc}$ | dc conductivity |
| $\tau$ | Relaxation time |

| Notation | Description |
| --- | --- |
| $\tau_{HN}$ | Relaxation time obtained by fitting Havriliak-Negami function |
| $\tau_c$ | Maxwell relaxation time |
| $\tau_d$ | Sample's optical depth |
| $\mathbf{V}$ | Volume |
| $\theta$ | Angle of incidence |
| $\theta_{air}$ | Angle of incidence in air |
| $\vec{D}$ | Electric displacement |
| $\vec{P}$ | Polarization |
| $\vec{m}$ | Dipole moment |
| $\vec{r}_i$ | Charge coordinate |
| $d$ | Thickness of the film |
| $dQ/dt$ | Heat flow |
| $dT/dt$ | Rate of the temperature change |
| $d_{33}$ | Piezoelectric coefficient |
| $f(T,t)$ | Heat flow from kinetic processes |
| $i(T)$ | Depolarization current |
| $j$ | Current density |
| $k$ | wavevector of light |
| $k_B$ | Boltzmann constant |
| $l$ | Ratio of the major and minor radii of the droplet |
| $n_{LC}$ | Refractive index of the LC |
| $n_P$ | Refractive index of the polymer |
| $n_{\textit{eff}}$ | Effective refractive index of the liquid crystal |
| $n_e$ | Extraordinary refractive index of the liquid crystal |
| $n_o$ | Ordinary refractive index of the liquid crystal |
| $q_i$ | Charge |
| $s$ | Inverse heating rate |
| $t$ | Time |

# Chapter 1

# Introduction

Polymer-dispersed liquid crystals (PDLCs) were first implemented in the mid-1980s [1]. Their suitability for light-valve applications, where the optical transmission depends on the applied electric field, was recognized [2, 3]. Typically, PDLCs consist of micrometer-sized liquid crystal (LC) droplets embedded in a transparent host polymer. In the absence of an external electric field, the LC molecules at the interface orient in a specific direction. Because of elastic forces, all LC molecules tend to orient parallel to each other. The phenomenon of orienting LC molecules at a surface is called anchoring [4]. In the absence of an external electric field, the optical axes ("directors") of the droplets are randomly aligned. Due to the mismatch in the refractive indices at the LC/polymer interface, they efficiently scatter light, rendering the sample translucent. An electric bias field orients the optical axes of the droplets. If the ordinary refractive index of the LC matches that of the polymer, the sample thus becomes transparent or the transmission of the PDLC film increases [5, 6].

PDLCs are attractive for large-area applications (such as windows with variable light transmission), since they require very little power to keep the light valve in the "open" state (the host polymer is generally a good electrical insulator) and do not require any additional optical elements [7]. When liquid-crystal droplets are embedded in ferroelectric polymers, the local electric field across the LC-filled cavities acts as a bias field to the LC which opens up a range of potential applications, from bi-stable electro-optical switches to pressure- and temperature-sensitive light valves.

## 1.1   Liquid crystals

One of the newly identified classes of materials in the 19th century was "Liquid Crystals". In 1888, an Austrian botanist, Friedrich Reinitzer, observed cholesteryl benzoate melted to a cloudy liquid at 145.5 °C and became a clear liquid at 178.5 °C which paved the way for the identification of a new phase of matter known as the liquid crystal phase. The term liquid crystal was first coined by German physicist Otto Lehmann in 1889. Liquid crystals are a class of materials which possess a phase of matter in between a highly ordered

crystalline state and the disordered or isotropic fluid state, known as the mesophase. The term "liquid crystal" (LC) refers to low molar mass liquid crystals whereas high molecular weight liquid crystals are referred as liquid crystalline polymers (LCP) [8].

## Types of liquid crystals

Beyond a critical concentration or temperature, chains with rigid rod-like segments will tend to form a mesophase. The rigid segment is known as a mesogen. Based on the factor which induces the ordering effect, liquid crystals are classified into two types, one being thermotropic liquid crystals, in which the temperature induces ordering effects, and the other one being lyotropic liquid crystals, in which the concentration of mesogens induces the ordering effect.

Broadly, mesophases are classified as nematic, chiral nematic, smectic and discotic. A lot of research has been done on the nematic and smectic LC molecules, shown in Fig. 1.1. The nematic phase is characterized by molecules having no positional order but being pointed in the direction of the director. The chiral nematic phase is also known as the cholesteric phase, in which the mesogenic molecules have a chiral center. It is nematic because each plane has a nematic director. The mesophase is in a twisted form which is due to the asymmetrical intermolecular forces between the nematic layers exerted by the chiral centers. When the chiral center is brought closer to the core, the pitch of the helix becomes shorter and therefore the chirality increases. Degree of chirality is determined by the pitch (P) of the helix [9]. The smectic phase shows both positional and orientational order and the molecules also arrange themselves in layers or planes. As shown in Fig. 1.1, based on the arrangement of molecules in the layer, smectic phases are called smectic A or smectic C. In smectic A the molecules are arranged normal to the layer whereas in smectic C the molecules are tilted at a particular angle. In the discotic phase, mesogens are of disc shape and they are packed in stack form. Since the local alignment of the LC molecules is the same on both the microscopic and the macroscopic scale, nematic liquid crystals (LC) are widely used in liquid crystal displays.



Nematic          Smectic A          Smectic C
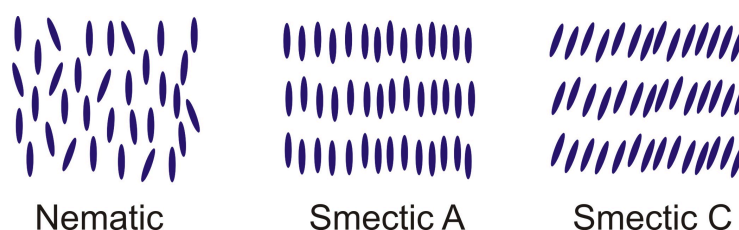
Figure 1.1: *Structure of nematic, smectic A and smectic C mesophases.*
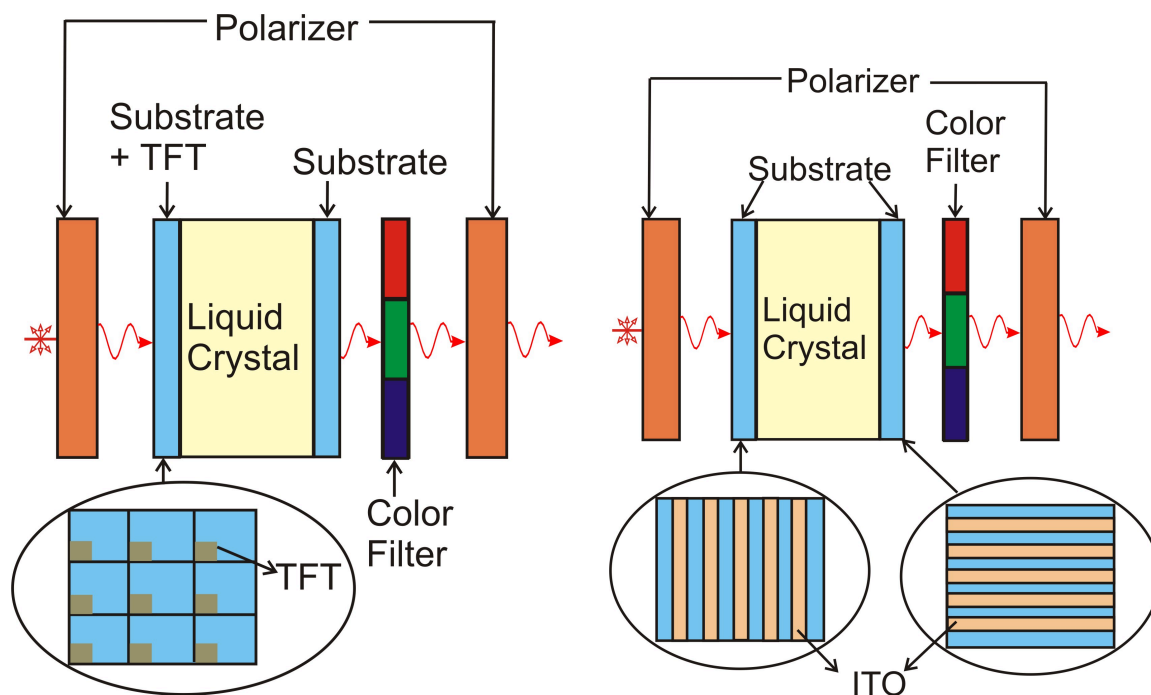
Figure 1.2: *Schematic representation of the working principle of the active and passive matrix liquid crystal display.*

## 1.2 Liquid-crystal displays

After the publication in Chemical Reviews [10] about the liquid crystal phase, the interest towards this new material increased which led to the first experimental liquid crystal display (LCD) in 1968. Fergason prepared an operating LCD in 1970 [11, 12], and already in 1971 the LCD was introduced in the market. There are two types of LC displays available in the market. One is active matrix LCD and the other one is passive matrix LCD. Liquid-crystal displays need a crossed polarizer to switch between an "OFF" and an "ON" state. In active matrix LCDs, the liquid-crystal is filled between two glass substrates, which in turn are placed between a crossed polarizer, as shown in Fig. 1.2. In the active matrix LCD, thin film transistors are arranged in a matrix on a glass-substrate. In the absence of an electric field, the orientation of the liquid crystals is determined by their alignment at the electrode surface. By applying an electric field, the liquid crystal molecules are re-oriented in a particular direction. Depending on the orientation of the LC molecules, the LC layer rotates (or does not rotate) the light polarization so that the light can (or can not) pass through the second polarizer. Here, thin film transistors are used to charge the LC, i.e. they are used to change the orientation of the LC molecules. Generally silicon is used for transistors. This type of LCD is also known as a thin-film transistor (TFT) LCD. They are of very good quality. The glass substrate has as many TFT as the number of pixels displayed and therefore it is expensive; this is the only disadvantage of this
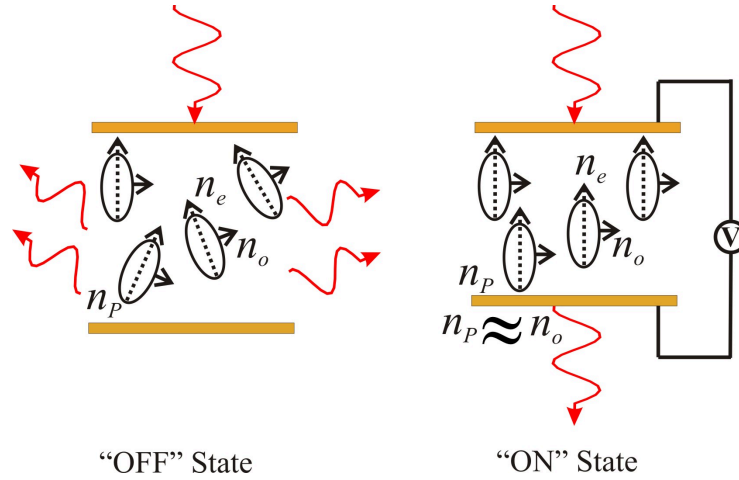
Figure 1.3: *Schematic representation of the "ON" and "OFF" states of PDLC film coated with semi-transparent gold electrodes. $n_e$ and $n_o$ represent the refractive indices of the liquid crystal parallel and perpendicular to the axis of anisotropy and $n_p$ represents the refractive index of the polymer matrix.*

technique. In passive matrix LCDs (Fig. 1.2), a simple grid of electrodes is used to charge the LC molecules. Transparent indium-tin-oxide is used as the electrode. Compared to active matrix LCDs, passive matrix LCDs are cheaper in price. Disadvantages of passive matrix are slow response time and imprecise voltage control. A lot of research is going on in improving the quality of passive matrix LCDs. One method is the usage of polymer dispersed liquid crystal film.

## 1.3 Polymer-dispersed liquid crystals

If a polymer dispersed liquid crystal film is used instead of a liquid crystal, there is no need for crossed polarizers to switch between a translucent off and a transparent on state. Polymer-dispersed liquid crystals (PDLCs) are a class of materials that consist of micrometer-sized liquid-crystal (LC) droplets embedded in a polymer matrix. Liquid crystals are birefringent due to their anisotropic nature. The birefringence of a material is characterized by the difference of the extraordinary $n_e$ and ordinary $n_o$ refractive indices of the LC molecules. $n_e$ and $n_o$ are the refractive indices of the LC parallel and perpendicular to the long axis of the molecule, respectively. The symmetry axis of each droplet in the PDLC film is oriented randomly. Due to the mismatch of the refractive indices of the LC and the polymer matrix, the composite film scatters light. When a voltage is applied to the composite film, the liquid crystal molecules tend to orient along the external electric field. Thereby the mismatch of the refractive indices of the LC and the polymer matrix decreases. If the refractive index of both the polymer matrix and the LC is nearly the same then the composite film becomes transparent [5, 6]. Unlike the LCD (section 1.2),

the polarization of the light remains the same. Only the effective refractive index of the LC is altered here.

In some PDLCs, e.g. poly(methyl methacrylate)-dispersed E7 nematic liquid crystal (Merck), the applied electric field induces either a memory effect or a persistence effect. In the memory effect, after the removal of the electric field the transmittance of the PDLC film decreases to a lower value (but higher than the zero-field transmittance), whereas in the persistence effect after the electric field is removed the PDLC film takes some time to reach the zero-field transmittance [13]. PDLCs are attractive for large-area applications (such as windows with variable light transmission), since they require very little power to keep the light valve in the "open" state (the host polymer is generally a good electrical insulator) and do not require any additional optical elements [7].

## PDLC preparation methods

PDLC films are prepared by the Polymerization-Induced Phase Separation (PIPS) method, the Solvent-Induced Phase Separation (SIPS) method or the Thermally-Induced Phase Separation (TIPS) method [2]. When the liquid crystal is miscible with the prepolymer, PIPS can be used to prepare the PDLC films. Phase separation takes place during the polymerization. In the case of resins, a curing agent is used to do the polymerization. Based on the system, either a free radical polymerization or a photo-initiated polymerization is carried out. As the polymerization proceeds, the solubility of the liquid crystal decreases, leading to the phase separation, thus forming droplets. The TIPS method can be used for thermoplastic materials which melt below their decomposition temperature. A homogeneous solution of liquid crystal and the polymer is formed at elevated temperature. Cooling the homogeneous solution leads to the phase separation of the liquid crystal. The droplet size depends on various parameters such as the rate of cooling, viscosity of the homogeneous solution etc. For thermoplastic materials which melt above their decomposition temperature, or when solvent coating techniques are used, the SIPS method is appropriate. A homogeneous solution of the liquid crystal and the polymer is prepared by dissolving them in a common solvent. The solvent is removed by evaporation which results in the phase separation. The droplet size depends on the solvent evaporation rate. The optical micrograph images of PDLCs prepared by SIPS, TIPS and PIPS are shown in Fig. 1.4.

## 1.4 Ferroelectric polymers

In 1921 Valasek discovered ferroelectricity in Rochelle salt [16]. Ferroelectric polymers, e.g. poly(vinylidene fluoride) (P(VDF)), exhibit both piezo- and pyro-electric properties. In addition to the ferroelectric property, P(VDF) exhibit a variety of properties like high mechanical strength, high impact strength, creep resistance, nonlinear optical properties and so on. Generally P(VDF) exhibits three crystalline forms, namely the $\alpha_{cr}$, $\beta_{cr}$ and $\gamma_{cr}$ phase as shown in Fig. 1.6. In the $\beta_{cr}$ phase all the molecules are in the trans conformation,
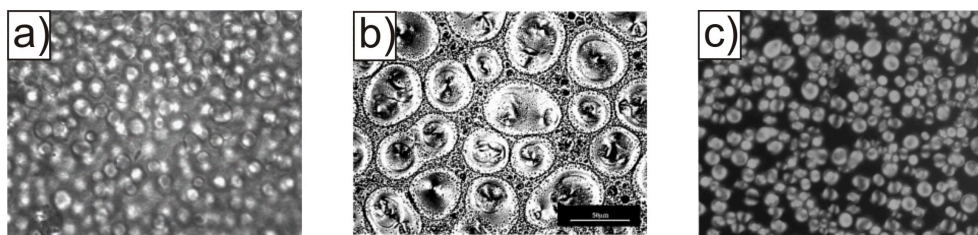
Figure 1.4: *Optical micrograph images of the PDLC films prepared by a)solvent-induced phase separation (SIPS), b)thermally-induced phase separation (TIPS) [14] and c)polymerization-induced phase separation (PIPS) [15] method.*



Poly(vinylidene fluoride)



Poly(vinylidene fluoride-trifluoroethylene)
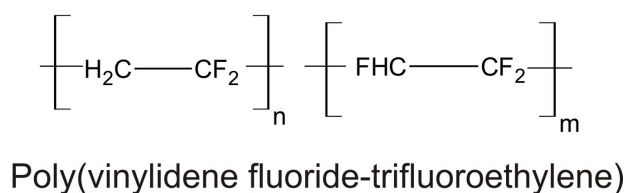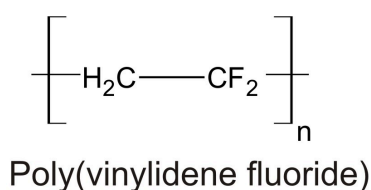
Figure 1.5: *Chemical structure of poly(vinylidene fluoride) and poly(vinylidene fluoride-trifluoroethylene).*

whereas in the $\alpha_{cr}$ phase, molecules of gauche and trans conformation are arranged alternatively. The $\beta_{cr}$ phase arranges in a planar zig-zag conformation; thereby the crystallinity of $\beta_{cr}$ phase is higher than that of the $\alpha_{cr}$ phase. The $\beta_{cr}$ phase exhibits both piezo- and pyro-electric properties. The most general way to get the $\beta_{cr}$ phase is by stretching $\alpha_{cr}$ P(VDF). To modify the physical properties of P(VDF), structural irregularity was introduced in the polymer by a copolymerization technique. The copolymerization of vinylidene fluoride with fluoropolymers results in a $\beta_{cr}$ phase. The $\beta_{cr}$ phase results from the steric hindrance of the fluorine molecules, so the molecules cannot form the usual TGTG' conformation [17]. Ferroelectric polymers possess a domain structure where dipoles are oriented randomly resulting in a zero net polarization. In order to break the centrosymmetry, high voltage is applied which results in a single domain structure. Only after poling with high electric field, do the ferroelectric polymers exhibit a piezo- and pyro-electric effect.
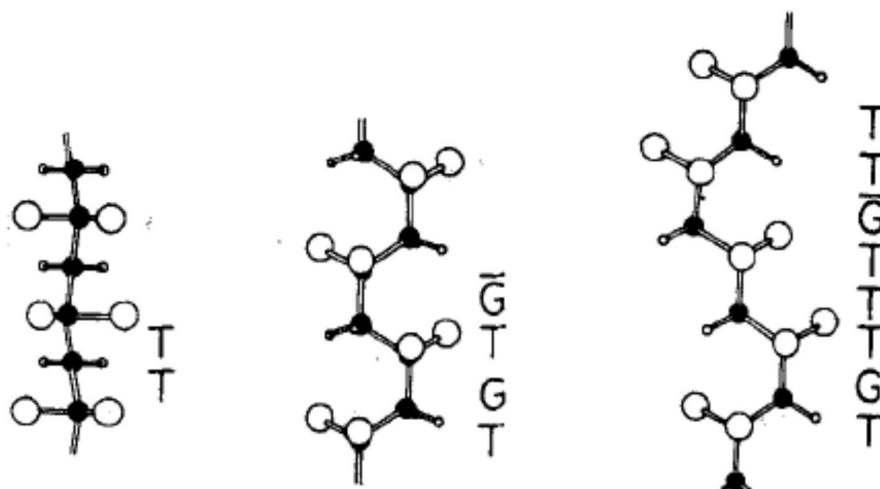
Figure 1.6: *Different chain conformations of P(VDF) and the resulting $\beta_{cr}$, $\alpha_{cr}$ and $\gamma_{cr}$ crystalline phases [18].*

## 1.5 PDLCs with ferroelectric hosts

Poled ferroelectric polymers exhibit pyro- and piezoelectric properties. For example, applying a mechanical stress changes their polarization and hence their internal electric field. Dubois suggested to use the charges generated by the PVDF bimorph to address the PDLC film [19]. When liquid-crystal droplets are embedded in ferroelectric polymers, the local electric field across the LC-filled cavities acts as a bias field to the LC. The first experimental studies of such systems were performed by Koda *et al.* [20]. Shah *et al.* developed an analog display which generates the desired wavelength of light depending on the applied electric field [21]. They used PVDF-based polymers to align the liquid-crystal molecules. In order to overcome the difficulty in the intermixing between the liquid-crystal and the surrounding polymer Andreau *et al.* prepared a new type of open-porosity PDLC [22]. They are the first to use the poly(vinylidene fluoride-hexafluoropropylene) as the matrix material. In this work, poly(vinylidene fluoride-trifluoroethylene) (P(VDF-TrFE)) is used as the matrix material. The mechanical properties (stress, strain) are coupled to the field-dependent optical transmission via the piezoelectric effect of the polymer matrix.

## 1.6 Thesis outline

In this thesis, the preparation of well-dispersed nematic LC in ferroelectric P(VDF-TrFE) polymer matrix is demonstrated. The working principles of differential scanning calorimetry, dielectric relaxation spectroscopy, infrared spectroscopy, thermally stimulated current measurement and electrical hysteresis measurement are presented. To understand the

electro-optical behavior of the PDLC film, the basic understanding of the light scattering effect of the PDLC film is outlined. The thermal behavior of the PDLC film and the influence of LC on the phase transitions of the polymer matrix are studied in detail. The anchoring effect of the LC dispersed in the highly polar material is addressed. Infrared spectroscopy reveals an overview of the phase composition in the PDLC film. The influence of the LC content on the ferroelectric properties of the polymer matrix is investigated. Finally, the optical transmission of the PDLC film under a mechanical load and applied electric field is shown.

# Chapter 2

# Sample preparation

As mentioned in section 1.3, for thermoplastic materials which melt above the decomposition temperature or where solvent coating techniques are used, the SIPS method is appropriate to prepare PDLCs. In order to obtain a homogeneous solution of the liquid crystal and the polymer, the liquid crystal and the polymer were dissolved in a common solvent. The solvent was removed by evaporation which results in a phase separation.

In this work, PDLC composite films were prepared by solvent-induced phase separation (SIPS) from a nematic liquid crystal (MDA-03-1767 from Merck Chemicals, Germany) and a copolymer of vinylidene fluoride and trifluoroethylene (Batch 2P0011, Solvay, France) whose molar composition is 65/35. Copolymers with a TrFE content higher than 11 mol% exist in a form analogous to the $\beta_{cr}$ phase of PVDF [23]. This polar phase exhibits pyro- and piezo-electric properties without mechanical stretching. This is the reason why P(VDF-TrFE) was used as the matrix material. Initially, it was attempted to dissolve the liquid crystal and the polymer in an acetone/dimethylsulfoxide (1:4) mixture (well-known as a good solvent for P(VDF-TrFE)), but the liquid crystal was insoluble. After several attempts, N-methyl pyrrolidone (NMP) was found to be a suitable solvent for the P(VDF-TrFE) and the liquid crystal.
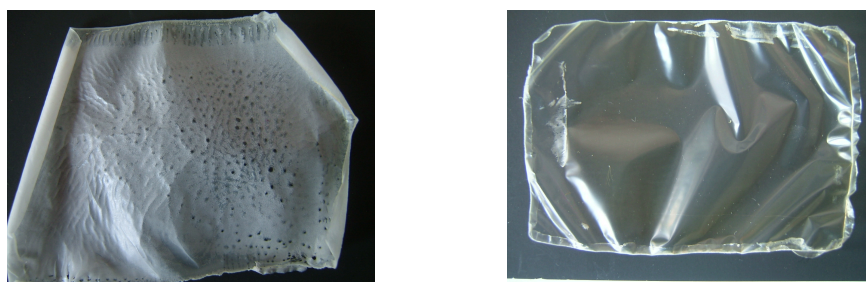


Figure 2.1: *Images of a PDLC film containing many air bubbles when quenched with water (left) and an oxidized film where solvent evaporation was done at $100°C$ for 70 min followed by subsequent annealing at $190°C$ for 9 min.(right)*
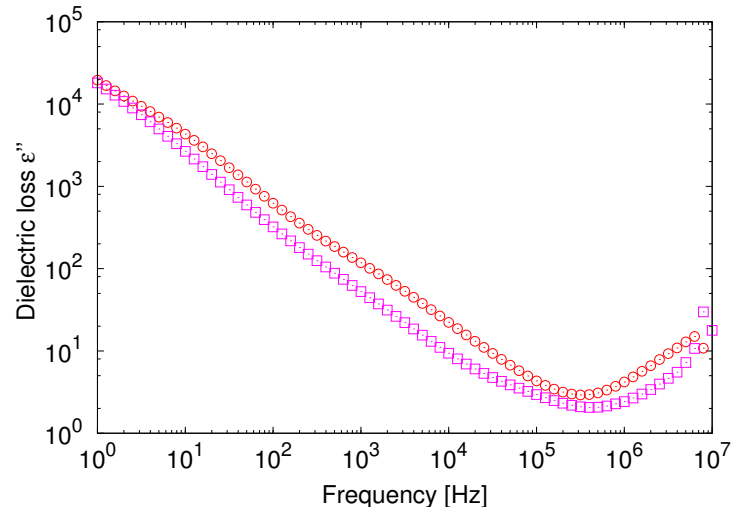
9

Figure 2.2: *Plot of the imaginary part of permittivity versus frequency at $100\,^{\circ}C$ for a pure P(VDF-TrFE) film prepared using NMP as the solvent, before ($\circ$) and after ($\Diamond$) the film was kept in vacuum at $100\,^{\circ}C$ for 24 h.*

The PDLC composite film was prepared by drop casting. Removal of the solvent induces phase separation. The solvent was evaporated at $100\,^{\circ}C$ for 70 min, then the film was annealed at $190\,^{\circ}C$ for 7 min. Initially the samples were quenched with water; however, the resulting film contained a large number of air bubbles as seen in Fig. 2.1 (left). Furthermore, annealing the film at $190\,^{\circ}C$ led to oxidation as shown in the Fig. 2.1 (right). Therefore the standard procedure for the preparation of the P(VDF-TrFE) film was modified in several ways. It was found that solvent evaporation at $100\,^{\circ}C$ for 35 min and subsequent annealing at $150\,^{\circ}C$ for 7 min are suitable conditions to avoid the above mentioned problem and to prepare a bubble free and (optically) transparent film. Due to the residual NMP in the P(VDF-TrFE) film, a high dielectric loss due to charge-carriers at low frequencies and at high temperatures was observed (Fig. 2.2) in the dielectric spectra of the P(VDF-TrFE) film. To overcome this problem, the sample was kept in vacuum for 24 h at $100\,^{\circ}C$. No significant change in the dielectric spectra was observed which can be seen in Fig. 2.2. Therefore, NMP was replaced by a mixture of dimethyl formamide (DMF) and toluene (2:1). Initially the solvent was evaporated at $100\,^{\circ}C$ for 35 min, but to ensure a complete evaporation of the solvent, the film was subsequently annealed at $100\,^{\circ}C$ in vacuum for 24 h and later at $150\,^{\circ}C$ for 7 min. In the following paragraphs this preparation method will be referred to as "method A".

The morphology of the PDLC films was checked using an optical microscope. The optical micrograph images of the PDLC films containing 10 and 20 weight percent (wt%) of liquid crystal are shown in Fig. 2.3. The surfaces of the PDLC film prepared by method A were rough and also clusters of LC droplets were formed in the PDLC films. Therefore,
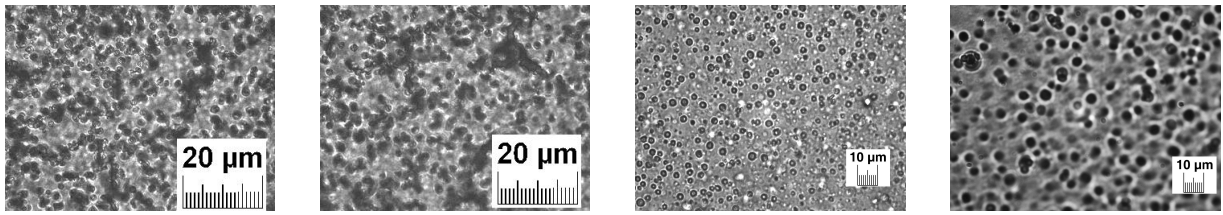
Figure 2.3: *Optical micrograph images of the PDLC film containing 10 wt% liquid crystal (first from the left) and PDLC film containing 20 wt% liquid crystal (second from the left), both prepared by the method A. PDLC film containing 10 wt% liquid crystal (third from the left) and PDLC film containing 20 wt% liquid crystal (fourth from the left), both prepared by the method B.*

the solvent evaporation step was further modified: a) the solvent was evaporated at 70 °C, b) to decrease the annealing time from 24 h to 4 h, the annealing temperature was increased to 140 °C. The above preparation method will be referred as "method B". As expected, the surface roughness of the film was decreased and also well-separated LC droplets were formed in the PDLC films which is shown in Fig. 2.3. From this it is clear that the morphology of the PDLC films strongly depends on the preparation conditions and "method A" is not suitable for obtaining ferroelectric polymer dispersed liquid crystal films. Thus, "method A" should only be considered as a step to optimize the preparation conditions. The results of the films prepared by the method B will be discussed in the following chapters. For the piezo-optical measurement, the solution was drop casted on an ITO-coated glass substrate and 15 nm gold was evaporated on top of the film. For the dielectric spectroscopy and the thermally stimulated current measurements, 50 nm aluminium electrodes were coated onto both sides of the free standing film. For comparison, a commercial P(VDF-TrFE) film from Piezotech, France was used.

# Chapter 3

# Differential scanning calorimetry

## 3.1   Introduction

The different thermal transitions, such as glass transition, Curie point, melting and crystallization can be determined from differential scanning calorimetry (DSC) thermograms.

The DSC set-up is shown in Fig. 3.1. The instrument consists of two pans; the samples are placed in the sample pan and the reference pan is generally left empty. The pans are placed in a closed chamber and they are placed above the heaters. A controller is connected to the heating chamber to regulate and monitor the heat flow. There are two types of DSC available in the market. One is the heat flux DSC where the sample and the reference pans are heated by the same heater. Since the heat absorption by the two pans is different, there will be a difference between the heat flow rates to the sample $\Phi_S$ and to the reference sample $\Phi_R$ which is proportional to the temperature difference between them: $\Phi_S - \Phi_R \propto \Delta T$. Here the temperature difference ($\Delta T = T_S - T_R$) will be measured and converted to a power difference. The other type is power compensated DSC in which both the sample and the reference pans are heated separately; thereby, the temperature difference is maintained close to zero. The electrical power i.e. $\Delta P = dQ/dt$ needed to maintain the zero temperature difference is measured and is directly proportional to the resultant heat flow ($dQ/dt$). In a DSC thermogram the heat flow is plotted against the temperature.
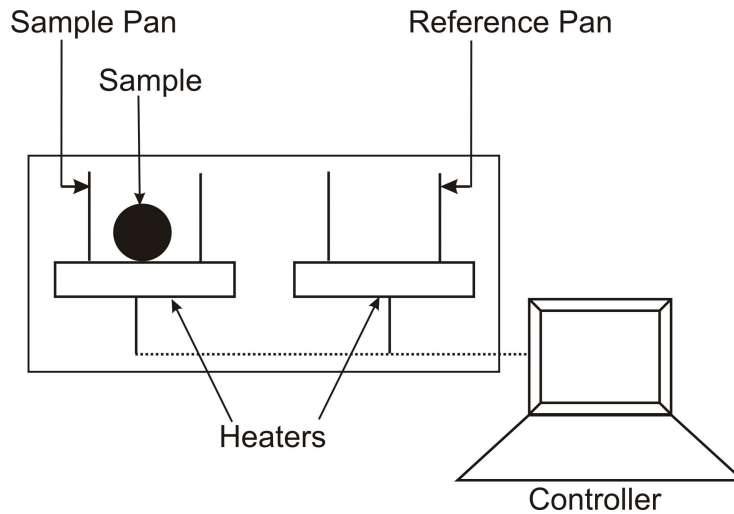
Figure 3.1: *General set-up of differential scanning calorimetry.*

## 3.2 Experimental setup

To study the thermal behavior of the LC, the copolymer of vinylidene fluoride and trifluoroethylene and the PDLC films, a power compensated PerkinElmer Pyris Diamond differential scanning calorimetry (DSC) was used. The sample and the reference material were placed in microfurnaces which are separated from each other. The microfurnaces are made of a platinum resistance thermometer (temperature sensor) and a platinum wire (heating resistor) [24]. The same heating power is applied to both the reference and the sample material, separately. When the temperature of the sample material rises (falls) the power is removed (applied) to the microfurnace to compensate the sample energy. The amount of power required to maintain the system at a "thermal null" state is directly proportional to the energy changes occurring in the sample.

## 3.3 DSC diagrams

A typical DSC plot of a semi-crystalline polymer is shown in Fig. 3.2. Crystalline and semi-crystalline polymers will show crystallization and melting transitions, whereas pure amorphous polymers will not show either crystallization or melting transitions. Both amorphous and semi-crystalline materials exhibit glass transitions. A glass transition is a second order transition (a thermal transition that involves a change in heat capacity but does not have a latent heat) whereas melting ($T_m$) and crystallization ($T_c$) are known as first order transitions (a thermal transition which involves both a latent heat and a change in the heat capacity of the material). The glass transition temperature ($T_g$) is the temperature below which the polymers are glassy and rigid and above which they are soft and rubbery.
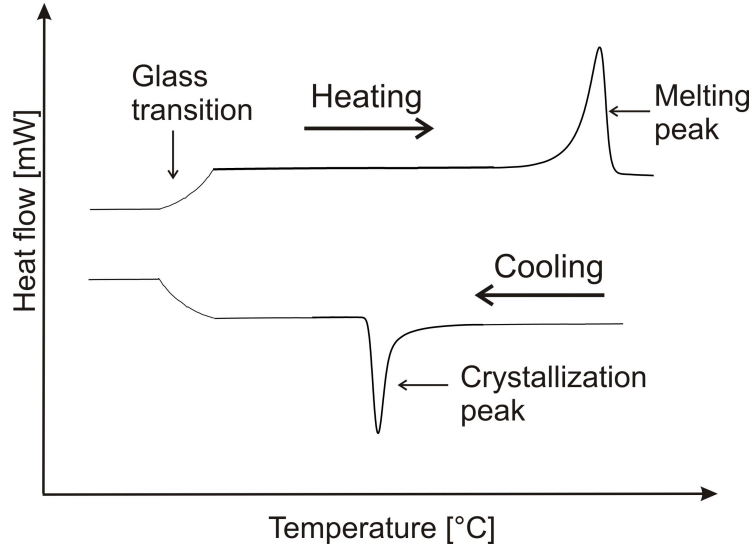
Figure 3.2: *Typical DSC plot of a semi-crystalline polymer exhibiting glass transition behavior ($T_g$), crystallization behavior ($T_c$) and melting behavior ($T_m$).*

## 3.4  StepScan DSC

The characterization of the glass transition process needs only the change in the heat capacity with temperature. A curved baseline influences the weak glass transition. Modulated temperature DSC (MTDSC) overcomes this problem. In addition to the linear temperature-time function, a sinusoidal modulation term is added in the MDSC. Therefore, the heating rate is also modulated. The resultant heat flow between the sample and the reference is given by [25]

$$\frac{dQ}{dt} = C_P \frac{dT}{dt} + f(T, t) \tag{3.1}$$

where $C_P$ is the heat capacity of the sample, $dT/dt$ is the rate of the temperature change and $f(T, t)$ is the heat flow from kinetic processes. The first and second terms represent the reversible and the kinetic aspects of the sample, respectively. By discrete Fourier transformation of the ratio of the modulated heat flow amplitude and the modulated heating rate amplitude the heat capacity is calculated. The difference between the total heat flow and the reversing heat flow gives the the kinetic component of the sample. In this work StepScan DSC measurement is used to characterize a weak glass transition process. StepScan DSC is a modulated temperature DSC technique in conjuction with the power compensated DSC. StepScan DSC does not use a modulated heat flow but it applies a series of short interval heating and isothermal hold steps (the temperature is kept constant for a certain period of time). When the sample is held in an isothermal condition, the

heating rate becomes zero and the equation 3.1 becomes

$$\frac{dQ}{dt} = f(T, t) \tag{3.2}$$

The sample's heat flow is then purely described by the kinetic term. The arithmetic difference between the total heat flow and the non-reversing heat flow or the kinetic component gives the reversing heat flow. The heat capacity is calculated from the ratio of the reversing heat flow and the rate of the temperature change. There is no need of a Fourier transformation to calculate the heat capacity.

## 3.5 Measurement

An approximately 5 - 15 mg sample was placed in the sample pan. For the DSC measurement the sample was heated and cooled at a rate of $20\,°\mathrm{C}/\mathrm{min}$. In the StepScan DSC measurement the sample was heated at a rate of 20 °C/min and the temperature was held at every $2\,°\mathrm{C}$ for 1 min.

# Chapter 4

# Dielectric relaxation spectroscopy

The electrical characterization of the insulating or semi-conducting materials in relation to their structure was done using dielectric relaxation spectroscopy (DRS). This technique is very sensitive to the dipoles and localized charges of the materials.

## 4.1 Types of polarization

When an electric field is applied to a material, the free electrons in the electrode, deposited on the material are displaced. The DC conductivity is zero in the case of an ideal dielectric material. They have only bound charges which can be displaced from their equilibrium positions until the electric field force and the oppositely acting elastic force are equal. This process is known as displacement polarization which can also be called electronic or ionic polarization. The dipole moments are oriented randomly. In the presence of an electric field, the dipole moments tend to orient along the external field. This phenomenon is known as orientational polarization.

The polarization $\vec{P}$ is defined as the dipole moment $\vec{m}$ per unit volume.

$$\vec{P} = \frac{d\vec{m}}{d\mathbf{V}} \tag{4.1}$$

The dipole moment can be defined as

$$\vec{m} = \sum_{i=1}^{N} q_i \vec{r_i} \tag{4.2}$$

where $q_i$ is charge and $\vec{r_i}$ are the coordinates of the charge. At small fields the polarization is proportional to the external field:

$$\vec{P} = \epsilon_0 \chi \vec{E} \tag{4.3}$$

where $\epsilon_0$ is the permittivity of the free space and $\chi$ is the electric susceptibility of the material. The electric displacement $\vec{D}$, the total charge per unit area deposited on the

electrodes, can be expressed as

$$\vec{D} = \epsilon^* \epsilon_0 \vec{E} \tag{4.4}$$

Here, $\epsilon^*(\omega) = \epsilon'(\omega) - i\epsilon''(\omega)$ is the complex permittivity of the material. Since $E(t)$ is a periodic sinusoidal function with respect to the frequency, the measuring regime is in the frequency domain. Due to the viscous motion and the dissipative force, the orientational polarization is not a resonant process. Therefore, the response of the orientational polarization to the change of the polarity is retarded. This process is known as dielectric relaxation and the time required to reach a new equilibrium state is called the relaxation time, $\tau$. Displacement polarization is a resonant process with resonant frequencies of $10^{15}$ to $10^{14}$ Hz for the electronic and $10^{13}$ to $10^{12}$ Hz for the ionic polarization.

As already mentioned, there is no dc conductivity in an ideal dielectric. But, real dielectric materials contain charge carriers which can be moved between the electrodes or between the crystalline and the amorphous interfaces. This results in a space charge polarization and the relaxation process is called charge-carrier relaxations. The relaxation time is given by the Maxwell relaxation time

$$\tau_c = \frac{\epsilon_0 \epsilon_r}{\sigma_{dc}} \tag{4.5}$$

where $\sigma_{dc}$ is the DC conductivity of the material. The relationship between the electric field and the current density $j$ is given as

$$j = \sigma^* \vec{E} \tag{4.6}$$

where $\sigma^* = \sigma' + i\sigma''$ is the complex electric conductivity. $\sigma'$ and $\sigma''$ are the real and the imaginary parts of the electric conductivity. Since the current density and the time derivative of the displacement polarization are equivalent quantities,

$$\vec{E} i\omega \epsilon^* \epsilon_0 = \sigma^* \vec{E} \tag{4.7}$$

$$\epsilon'' = \frac{\sigma'}{\omega} \tag{4.8}$$

At low frequencies, conductivity contributions lead to a divergence of $\epsilon''(\omega)$ [26].

## 4.2 Models for ideal and real systems

Dielectric spectroscopy measures the dielectric permittivity as a function of frequency and temperature. The simplest model to describe the dielectric spectrum is the Debye model. The Debye system is an ideal system which consists of non-interacting dipoles in a non-polar viscous environment. The complex permittivity or the Debye function can be expressed as

$$\epsilon^* = \frac{\epsilon_s - \epsilon_\infty}{1 + i\omega\tau} + \epsilon_\infty \tag{4.9}$$

where $\epsilon_s$ and $\epsilon_\infty$ are the static and unrelaxed permittivity, respectively. The complex permittivity can be separated into real and imaginary part. The real part of the permittivity ($\epsilon^{'}$) is usually known as permittivity (eq. 4.10) and the imaginary part of the permittivity ($\epsilon^{''}$) is known as the dielectric loss (eq. 4.11) which is due to the energy dissipated from the sample's internal friction. Debye's equation holds only for a single relaxation.

$$\epsilon^{'} = \frac{\epsilon_s - \epsilon_\infty}{1 + \omega^2\tau^2} + \epsilon_\infty \tag{4.10}$$

$$\epsilon^{''} = \frac{\epsilon_s - \epsilon_\infty}{1 + \omega^2\tau^2}\omega\tau \tag{4.11}$$

Debye's equation describes a symmetric loss peak with a half width of 1.14 decades [27], whereas in reality the loss peaks are broadened and asymmetric because the molecules contain interacting dipoles and the high frequency behavior is more pronounced than the low frequency one. The broadening of the loss peak can be explained by using the Cole-Cole function

$$\epsilon^{*}_{CC} = \frac{\epsilon_s - \epsilon_\infty}{1 + (i\omega\tau_{CC})^\beta} + \epsilon_\infty \tag{4.12}$$

The asymmetry of the loss peak can be described by the Fuoss-Kirkwood or by the Cole-Davidson function

$$\epsilon^{*}_{CD} = \frac{\epsilon_s - \epsilon_\infty}{(1 + i\omega\tau_{CD})^\gamma} + \epsilon_\infty \tag{4.13}$$

The Havriliak-Negami function (eq. 4.14) [27] is a combination of the Cole-Cole and the Cole-Davidson functions and takes into account both the broadening and asymmetry of the loss peak.

$$\epsilon^{*}_{HN} = \frac{\epsilon_s - \epsilon_\infty}{(1 + (i\omega\tau_{HN})^\beta)^\gamma} + \epsilon_\infty \tag{4.14}$$

$\beta$ and $\gamma$ describe the symmetric and asymmetric broadening of the loss peak, fulfilling the conditions $0 < \beta \leq 1$ and $0 < \gamma \leq 1$. The relaxation strength ($\Delta\epsilon = \epsilon_s - \epsilon_\infty$), relaxation time ($\tau$) and the two shape parameters ($\beta$ and $\gamma$) give the complete phenomenological description of a relaxation process. These values can be obtained by performing a least squares fit of Havriliak-Negami (HN) function known as HN analysis.

## 4.3 Dielectric relaxations

Dielectric spectroscopy is used to understand the molecular dynamics of a polymer. Motional processes of the polymer are investigated over a broad range of frequency and temperature. Amorphous polymers exhibit both a $\boldsymbol{\beta}$ or secondary relaxation and an $\boldsymbol{\alpha}$ or primary relaxation. Compared to the $\boldsymbol{\beta}$ relaxation, the $\boldsymbol{\alpha}$ relaxation occurs at lower frequencies or higher temperatures. The $\boldsymbol{\alpha}$ relaxation is related to the dynamic glass transition behavior

which is the onset of Brownian motion of polymer. The temperature dependence of its relaxation time obeys the Vogel-Fulcher-Tammann (VFT) law:

$$\tau(T) = \tau_0 \exp\left(\frac{T_A}{T - T_0}\right),\tag{4.15}$$

where $T_A$ is the activation temperature and $T_0$ is the Vogel or ideal glass transition temperature, which is 30-40 K below the calorimetric glass transition [28]. At the calorimetric glass transition, the relaxation time reaches a value of 100 s [29]. Since the $\boldsymbol{\alpha}$ relaxation has the highest strength it is known as a primary relaxation. The $\boldsymbol{\beta}$ relaxation arises from the local intramolecular movement. The temperature dependence of the $\boldsymbol{\beta}$ relaxation time obeys the Arrhenius law.

$$\tau(T) = \tau_0 \exp\left(\frac{E_A}{k_B T}\right),\tag{4.16}$$

where $E_A$ is the activation energy and $k_B$ is the Boltzmann constant. Sometimes a $\boldsymbol{\beta}$ relaxation is followed by a $\boldsymbol{\gamma}$ relaxation due to the smaller molecular units. The $\boldsymbol{\delta}$ relaxation occurs at high-frequency at the end of spectrum and is due to isolated molecules of impurities. Both $\boldsymbol{\gamma}$ and $\boldsymbol{\delta}$ relaxations obey the Arrhenius temperature dependence law.

## 4.4   Experimental setup and measurement

The DRS experimental set-up is shown in Fig. 4.1. Dielectric relaxation spectroscopy was performed from $-100\,^{\circ}\mathrm{C}$ to $+100\,^{\circ}\mathrm{C}$ and from 0.1 Hz to 10 MHz on pure P(VDF-TrFE) and the PDLC films. For measurement, 50 nm aluminium electrodes were coated onto both sides of the sample. The sample was placed between two metal electrodes whose diameter was approximately equal to the diameter of the electrode coated on the sample. The sample was placed on the sample holder and the sample holder was mounted inside a cryostat to control the temperature. A Novocontrol Alpha frequency-response analyzer was employed together with the Quatro cryosystem. The experiment was done both in the presence and in the absence of a bias voltage of 20 V. For higher ac amplitudes, the Novocontrol Alpha-A frequency analyzer (0.1 Hz to 10 kHz) was used together with the high-voltage booster HVB 1000 and the Quatro cryosystem. The measurements were performed under dry nitrogen. For DRS studies of the pure LC, a 100 µm thick Teflon spacer filled with the LC was placed between two glass plates coated with copper electrodes. The data was transferred automatically to the computer.
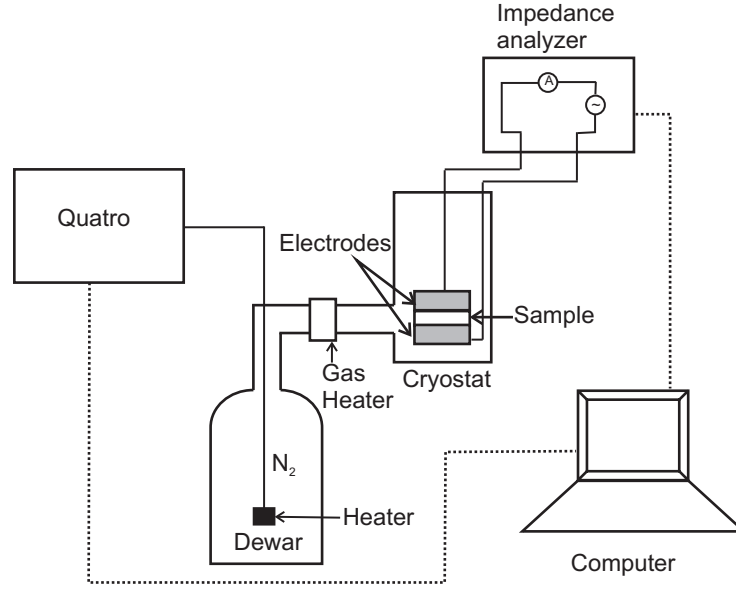
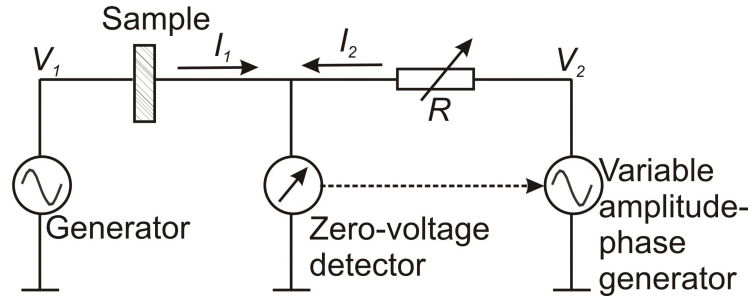Figure 4.1: *Experimental set-up for dielectric spectroscopy measurement.*



Figure 4.2: *Simplified measuring circuit of the dielectric spectroscopy measurement.*

The simplified measuring circuit is shown in Fig. 4.2. The potential $V_1$ was applied at the high terminal of the sample. Using the zero-voltage detector, the potential at the sample's low terminal was detected. The detector adjusted the magnitude and phase of the output $V_2$ of the variable amplitude-phase generator until the current $I_2$ generated by the range resistor and the sample balanced. Thus, the potential at the sample's low terminal became zero. The current produced by the sample $I_1$ and the range resistor $I_2$ can be defined as

$$I_1 = \frac{V_1}{Z} \tag{4.17}$$

$$I_2 = \frac{V_2}{R} \tag{4.18}$$

where $Z$ is the sample's impedance and $R$ is the resistance of the range resistor. When the range resistor current balanced the sample current i.e. $I_1 = -I_2$, the impedance of the

sample can be calculated as

$$Z = -\frac{V_1}{V_2}R. \tag{4.19}$$

Impedance was directly measured by the impedance analyzer. Therefore, dielectric spectroscopy is also known as Impedance Spectroscopy. Using impedance, one can find the capacitance and the permittivity of the sample (appendix A).

# Chapter 5

# Infrared spectroscopy

Infrared (IR) spectroscopy is a well recognized technique used to characterize, identify and quantify solid, liquid and gaseous substances. The mid-infrared region (4000 cm$^{-1}$ to 400 cm$^{-1}$) is used to study the vibrational energies within molecules. Infrared radiation is absorbed by organic molecules and converted into vibrational energy either stretching or bending. Not all possible vibrations will result in an absorption band in the IR region. When infrared radiation interacts with a molecule, the vibration must result in a change in dipole moment. The change in dipole moment may arise from symmetrical and asymmetrical stretching, scissoring, rocking, wagging and twisting of the bonds. Every bond and functional group absorbs IR radiation of different wavelength. In 1940's dispersive IR spectrometers emerged which are used to analyse organic compounds. Later, the Fourier-transform IR spectrometer replaced the dispersive IR spectrometer due to the increase in speed and no need of external calibration.

## 5.1   Dispersive infrared spectrometer

A dispersive infrared spectrometer is also known as a grating or scanning spectrometer. A simplified schematic diagram of the working principle of the dispersive IR spectrometer is shown in Fig. 5.1. The IR radiation is sent through a sample and sometimes through a chopper to moderate the energy reaching the detector- and then directed to a diffraction grating or prism. The prism separates the wavelengths of light in the spectral range and directs each wavelength individually to the detector. Each wavelength is measured subsequently and therefore the scanning speed is slow.
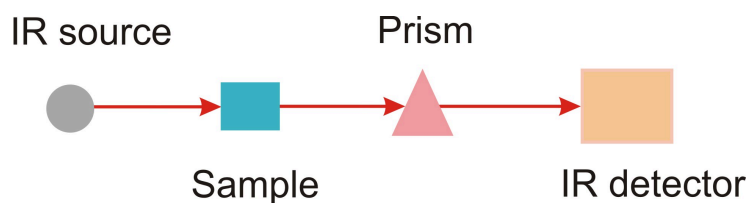
Figure 5.1: *Simplified schematic diagram of the dispersive infrared spectrometer.*
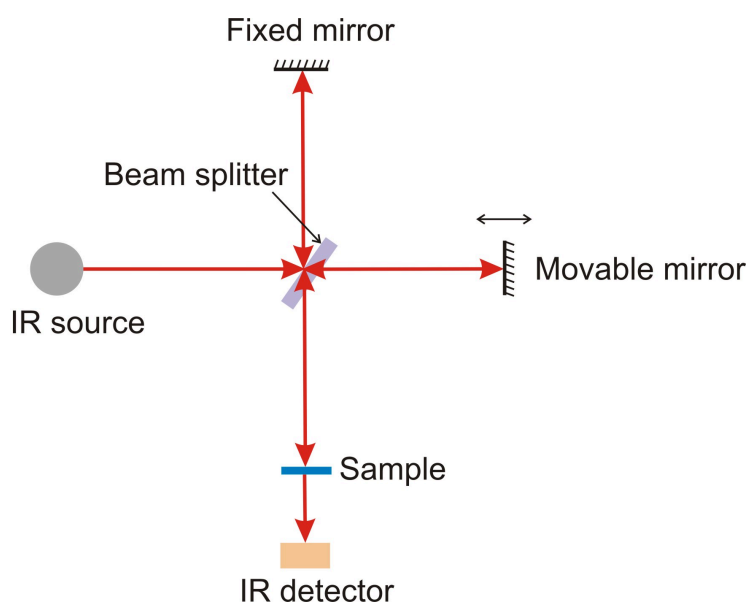


Figure 5.2: *Simplified schematic diagram of the fourier transformer infrared spectrometer.*

## 5.2    Fourier-transform infrared spectrometer

The Fourier-transform infrared (FTIR) spectrometer is based on the Michelson interferometer. Generally, the IR source is a ceramic material e.g. Globar (silicon carbide). The interferometer consists of two mutually perpendicular mirrors. One is fixed and the other one can move along an axis that is perpendicular to its plane. The movable mirror is either moved at a constant velocity or is held at certain positions for a short period of time [30]. The light emerging from the source strikes the beam splitter which reflects 50% of the light to the moving mirror and 50% of the light to the fixed mirror. The reflected light from the mirrors return to the beamsplitter where the light interferes. Again the light is partially reflected back to the source and partially transmitted to the sample. The intensity of the beam reaching the beamsplitter depends on the path difference between the beams traveling to the fixed and movable mirrors. From the beamsplitter, the interfered light goes
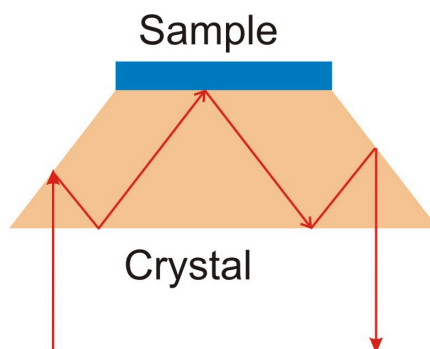
23

Sample

Crystal

Figure 5.3: *Simplified schematic diagram of the attenuated total reflection infrared spectrometer.*

to the sample where the energy is either absorbed or transmitted. Finally, the transmitted light reaches the detector. The detectors can be a liquid nitrogen cooled detector or room temperature detector e.g. deuterated triglycine sulfate (DTGS). The detector reads information about every wavelength in the IR range simultaneously. To convert it to a single spectrum, a Fourier transformation is performed (by software) on the interferogram. Without a sample, a background single beam is measured. The ratio of the sample single beam to the background single beam results in the transmittance of the sample. By taking the negative $\log_{10}$ of the transmittance, the absorbance spectrum can be obtained.

## 5.3 Attenuated total reflection infrared spectrometer

Attenuated total reflection (ATR) IR spectrometer is used for the analysis of powder, liquids, surfaces, thick samples and highly absorbing materials. The sample is placed on an optically dense material (crystal) with a high refractive index. The IR beam is directed onto the crystal at a certain angle allowing the radiation to reflect within the crystal, as indicated in Fig. 5.3. The internal reflectance creates an evanescent wave that propagates along the boundary and decays exponentially with increasing distance from the boundary. This means that the evanescent wave extends beyond the surface of the crystal into the sample held in contact with the crystal. When the sample absorbs energy the evanescent wave will be attenuated and the attenuated wave exits the opposite end of the crystal and is passed to the detector. A background measurement is done without a sample. Compared to the sample the crystal must have a very high refractive index. Zinc Selenide (ZnSe) and Germanium are the most commonly used crystals, but Diamond is the best ATR crystal.

## 5.4 Measurement

The platinum ATR module of a Bruker Alpha FTIR was used to measure the IR spectrum of the liquid crystal. A drop of liquid crystal was placed on the diamond crystal. The

liquid crystal was pressed by the ergonomic pressure device on the crystal. Then the measurement was carried out. Similarly, the IR transmission spectrum of the PDLC films were taken. The results were inconsistent because the PDLC film is not a homogeneous material. Some parts of the film may have high a droplet density and others may not. Therefore the unviersal sampling module of Bruker Alpha FTIR was used to obtain the IR spectrum of the pure P(VDF-TrFE) and the PDLC films. The alpha interferometer is based on a RockSolid interferometer. Spectra were taken by the FTIR spectrometer using an iris diaphragm. Bormashenko *et al.* [31] found that the spectral data depends strongly on the diameter of diaphragm. The FTIR spectra obtained with a diaphragm of 13 mm size. When the diaphragm size is bigger than the LC droplet size ($\approx$ 2-6 µm) and $\beta_{cr}$ inclusion size ($\approx$ 100 µm), an averaged spectrum is obtained.

# Chapter 6

# Thermally stimulated current

## 6.1 Introduction

Frei and Groetzinger proposed a thermal stimulation of the decay of the spontaneous polarization of electrets, in order to perform the decay measurement in a reasonable time [32,33]. Later Bucci *et al.* proposed a method called "ionic thermoconductivity" (ITC) to investigate the polarization in inorganic dielectrics [34] which is very similar to the technique suggested by Groetzinger *et al.*. Bucci *et al.* increased the temperature linearly to measure the depolarization current. Thermally stimulated current (TSC) measurement is used to understand the dynamics of thermally induced relaxation processes of the polymer films. Due to the hindered motion of the permanent dipoles and the free charges of the polymer by frictional forces, polar polymers can not be charged immediately after applying an electric field. Similarly, the polymers can not be discharged immediately after the removal of the electric field. Either by increasing or decreasing the temperature the relaxation process of the polymer is accelerated or slowed down. Above the glass-transition temperature, the polymers can be poled permanently.

## 6.2 Global and windowing polarization method

The TSC measurement scheme is shown in Fig. 6.1. In the TSC measurement, initially the polymer is heated to a higher temperature (above the glass transition temperature and below the melting temperature), to remove the charges stored in the electrode. Then the polymer is cooled down to a temperature above the glass transition temperature $T_\mathrm{g}$, so that the dipoles and free charges are mobilized. Next, at time $t_\mathrm{o}$, an electric field $E$ is applied which results in an alignment of dipoles and a drift of free charges to the electrodes. The temperature at which the electric field is applied is known as the polarization temperature $T_\mathrm{p}$. After a certain time $t_\mathrm{f}$, the charged polymer is cooled down to a temperature $T_\mathrm{d}$ where the permanent dipoles and charges are frozen. Therefore, no depolarization takes place. The electric field is switched off at $t_\mathrm{d}$. Then the polymer is subjected to a pure heating process to set free the molecular motions and hence, the measured current is
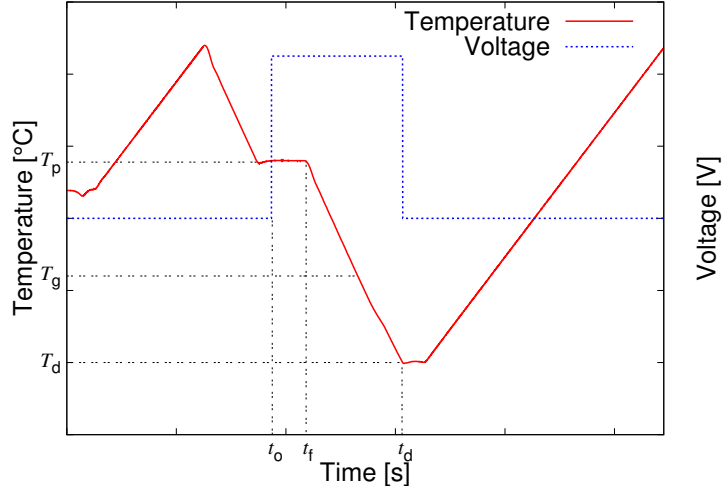
Figure 6.1: *TSC measurement scheme.*

the depolarization current $i(T)$. The current obtained is also known as the global TSC depolarization current which contains different relaxation process. The result obtained is similar to the one obtained by DRS operating at a very low frequency ($10^{-3}$ to $10^{-4}$ Hz) [35]. In order to isolate the different relaxation processes, Collins *et al.* used the windowing polarization method [35].

In the windowing polarization method, the polarization voltage is applied to the sample at the polarization temperature and it is held for a period of time $t_p$. The dipoles which have mobility at or below this temperature are oriented. The sample is cooled down to a temperature $T_o$ and then the voltage is switched off. The sample is held at this temperature for a period of time $t_w$. $T_o$ is only few degrees (2 - 5 °C) less than $T_p$. The dipoles which have mobility at or below $T_o$ start to move resulting in a depolarization. The dipoles which have mobility between $T_p$ and $T_o$ remain oriented. The sample is cooled down to $T_d$ where all the charges and dipoles are frozen and then the sample is heated in a linear fashion. The resulting depolarization current arises from the dipoles that remain oriented in the temperature window. Similarly, the measurement is carried out at different polarization temperatures and the resulting depolarization curves are the constituents of the global TSC curve.

## 6.3 Bucci equation

Using the Bucci formalism [36], the temperature dependence of the relaxation time of the processes can be calculated:

$$\ln\tau(T) = \ln\tau_0 + \frac{E_A}{k_B T} = \ln\left[s\int_T^\infty i(T)dT\right] - \ln i(T) \qquad (6.1)$$

where $s$ is the inverse heating rate $(dT/dt)$. In the Bucci plot or the relaxation map, the logarithm of the relaxation time is plotted against the inverse of the temperature. For a single Debye relaxation, the Bucci plot yields a straight line. The slope and the intercept of the line gives the activation energy $E_A$ and the time constant $\tau_0$ of the relaxation process, respectively.

## 6.4 Experimental setup and measurement

In this work, Global TSC measurements were done. The experimental setup is shown in Fig. 6.2. The polymer is placed between two steel electrodes which are mounted in a sample holder. The sample holder is placed inside a cryostat and it is connected to a electrometer. The electrometer is used to measure the output current and as the voltage source. The sample is heated and cooled with dry nitrogen gas from a dewar and heated or cooled using a gas heater. The quatro system and the electrometer are fully controlled by a computer.

To remove all charges, the sample was heated to 120 °C. Then, the sample was cooled down to the polarization temperature $T_p$ (40 °C) well above the glass transition temperature of the polymer matrix ($-37$ °C) and the temperature at which the LC changes from solid crystalline to nematic transition ($-20$ °C to 10 °C). Under the electric field the sample was polarized at the polarization temperature for 10 min. The applied electric field was maintained at 0.5 MV/m. The sample was quenched to the freezing temperature $T_d$ of $-100$ °C. Later, the sample was heated at a rate of 3 °C/min. The polarization current was measured using the electrometer. The measurement was stopped at 70 °C. To understand the physical properties of the PDLC film, the polarization temperature was varied between $-10$ °C and 40 °C and to investigate the peak character the electric field was varied from 0.2 MV/m to 1 MV/m.
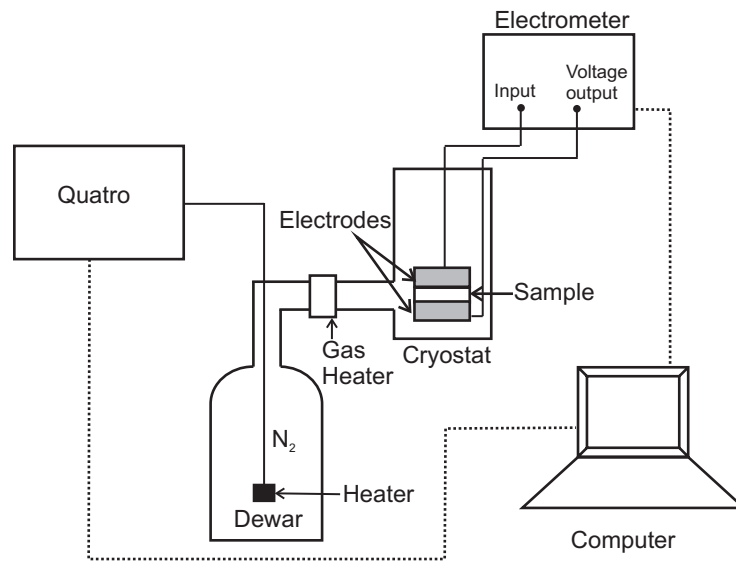
Figure 6.2: *TSC experimental setup.*

# Chapter 7

# Electrical hysteresis

## 7.1   Electric poling

Poly(vinylidene fluoride-trifluoroethylene) exists in a crystalline form ($\beta_{cr}$) which exhibits ferroelectricity. Before poling, the spontaneous polarization in the polar crystallites is randomly distributed resulting in a zero net polarization, which is why the ferroelectric polymer does not show either a piezoelectric effect or a pyroelectric effect. The samples can be poled by a corona discharge [37, 38] or by poling of metalized samples with direct electrode contact. In direct contact method, poling can be done either by using a constant (square, etc) electric field (Fig. 7.1) or by using a varying (sinusoidal, triangular, etc) electric field (Fig. 7.2). When the polymer is poled with a suitable electric field the molecular dipoles are oriented in the field direction and a spontaneous or remanent polarization is formed in the crystallites which remains even after the removal of the electric field. Poled ferroelectric materials are characterized by remanent polarization and a coercive field. Remanent polarization is the polarization remaining after the sample has been poled and the applied field is switched off. The coercive field is the field required to reduce the polarization to zero. To estimate the remanent polarization and the coercive field, Dickens *et al.* described different measurement and calculation procedures which are based on the application of a sinusoidally varying electric field and a combination of bipolar and unipolar electric-field cycles [39].
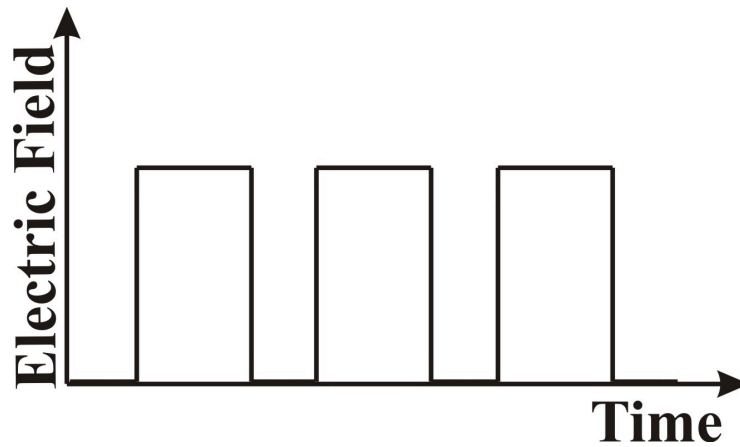
Figure 7.1: *Time dependence of the square wave electric field.*
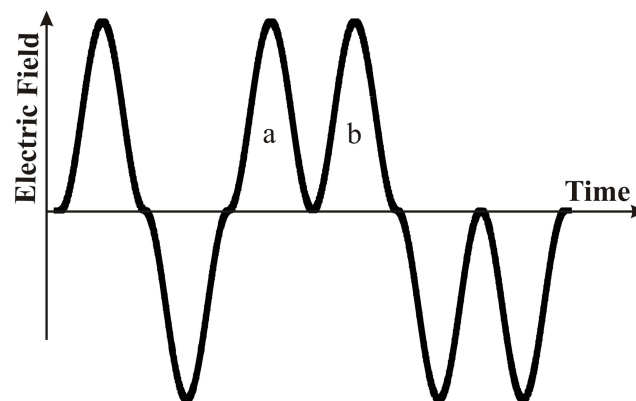


Figure 7.2: *Time dependence of the unipolar and bipolar poling scheme.*

During poling, orientation of dipoles, orientation of domains, trapping of charges and ageing effects can occur. Here, ageing effects were neglected. When a voltage is applied to the ferroelectric material, the current measured is called the poling current, $I$. The poling current (eq. 7.1) is the sum of the polarization build-up current, $I_p$, the current due to the capacitance, $I_c$, and the current due to the conductivity, $I_{cond}$ [39]. $A$ is the sample area, $R$ is the resistance, $C$ is the capacitance of the sample, $P$ is the polarization and $V_p$ is the poling voltage.

$$I(t) = I_p(t) + I_c(t) + I_{cond}(t) = A\frac{dP}{dt} + C\frac{dV_p}{dt} + \frac{V_p}{R} \tag{7.1}$$

In order to separate the polarization contribution from the other contributions, such as conductivity, capacitance of the sample, Dickens *et al.* used a unipolar/bipolar loop. In this work, a unipolar/bipolar poling scheme is used to pole the sample and to characterize the ferroelectric polymer matrix and the PDLC films. When the applied electric field is above the coercive field the polarization (the dipoles) can be reversed. In the bipolar poling scheme, the polarization will be flipped twice. The bipolar poling scheme is followed by two positive unipolar cycles and two negative unipolar cylces. The poling current obtained from the first unipolar poling scheme ('a' in Fig. 7.2) is $I_a$ which is nothing but $I(t)$. If the orientation is saturated and if no relaxation occurs, a second unipolar poling scheme ('b' in Fig. 7.2) with the same polarity yields a poling current $I_b$ which is only due to the capacitance and conductivity of the sample. By using the equation

$$I_p(t) = I_a(t) - I_b(t) \tag{7.2}$$

the current due to the polarization alone can be obtained, from which the polarization ($P$) can be calculated as

$$P = \frac{1}{2A} \int I_p(t)dt \tag{7.3}$$

The above calculation was proposed by Wegener [40].

## 7.2   Experimental setup and measurement

The hystersis and electro-optical measurement setup is shown in Fig. 7.3. The electro-optical measurement will be discussed in the next chapter. The setup consists of a high voltage power supply, which is connected in series with the sample, a resistor and an electrometer in current mode. To apply the unipolar/bipolar wave form to the sample a function generator is connected to the high voltage source to generate an electrical field of unipolar/bipolar waveform. The poling voltage, the frequency and the waveform are controlled by the computer. The measurement was started with a low electric field of 5 MV/m and each time the electric field was increased stepwise by 5 MV/m. The measurement was carried out until a saturated hysteresis curve was obtained. By plotting the polarization against the electric field, the hysteresis behavior of the polymer matrix and the PDLC films is studied.
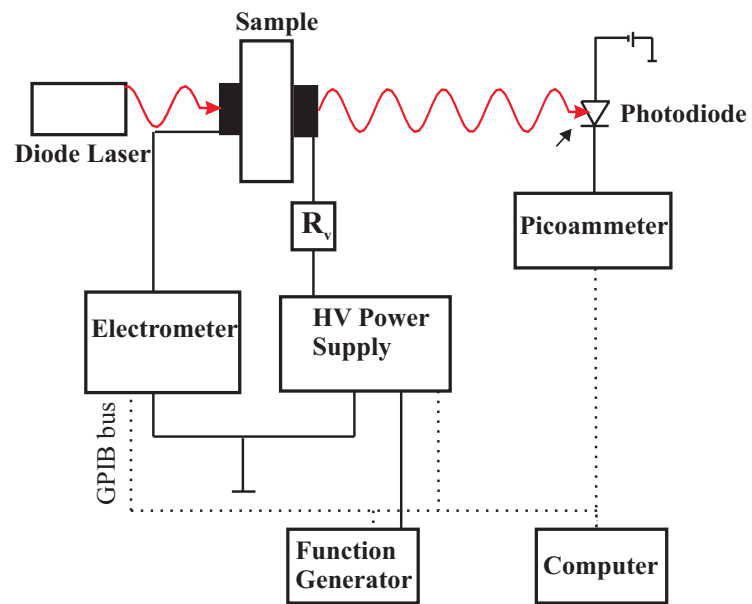
Figure 7.3: *Set-up for hysteresis and electro-optical measurement.*

# Chapter 8

# Electro-optical behavior

## 8.1   Light scattering

The electro-optical effects seen in the PDLC films make them interesting candidates for a variety of electro-optic applications ranging from displays to light shutters. For this the basic understanding of light scattering of the PDLC film is necessary.

The light scattering properties of a PDLC film depends on the droplet size, droplet shape, density of LC droplets, the refractive index mismatch between the LC and the matrix polymer, the wavelength of light, the polarization of light and the angle of incidence. When the LC possesses positive dielectric anisotropy ($\Delta\epsilon = \epsilon_{||} - \epsilon_{\perp} > 0$), where $\epsilon_{||}$ is the dielectric coefficient parallel to the director and $\epsilon_{\perp}$ is the dielectric coefficient perpendicular to the director of the LC molecules, the PDLC film will exhibit a scattering effect in the OFF state (at zero electric field) and a transparency in the ON state (at high electric field). When the LC possesses negative dielectric anisotropy ($\Delta\epsilon < 0$), the PDLC film will exhibit a transparency in the OFF state and a scattering effect in the ON state [41]. The orientation of the nematic molecules inside the droplet plays the main role in switching the PDLC film between the highly scattering "OFF" to the transparent "ON" state.

In the absence of an electric field, the symmetry axis of each droplet is oriented randomly. When light passes through the PDLC film, the refractive index varies from droplet to droplet resulting in a strong scattering. At intermediate field, some of the droplets are oriented and others are either partially oriented or remain unchanged. In this case, the effective birefringence and scattering are reduced. When the applied electric field is high enough to orient all the LC molecules in the droplet, the scattering will depend on the refractive-index mismatch between the polymer matrix and the LC.

### Single and multiple scattering

If the mutual distance between the droplets is 20 times the radius of the droplet, then it is possible to study the scattering of one droplet without reference to the other droplets.

This is called *independent scattering* [42]. When the scattered intensity of the PDLC film is equal to the product of the number of droplets and the intensity scattered by a single droplet, then it is known as *single scattering* [42]. In the *multiple scattering* the LC droplet is not only exposed to the incident beam but also to the light scattered by the other droplets. When the total scattering is small, the transmitted intensity $I_t$ is given as

$$I_t = I_0 e^{-\tau_d} \tag{8.1}$$

where $I_0$ is the incident intensity and $\tau_d$ is the optical depth of the sample. If $\tau_d > 0.3$, then multiple scattering becomes important.

## 8.2 Light-scattering models

Based on droplet size, droplet density and refractive index of the LC and the polymer matrix, different scattering models can be selected. The *anomalous diffraction approximation* and *Rayleigh-Gans approximation* are the two most widely used light scattering models.

### 8.2.1 Anomalous diffraction approximation

The anomalous diffraction (AD) approximation [42, 43] assumes that $kR_d \gg 1$ and $(n_{LC}/n_P) \gg 1$ where $k = 2\pi/\lambda$ is the wavevector of light and $\lambda$ is the wavelength of light, $R_d$ is the droplet radius, $n_{LC}$ is the refractive index of the LC and $n_P$ is the refractive index of the polymer matrix. The first assumption allows the use of a ray approximation for the incident light whereas the second assumption assumes that refraction and reflection at the LC/polymer interface will be negligible. The droplet introduces only a phase shift in the incident light. The transmitted radiation interferes in the far field producing a diffraction pattern similar to Fraunhofer diffraction pattern.

### 8.2.2 Rayleigh-Gans approximation

The Rayleigh-Gans (RG) approximation [42, 43] assumes that $2kR_d(n_{LC}/n_P - 1) \ll 1$. Here, the induced phase shift of the light is weak. Each LC droplet acts independently and scatters light similar to Rayleigh scattering which forms the basis for the approach.

By applying the RG approximation, the light scattering of three-dimensional spherulites [44], isotropic and anisotropic spheres [45] and liquid crystalline droplets in an isotropic polymer has been studied [46]. Meet *et al.* used the AD approximation to study the light scattering of both anisotropic and isotropic spheres [45], and Biganska *et al.* calculated the theoretical angle of the liquid crystalline droplets with an axial director orientation using the AD approximation [46]. These models were mostly applied for weakly-scattering films which simplifies the analysis.

## 8.3 Light scattering of high-droplet-density films

The PDLC film having low droplet-density scatters less. At high fields, the scattering will depend on the refractive-index mismatch between the polymer matrix and the LC. The PDLC films having high droplet-densities are highly scattering and multiple scattering is predominant. The light scattering property is dominated by the refractive index difference between the neighboring droplets [43]. The volume fraction of the liquid crystal $\nu_{LC}$ can be calculated using Bruggeman's formula [47]

$$1 - \nu_{LC} = \frac{\epsilon_{LC} - \epsilon_m}{\epsilon_{LC} - \epsilon_P} \left( \frac{\epsilon_P}{\epsilon_m} \right)^{1/3} \tag{8.2}$$

where $\epsilon_{LC}$ is the dielectric constant of the liquid crystal, $\epsilon_P$ is the dielectric constant of the polymer matrix, and $\epsilon_m$ is the dielectric constant of the composite film.

## 8.4 Factors affecting light scattering

### 8.4.1 Refractive index of the droplet

A schematic representation of the PDLC film indicating the path of the polarized light is shown in Fig. 8.1. At high electric field, the transparency of the PDLC film depends on the mismatch between the effective refractive index of the LC droplet and the refractive index of the polymer matrix. The effective refractive index $n_{eff}$ of the LC droplet depends on the angle of incidence and the polarization of the light. The effective refractive index is given as [48, 49]

$$n_{eff} = \frac{n_e n_o}{\sqrt{n_e^2 \cos^2\theta + n_o^2 \sin^2\theta}} \tag{8.3}$$

where $\theta$ is the angle of incidence, $n_e$ and $n_o$ are the extraordinary and ordinary refractive indices of the LC, respectively. They are the refractive indices parallel and perpendicular to the direction of the molecular alignment, shown in Fig. 8.1. At normal incidence the light will be parallel to the LC director and $n_{eff}$ is equal to $n_o$. For the light polarized perpendicular to the plane of incidence, $n_{eff}$ remains constant and equal to $n_o$ for all $\theta$. Using both horizontally and vertically polarized light Wu *et al.* studied the angular dependency of the transmitted light intensity for various $n_P/n_o$ ratios [48]. Including the Snell's-law correction for the refraction of light at the air/PDLC interface, eq. 8.3 can be re-written as [50]

$$n_{eff} = \frac{n_o}{\sqrt{1 - \left( \frac{\sin^2\theta_{air}}{n_P} \right) \left( 1 - \left( \frac{n_o}{n_e} \right)^2 \right)}} \tag{8.4}$$

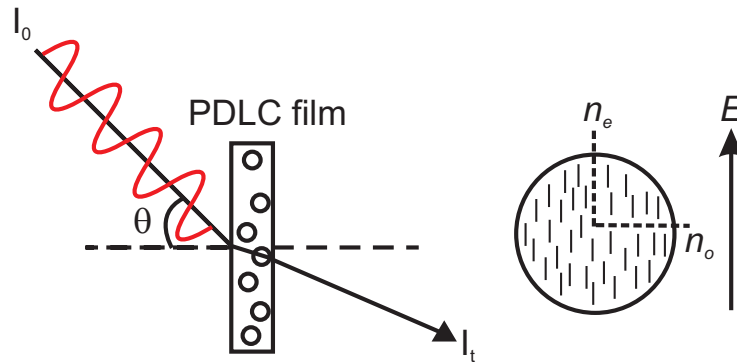where $\theta_{air}$ is the angle of incidence in air.

Figure 8.1: *Schematic sketch of the PDLC film indicating the path of light polarized perpendicular to the plane of incidence. Illustration of the aligned nematic radial droplet along the electric field, where $n_e$ and $n_o$ are the refractive indices of the LC parallel and perpendicular to the axis of anisotropy, respectively.*
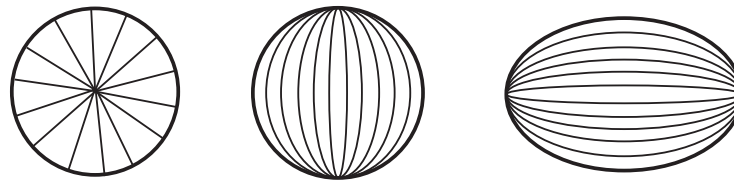


Figure 8.2: *Director configuration within a radial, a spherical bipolar and an ellipsoidal bipolar droplets.*

### 8.4.2  Droplet configuration

Bipolar configuration is the most common droplet alignment, shown in Fig. 8.2. Parallel alignment of the nematic is induced by most of the polymers, therefore bipolar droplets are the most commonly found in the PDLC films where the director is anchored parallel at the interface. The major elastic deformation present in bipolar droplets is a bend deformation at the curvature [43]. When a strong electric field is applied to the bipolar droplets, the director will tend to orient along the electric field. In radial droplets, the liquid crystal molecules are aligned perpendicular to the cavity wall. At high droplet concentration, the refractive index difference between the neighboring droplets is small and results in weak scattering.

### 8.4.3  Wavelength

For every droplet size, there is a short wavelength ($\sim 400$ nm) where the absorbance decreases and the transmission increases. At long wavelength($\sim 700$ nm) the transmission decreases rapidly and the absorbance increases [51]. Selection of the wavelength within this window range is important for the electro-optical measurement.

## 8.5   Characterization of electro-optical behavior

The electro-optical property of the PDLCs is characterized by the transmission $T$, contrast ratio and the voltage $V_{on}$ required to make the PDLC film transparent. The $V_{on}$ is also known as switch on voltage. *Transmission* is the ratio of the transmitted light intensity to the incident light intensity. *Contrast ratio* is the ratio of the transmission of the PDLC film at "ON" state (high field) to the transmission at "OFF" state (zero field). The switch on voltage is given as [52]

$$V_{on} \sim \frac{d}{R_m}(l^2 - 1)^{1/2} \left( \frac{4\pi K}{\Delta\epsilon} \right).$$
(8.5)

where $d$ is the thickness of the PDLC film, $R_m$ is the mean droplet radius, $l$ is the ratio of the major and minor radii of the droplet, $K$ is the elastic constant of the LC and $\Delta\epsilon$ is the dielectric anisotropy of the LC.

## 8.6   Experimental setup

The field-dependent optical transmission of both the PDLC and the pure P(VDF-TrFE) films was measured while poling the sample. The experimental setup is shown in Fig. 7.3. The electric field was applied using a high-voltage power supply. A function generator was connected to the high-voltage source to generate a unipolar/bipolar electrical field. A diode laser emitting red light with a wavelength of 785 nm and a power of 50 mW was used as the light source which generates polarized light. The PDLC film was placed between the laser diode and the photodiode. The sample was irradiated normal to the film surface. In this work, the transmitted light intensity (without any polarizer and filter) was measured using a photodiode. The change in the transmitted intensity with the electric field has been focused on in this thesis.

# Chapter 9

# Piezo-optical measurement

## 9.1 Conceptual background

As mentioned in section 1.5, the local electric field developed by the ferroelectric polymer matrix under stress acts as a bias field to the LC droplet. A piezo-optical measurement is not found in the literature. Once the PDLC film is poled with an electric field above the coercive field, the molecular dipoles of the ferroelectric polymer are oriented in the field direction which persists after removal of the external field, as shown in Fig. 9.1. Now, the PDLC film can exhibit both the piezo- and pyro-electric effect. In this work, the piezoelectric effect of the ferroelectric polymer is coupled to the electro-optical effect of the LC molecules. When unstressed, the LC molecules are aligned parallel to the major axis of the droplet. When the PDLC film is compressed, the dipole density of the polymer matrix changes, thereby a change of electric-field is generated of the same polarity as the poling voltage. The local electric field across the LC-filled cavities acts as a bias field to the LC. The nematic molecules tend to align along the field direction, resulting in the decrease of the birefringence, thus the scattering is reduced, as shown in Fig. 9.1. If the ordinary refractive index $n_o$ of the LC matches that of the polymer $n_P$, the sample thus becomes transparent or the transmission of the PDLC film increases. Applying a load (force) to the PDLC film can switch it from the "OFF" state to the "ON" state.
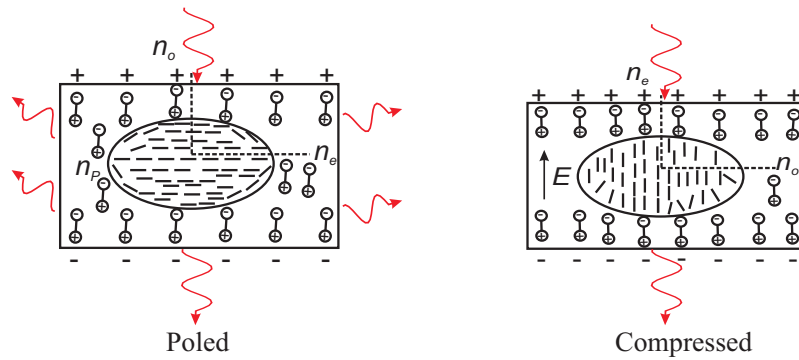
Figure 9.1: *Schematic representation of the poled PDLC film and the poled PDLC film under compression.*
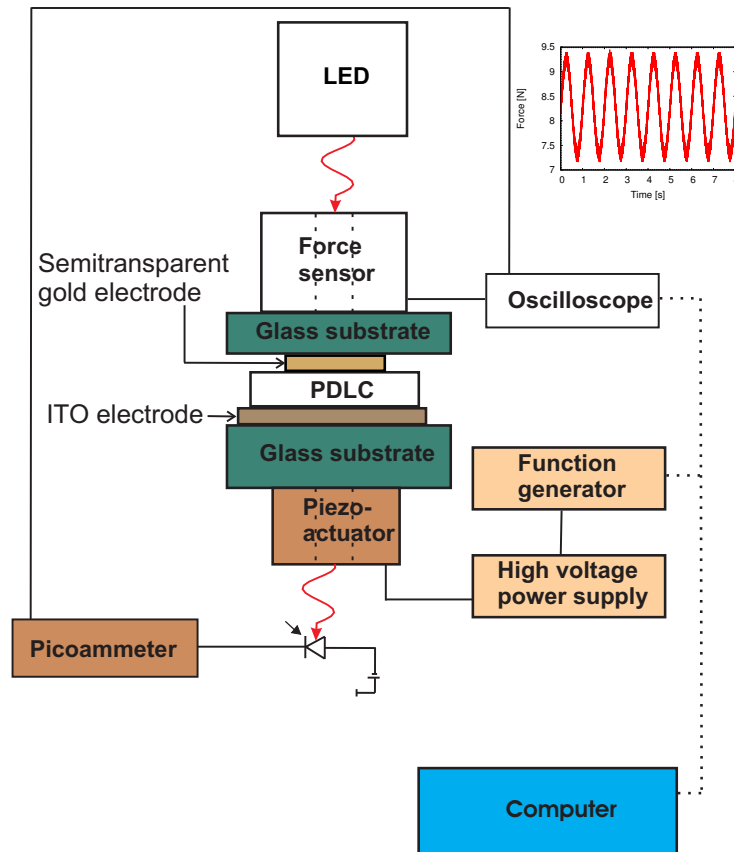


Figure 9.2: *Schematic diagram of the piezo-optical measurement system. Inset: Time dependence of the dynamic force.*

## 9.2  Experimental setup

The schematic diagram of the measurement system is shown in Fig. 9.2. During the measurement the light needs to pass through the compressed area of the sample. Therefore, a ring-shaped force sensor and ring-shaped piezo-actuator are used. When a free-standing film is used, the film will bend. Thereby, specially prepared samples (see section 2 for the sample preparation) were used for the measurement. The sample was placed between a force sensor and a piezo-actuator. To avoid bending of the sample, another glass substrate was placed on top of the film. Using the force sensor, the force applied to the sample was measured. The actuator was pre-loaded with an offset voltage. To generate a sinusoidal dynamic force at a frequency of 1 Hz, a sinusoidal voltage with a frequency of 1 Hz was applied to the actuator. In the first measurement setup, the piezo-actuator having a maximum displacement of 5 µm and a stiffness of 230 N/µm was used to apply the dynamic force on the sample. A laser diode emitting a red light at a wavelength of 785 nm was used as the light source and the transmitted light intensity was measured with a photo-diode. The resulting light-intensity waveform exhibited sub-peaks in every period which might have come from the interference effect in the sample and the substrate (Fig. 9.3 (left)). In order to avoid the interference effect, the laser diode was replaced by a light-emitting diode, as can be seen in Fig. 9.3. An LED emitting red light at a wavelength of 660 nm was used. It was also necessary to increase the force applied to the sample. Therefore, the piezo-actuator was replaced with a piezo-actuator having a high maximum displacement of 60 µm and a stiffness of 29 N/µm. The piezo-optical measurement setup is shown in Fig. 9.4. The modulation of the optical transmission under dynamic mechanical excitation was measured for both the PDLC film and the pure P(VDF-TrFE) films. The photo-diode current and the electrical signal from the force sensor were fed to a digital storage oscilloscope.
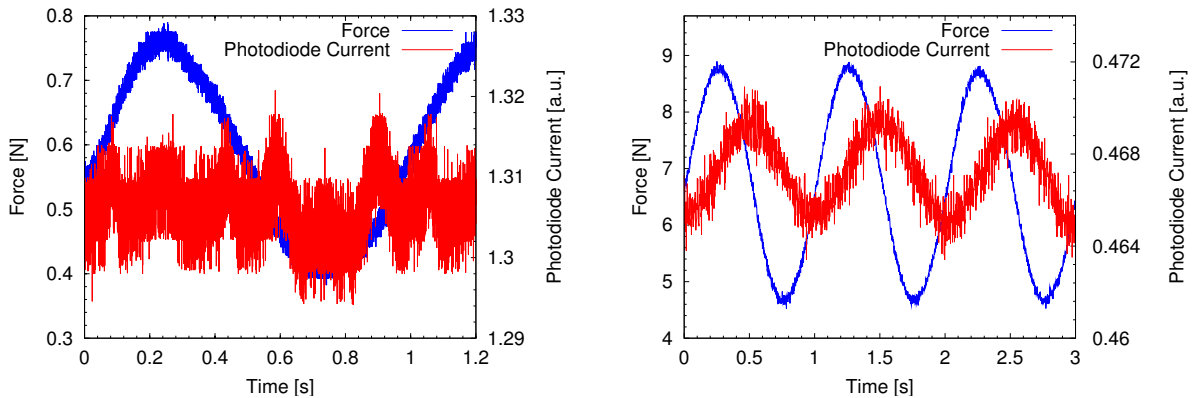


Figure 9.3: *The photodiode current variations of the PDLC film containing 10 wt% LC when the laser diode (left) and LED (right) were used as light source.*
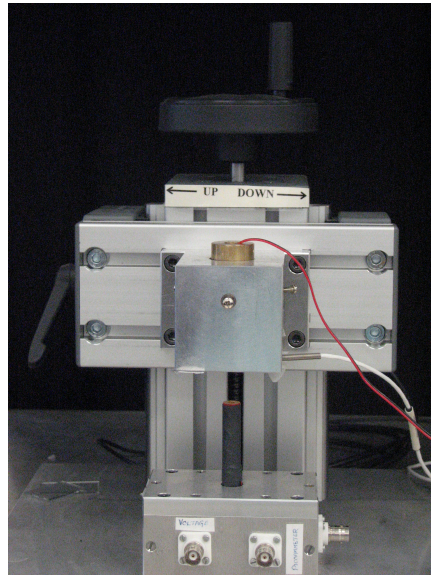
Figure 9.4: *Piezo-optical measurement setup.*

# Chapter 10

# Results and Discussion

## 10.1 Thermal behavior

### 10.1.1 Liquid crystal

The DSC thermogram of the LC is shown in Fig. 10.1 . During heating a transition was observed around $-10\,°C$. This is the transition from solid crystalline phase to anisotropic nematic phase. Here the transition does not occur at a definite temperature but takes place over a temperature range because the LC used is a mixture of LCs. Below this transition the LC molecules exist in a crystalline form. At $75\,°C$, the LC undergoes a transition from the anisotropic nematic phase to isotropic liquid phase.
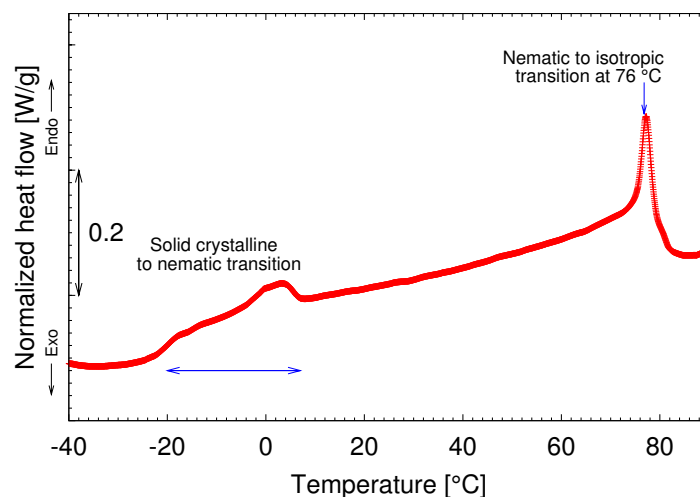


Figure 10.1: *DSC thermogram of the LC during heating at the rate of $20°C/min$.*
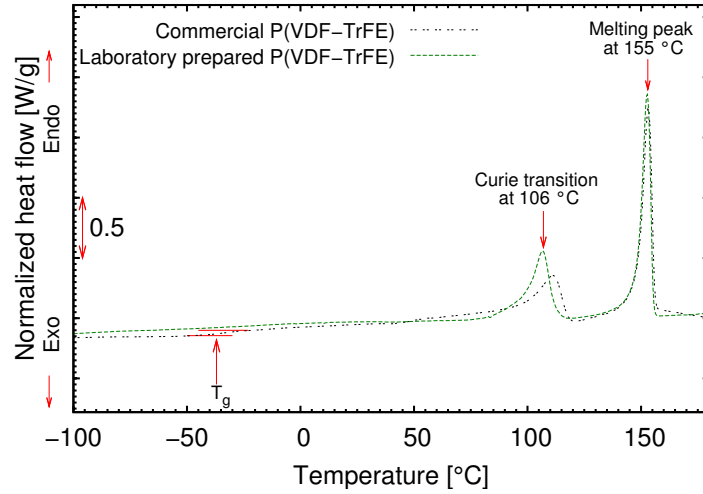
Figure 10.2: *DSC thermogram of the commercial and laboratory-prepared P(VDF-TrFE) film during the first heating.*

## 10.1.2 Comparison of commercial and laboratory-prepared P(VDF-TrFE)

P(VDF-TrFE) is a semi-crystalline polymer. The P(VDF-TrFE) film showed two endothermic peaks in the DSC thermogram. The Curie point $T_C$, is the point at which the polymer changes from the ferroelectric to the paraelectric phase and the melting point $T_m$ of both the laboratory-prepared and the commercial P(VDF-TrFE) film are found to be 106 °C and 155 °C, respectively, as shown in Fig. 10.2. At about −39 °C a glass transition is observed in the DSC thermogram of the commercial P(VDF-TrFE) film. Due to the annealing process, the crystallinity of the laboratory-prepared P(VDF-TrFE) film ($\Delta H_m = 29.7$ J/g) is slightly higher than that of the commercial P(VDF-TrFE) ($\Delta H_m = 28.9$ J/g) which can be seen from the height of the melting peak and from the melting enthalpy.

## 10.1.3 Comparison of P(VDF-TrFE) and PDLC

Hereafter, the laboratory-prepared P(VDF-TrFE) film will be mentioned only as P(VDF-TrFE). The thermal behavior of the pure P(VDF-TrFE) film and the PDLC films containing different wt% of LCs are compared. Between −10 °C and 25 °C a flat heat flow peak is visible in the PDLC films (Fig. 10.3) which could be attributed to the solid crystalline to nematic transition of the LC. The shift of the transition to higher temperature could be caused by the fact that the LC is constrained in small droplets embedded in the polymer matrix. Since the change in the heat flow of the LC during the transition from solid crystalline to nematic is ca. 0.13 W/g, the transition in the PDLC film is flat and cannot be seen distinctly.
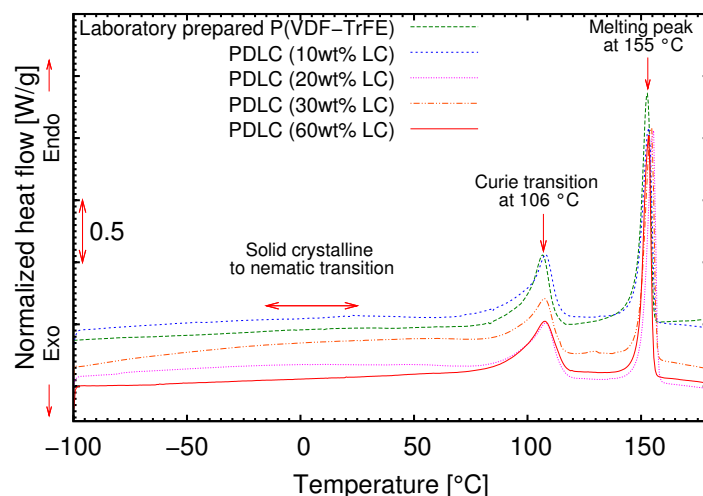
Figure 10.3: *DSC thermogram of the laboratory prepared P(VDF-TrFE) film and the PDLC film containing 10 wt% LCs, 20 wt% LCs, 30 wt% LCs and 60 wt% LCs during the first heating.*

Even though the weight percentage of P(VDF-TrFE) is decreased in the PDLC composites, no remarkable change in the melting behavior of the P(VDF-TrFE) is observed in the PDLC films, as shown in Fig. 10.3. The melting temperature and the melting enthalpy of the PDLC composites are plotted versus the LC content in Fig. 10.4. Addition of LC in the polymer matrix results in a small change in the melting temperature and in the melting enthalpy of the P(VDF-TrFE). A small change in the melting enthalpy means that the LC acts as a nucleator for the polymer matrix and the interaction between the LC and the polymer matrix is very weak. Zhang *et al.* observed a similar behavior in the melting and crystallization behavior of unmaleated polyethylene and fibrous cellulose blends [53].
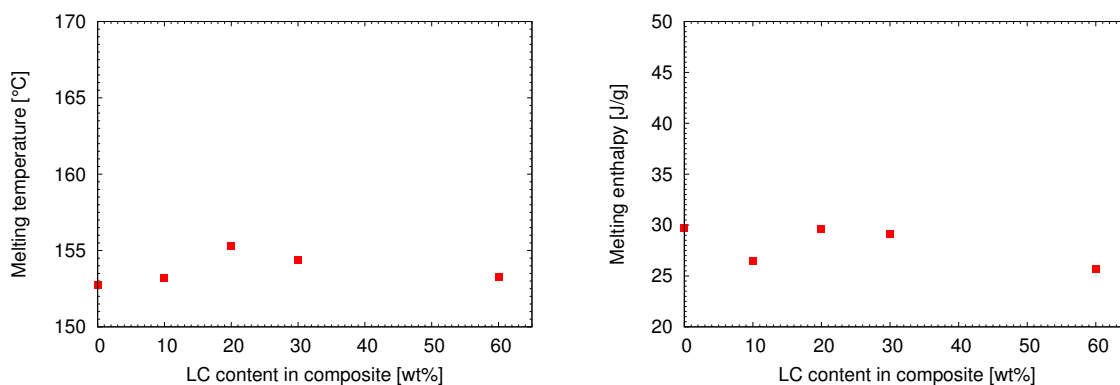


Figure 10.4: *The effects of the LC content in the PDLC composite on the melting temperature(left) and melting enthalpy of the composites (right).*
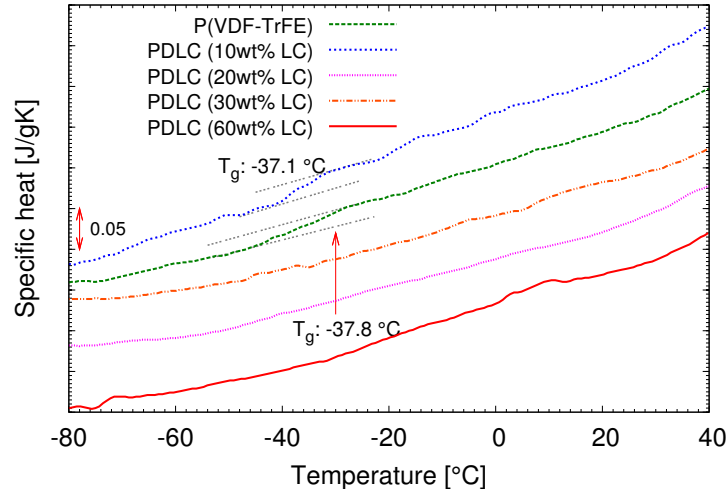
Figure 10.5: *StepScan DSC thermogram of a pure P(VDF-TrFE) film and of PDLC film containing different weight percentages of LCs.*

Because of its higher crystallinity the pure P(VDF-TrFE) film and PDLC films do not show a glass step in the DSC thermogram. The weak glass-transitions of the pure P(VDF-TrFE) film and of the PDLC film containing 10 wt% LC are visible in the Step-Scan DSC thermogram (Fig. 10.5). The glass transition temperature $T_g$ of the pure P(VDF-TrFE) film is found to be $-37.8\,°C$; it is close to the value $(-34\,°C)$ obtained by Menegotto *et al.* [54]. The glass transition of the PDLC film containing 10 wt% LC is found at $-37.1\,°C$, it is close to the $T_g$ of the P(VDF-TrFE) film. Therefore, it can be concluded that the LC molecules do not plasticize the matrix material, i.e. they are not dissolved in the polymer matrix; they are only dispersed as droplets. In the StepScan DSC thermogram of the PDLC film containing 20 wt%, 30 wt% and 60 wt% LCs, the specific heat capacity changes in the order of $10^{-3}$ J/(gK) which results in difficulty in finding the glass transitions of the PDLC composites. Here, with the increase in LC content, the crystalline portion of the PDLC films is increased which in turn leads to the decrease in the amorphous portion.

## 10.2   Optical micrographs

After the films were prepared they were examined using a polarizing microscope. The anisotropic liquid crystal dispersed in the P(VDF-TrFE) is a birefringent material, i.e. it has two indices of refraction. The transmission axis of the sample was placed between two crossed polarizers and it was aligned at some angle between the fast and the slow direction of the material. When polarized light passes through the liquid crystal droplets, the light is divided into two components with different propagation speeds. The difference in speed gives rise to a phase difference when the two beams interfere. The relative phase difference
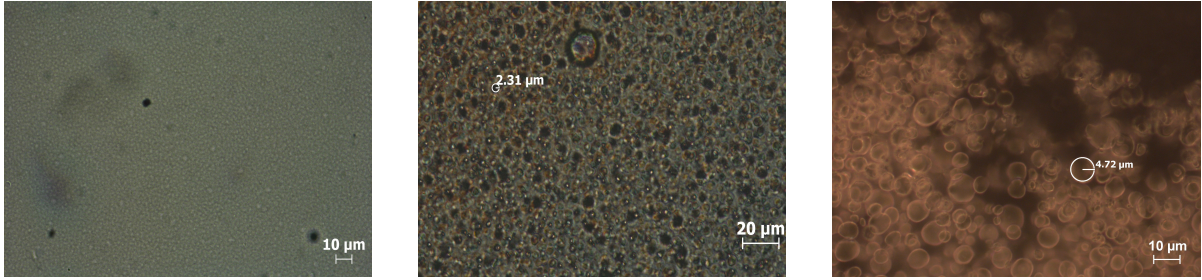
Figure 10.6: *Optical micrograph images of the pure P(VDF-TrFE) film (left), the PDLC films containing 10 wt% (center) and 60 wt% (right) liquid crystal.*

can be expressed as [55]

$$\Gamma = \frac{2\pi\Delta nL}{\lambda} \tag{10.1}$$

where $\Delta n$ is the birefringence, $L$ is the thickness of the sample and $\lambda$ is the wavelength of the light. Due to the birefringent nature and non-uniform thickness of the PDLC film the incoming linearly polarized light becomes elliptically polarized. From the optical micrograph the texture of the samples was studied.

Optical micrographs of pure P(VDF-TrFE) film and the PDLC films containing 10 and 60 weight percent of liquid crystals are shown in Fig. 10.6. Compared to PDLC with 10 wt% LCs, the PDLC with 60 wt% LCs contains relatively larger droplets and has a wider distribution of droplet size. The LC droplets are a few micrometers in size. The mean diameter and the morphology of the droplets can be determined from SEM (Scanning electron microscope) micrographs.

## 10.3 Scanning electron microscope images

Scanning electron microscope images of the pure P(VDF-TrFE) film, the PDLC film containing 10 wt% of LC and the PDLC film containing 60 wt% LC on the glass substrate are shown in Fig. 10.7. The SEM images of the PDLC film containing 10 wt% LC reveals that the liquid crystal domains appear as relatively distinct droplets within the polymer matrix. The thickness of the interfacial layer is in the supramicron range whereas, the thickness of the interfacial layer in the PDLC film with 60 wt% LC, is in the range of submicron to a few μm. In the case of the PDLC film containing 60 wt% LC, the LC droplets mostly appear as distinct droplets. In some places the interfacial layer is so thin that the two LC droplets collapse and form interconnected droplets. The films have the oblate spheroidal (disk) droplet morphology. The oblate spheroidal droplets are formed by anisotropic shrinkage (along the direction perpendicular to the film plane) of the film during annealing process [56]. The major axis of the droplet is parallel to the film surface.
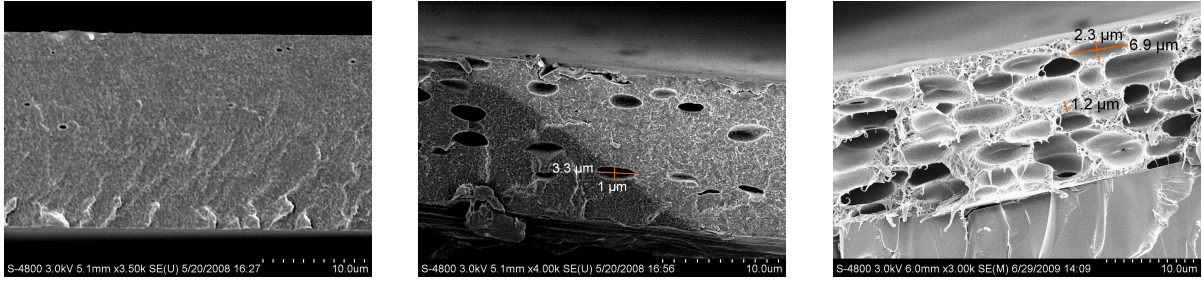
Figure 10.7: *Scanning electron microscopic images of the pure P(VDF-TrFE) film (left), the PDLC films containing 10 wt% (center) and 60 wt% (right) liquid crystal.*

The major and minor radii of the PDLC film containing 10 wt% and 60 wt% LCs are approx., 3 µm and 1 µm, and, 6.9 µm and 2.3 µm, respectively, as shown in Fig. 10.7. The oblate spheroidal droplets favor the orientation of LC molecules along the maximum cross-sectional area (major axis) of the droplet and the optical axis lies in the film plane [43,57].

## 10.4 Dielectric relaxation behavior

### 10.4.1 Liquid crystal

The dielectric measurement of the liquid crystal was done in the presence and in the absence of a bias voltage. A 100 µm thick Teflon spacer was placed between two glass plates coated with a copper electrode. Then the Teflon spacer was filled with the LC. Fig. 10.8 shows the imaginary part of the permittivity $\epsilon''$ versus frequency of the LC in the absence of a bias voltage. Below $0\,°C$ four dispersion regions are seen. As already mentioned in section 10.1.1, the LC used in this work is a mixture of LC and below $10\,°C$ they exist in a crystalline form. Each dispersion region belongs to a different crystalline LC present in the mixture. The loss peaks "a" and "b" appear below $-70\,°C$ whereas the loss peaks "c" and "d" appear above $-70\,°C$. Above $0\,°C$ only one loss peak appears which is related to the angular motions of the dipole moments of the mesogenic molecules with respect to the director ($\boldsymbol{\delta}$ process) [58]. In the absence of an external electric field, the nematic molecules at the interface orient in a specific direction depending mainly on the interfacial energy and the wetting behavior. Because of elastic forces, all the LC molecules tend to orient parallel to each other. As the temperature is increased, the loss peak is shifted to higher frequencies because the rate of molecular motion increases with temperature. At low frequencies, the slope of the loss curve approaches $-1$. Thus, the dielectric loss is given by $\epsilon''(\omega) = \sigma_{dc}/(\omega\epsilon_0)$ where $\sigma_{dc}$ is the DC conductivity of the sample and $\omega = 2\pi f$. It is caused by unipolar charges which can move easily at higher temperatures.
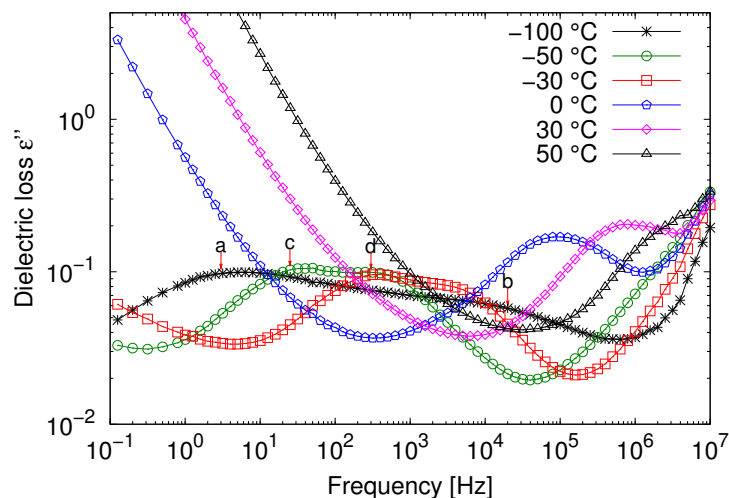
Figure 10.8: *Imaginary part of the permittivity ($\epsilon''$) versus frequency at selected temperatures for the LC in the absence of bias field. The four dispersion regions of the solid form of the LC are denoted by "a", "b", "c" and "d".*
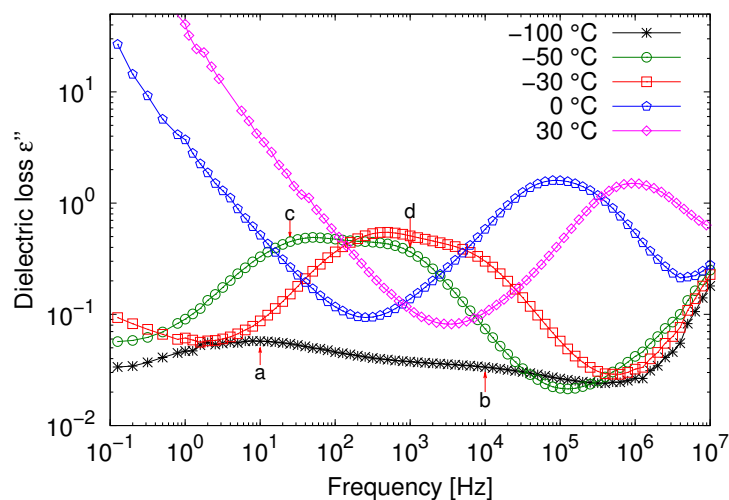


Figure 10.9: *Imaginary part of the permittivity ($\epsilon''$) versus frequency at selected temperatures for the LC in the presence of bias field (0.2 MV/m). The four dispersion regions of the solid form of the LC are denoted by "a", "b", "c" and "d".*

When a bias voltage is applied to the sample the director tends to orient along the electric field. The loss peak due to the $\boldsymbol{\delta}$ relaxation process is increased when a bias field of 0.2 MV/m is applied to the sample as seen in Fig. 10.9. As the temperature is increased

the loss peak is shifted to higher frequencies.

At 10 °C, the maximum loss of the $\boldsymbol{\delta}$ peak shows a pronounced dependence on the external bias field. When a bias voltage is applied to the LC, the director tends to orient along the electric field direction and therefore, the loss peak increases with the bias field and saturates at about 0.24 MV/m (Fig. 10.10). Thus, the fully homeotropic alignment of the LC occurs at 0.24 MV/m. Below −30 °C, no bias field dependence was found (Fig. 10.11). Consequently, the dispersion regions appearing below 10 °C are related to the crystalline phase of the LCs, in which the nematic molecules cannot change their orientation.
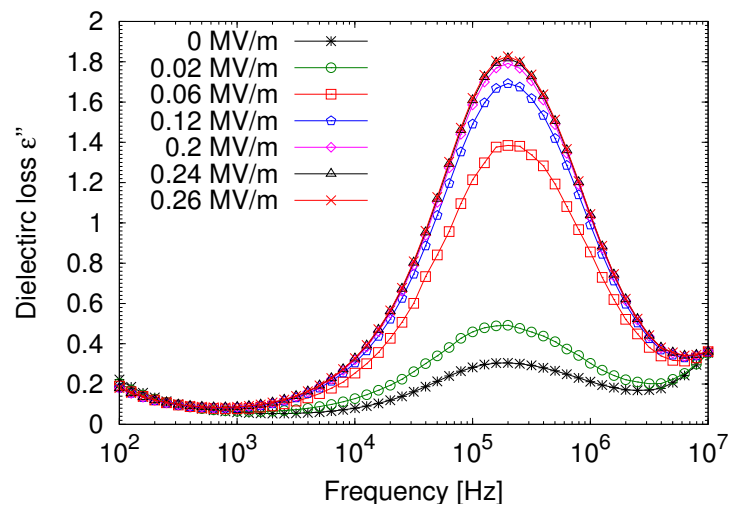


Figure 10.10: *Imaginary part of the permittivity ($\epsilon''$) versus frequency at 10° C for the LC with several bias fields, as indicated.*
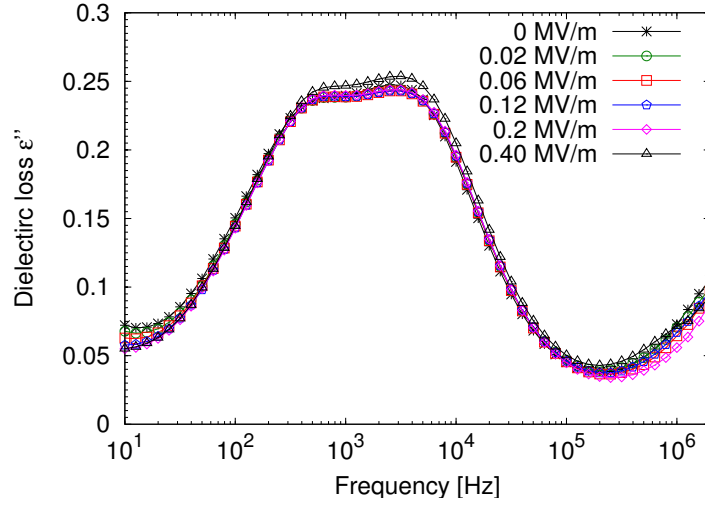
Figure 10.11: *Imaginary part of the permittivity ($\epsilon''$) versus frequency at $-30\,°C$ for the LC with several bias fields, as indicated.*

## 10.4.2    Commercial P(VDF-TrFE)

Two distinctly separated dispersion regions ("a" and "b") are observed in the dielectric spectra of the commercial P(VDF-TrFE) film. Both relaxations are shifted to higher frequencies as the temperature increases (Fig. 10.12). At higher temperatures, the film shows relatively high conductivity which probably comes from the presence of impurities. The conductivity was significantly reduced by annealing at $140\,°C$ for 4 h. After annealing, however, only one relaxation peak is observed in the dielectric spectra (Fig. 10.13).

Figure 10.12: *Imaginary part of the permittivity ($\epsilon''$) versus frequency at selected temperatures for the commercial P(VDF-TrFE) film. The two dispersion regions are denoted by "a" and "b".*

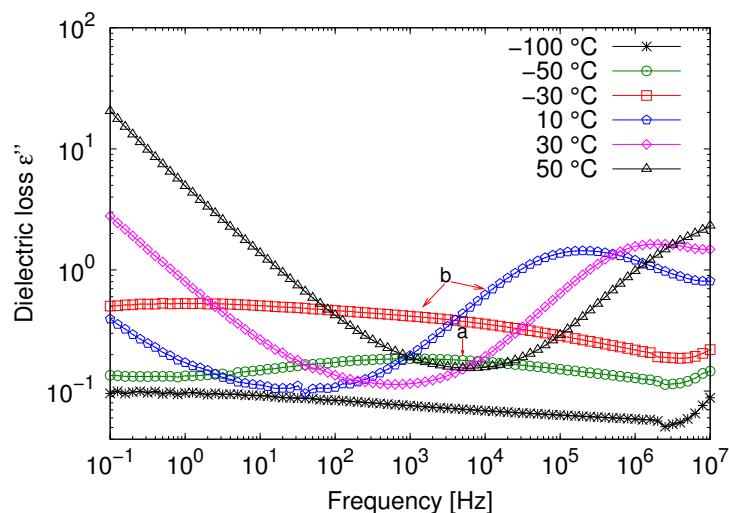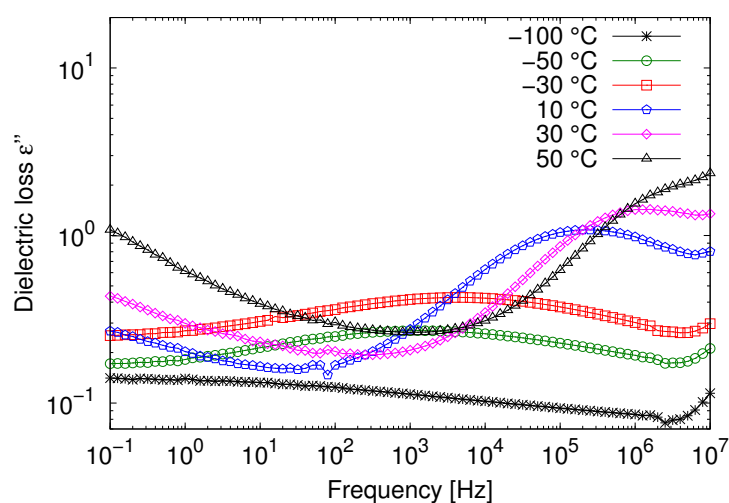

Figure 10.13: *Imaginary part of the permittivity ($\epsilon''$) versus frequency at selected temperatures for the annealed commercial P(VDF-TrFE) film.*

### 10.4.3   Laboratory-prepared P(VDF-TrFE)

In the case of the pure P(VDF-TrFE) film, which was also annealed, only one loss peak is observed in the dielectric spectrum (Fig. 10.14). At higher temperatures this loss peak was
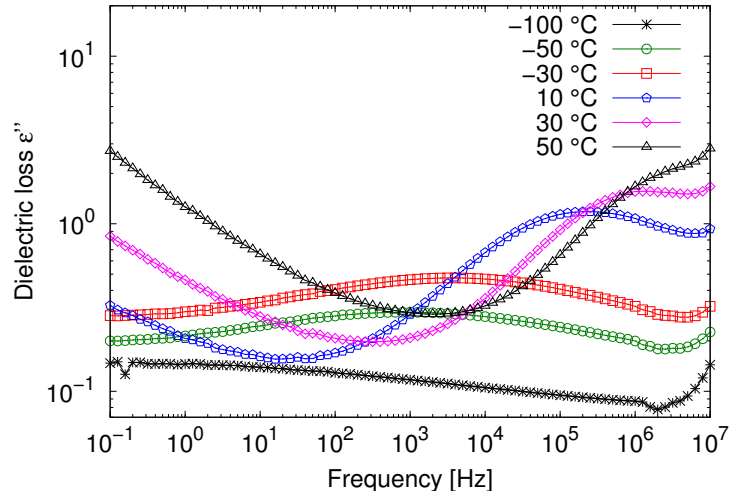
Figure 10.14: *Imaginary part of the permittivity ($\epsilon''$) versus frequency at selected temperatures for the laboratory-prepared P(VDF-TrFE) film.*

shifted to higher frequencies. The dielectric loss behavior of the commerical unannealed and annealed P(VDF-TrFE) films was compared with that of the laboratory prepared P(VDF-TrFE) film.

## 10.4.4  Comparison of commercial and laboratory-prepared P(VDF-TrFE) films

After annealing, the dispersion regions of the commercial and the laboratory-prepared P(VDF-TrFE) films look similar, as shown in Fig. 10.15. As already mentioned, annealing the polymer film above the Curie point $T_\mathrm{C}$ results in an increase in crystallinity which in turn may lead to the merging of the two relaxation processes visible in the non-annealed commercial film. The increase of the peak height with increasing temperature is probably caused by the superposition of the two relaxation processes. The origin of these loss peaks will be discussed later.
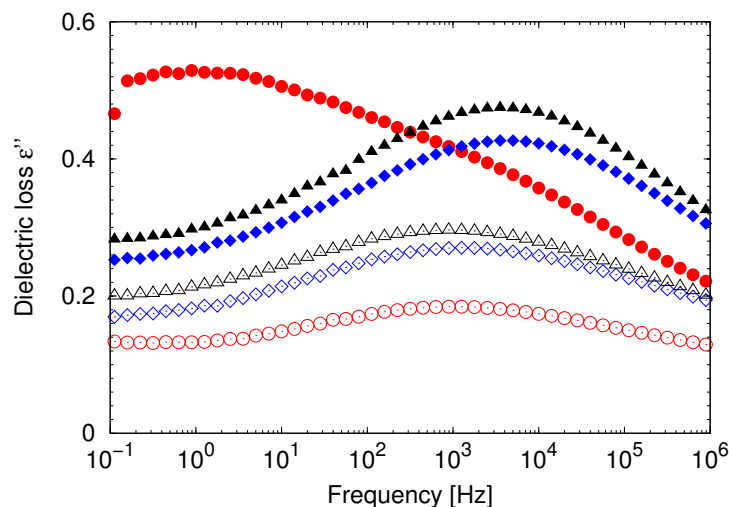
Figure 10.15: *Comparison of the imaginary part of the permittivites of commercial ($\bigcirc$), annealed commercial ($\diamond$) and laboratory-prepared ($\triangle$) P(VDF-TrFE) film at $-50\,^{\circ}C$ (open symbols) and at $-30\,^{\circ}C$ (solid symbols).*

### 10.4.5 PDLC

The relaxation spectra of the PDLC film containing 10 wt% LC show two well-separated loss peaks (Fig. 10.16). One is a low-frequency peak and the other one is a high-frequency peak. As the temperature increases both peaks shift to higher frequencies. The dielectric loss behavior of the PDLC films containing 10, 20, 30 and 60 wt% LCs is compared. There is no considerable difference between the dielectric spectra of the PDLC films containing 10, 20 and 30 wt% of LC, whereas the low-frequency peak of the PDLC film containing 60 wt% LC is shifted to higher temperature, as can be seen in Fig. 10.17. The relaxation spectra of the PDLC film containing 60 wt% LC is shown in Fig. 10.18. Due to the higher LC content, the low-frequency relaxation becomes stronger. For further studies, the PDLC films containing 10 and 60 wt% LC were used.
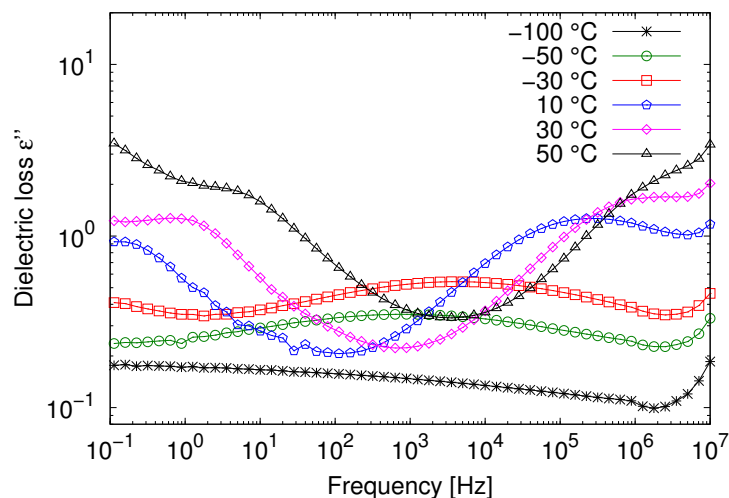
Figure 10.16: *Imaginary part of the permittivity ($\epsilon''$) versus frequency at selected temperatures for the PDLC film (10 wt% LC) in the absence of bias voltage.*
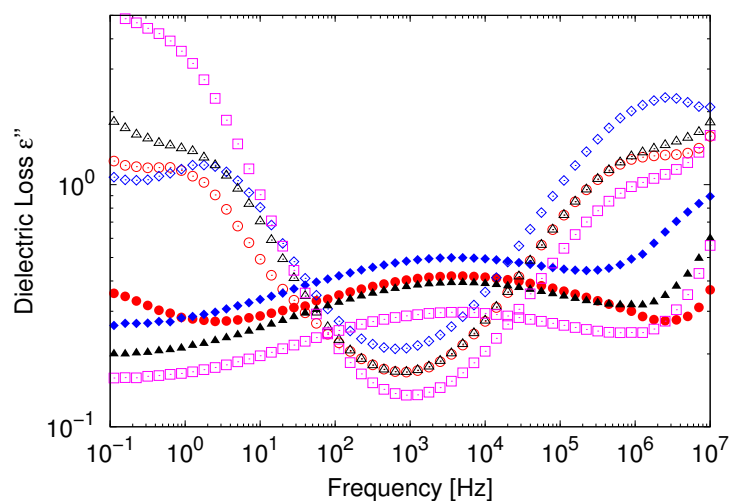


Figure 10.17: *Comparison of the imaginary part of the permittivites of PDLC films containing 10 wt% ($\bigcirc$), 20 wt% ($\diamond$), 30 wt% ($\triangle$) and 60 wt% ($\square$) LCs at $-30\,^{\circ}C$ (solid symbols) and at $30\,^{\circ}C$ (open symbols).*
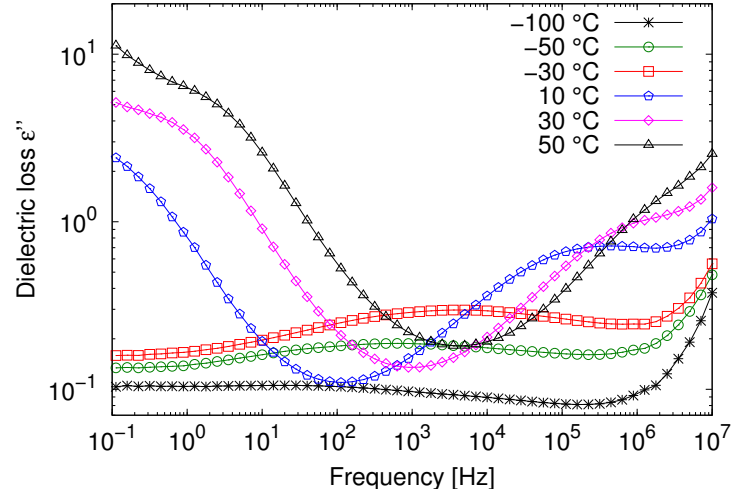
Figure 10.18: *Imaginary part of the permittivity ($\epsilon''$) versus frequency at selected temperatures for the PDLC film (60 wt% LC) in the absence of bias voltage.*

### 10.4.6 Comparison of P(VDF-TrFE) and PDLC film

Hereafter, the laboratory-prepared P(VDF-TrFE) film will be mentioned only as P(VDF-TrFE). Compared to the pure P(VDF-TrFE) film, the PDLC films containing 10 and 60 wt% LC have an additional low-frequency peak. The high frequency loss peak of the PDLC films corresponds to the loss peak of the pure P(VDF-TrFE) film which can be seen in Fig. 10.19. The low frequency dispersion region is due to the dispersed LC in the polymer matrix.
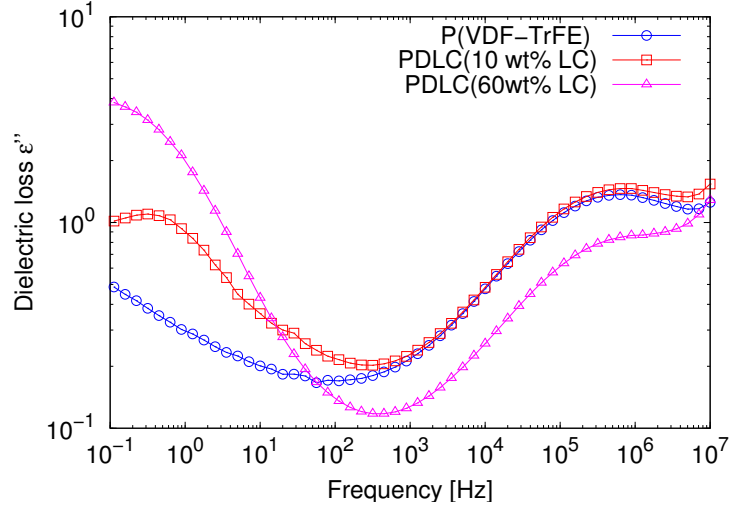
Figure 10.19: *Comparison of the dielectric loss of the pure P(VDF-TrFE) film and of the PDLC film containing 10 and 60 wt% LC at 20°C.*

### 10.4.7   Arrhenius plot

The loss peaks of both the pure P(VDF-TrFE) and the PDLC films are broadened and asymmetric; therefore the Havriliak-Negami (HN) function (eq. 4.14) was used to fit the curves. By fitting the HN function to the loss peak, the relaxation time $\tau_{HN}$ was determined. In most polymers the loss peaks are not symmetrical; therefore, the asymmetric shape parameter $\gamma$ is not equal to one. By using the explicit equation (eq. C.1) proposed by Boersma *et al.* [59], the relaxation time $\tau$ at which the maximum loss occurs can be calculated as (eq. 10.2).

$$\tau = \tau_{HN} \left( \frac{\sin\left(\frac{\pi\gamma\beta}{2(1+\beta)}\right)}{\sin\left(\frac{\pi\beta}{2(1+\gamma)}\right)} \right)^{1/\gamma} \tag{10.2}$$

In the Arrhenius plot (Figure. 10.20), the relaxation time, $\tau$ is plotted against the inverse temperature. Well-separated $\boldsymbol{\alpha}$ and $\boldsymbol{\beta}$ processes can be seen in the Arrhenius plot only for the non-annealed commercial film, whereas only one loss peak could be fitted to the annealed commercial and laboratory-prepared P(VDF-TrFE) films. Thus, in the Arrhenius diagram, a superposition of both processes is seen. The relaxation process observed above the glass-transition temperature exhibits Vogel-Fulcher-Tammann (VFT) behavior and bends towards $T_g$, which is defined as the intercept with the line $\tau = 10^2$ s. It is due to the dynamic glass transition behavior of the P(VDF-TrFE) which was seen in the differential scanning calorimetry measurement (Fig. 10.5). The relaxation process below $T_g$ obeys Arrhenius' law which was already reported by Menegotto *et al.* [54]. This relaxation process is a manifestation of the secondary relaxation process ($\boldsymbol{\beta}$ process). Both the annealed

commercial and the laboratory-prepared P(VDF-TrFE) films behave similarly. The two relaxation processes merge at a temperature above $T_g$ and result in the single loss peak.

The PDLC films containing 10 and 60 wt% LC do not show the typical VFT behavior, but behave very similarly to the annealed P(VDF-TrFE) films. Their low-frequency dispersion appears in the same temperature range as the $\boldsymbol{\delta}$ relaxation of the LC, and both follow the Arrhenius law. This gives rise to the conclusion that both peaks are related and that the low-frequency peak is caused by the movement of the LC molecules in the PDLC. Since the movement of the LC molecules in the polymer matrix is hindered by the polymer molecules [60], the low-frequency peak of the PDLC film containing 10 wt% LC appears at much lower frequencies and needs a higher activation energy, as shown in Tab. 10.1. The PDLC film containing 60 wt% LC contains relatively bigger and more droplets than the PDLC film with 10 wt% LC (Fig. 10.7). Because of the higher number of LC molecules at the interfaces, the low-frequency peak of the PDLC film with 60 wt% LC is shifted to lower frequencies. The LC molecules in the center of the droplet behave as in the bulk state, therefore the low-frequency relaxation process needs an activation energy close to the activation energy of the $\boldsymbol{\delta}$ relaxation of the LC, as can be seen in Tab. 10.1.
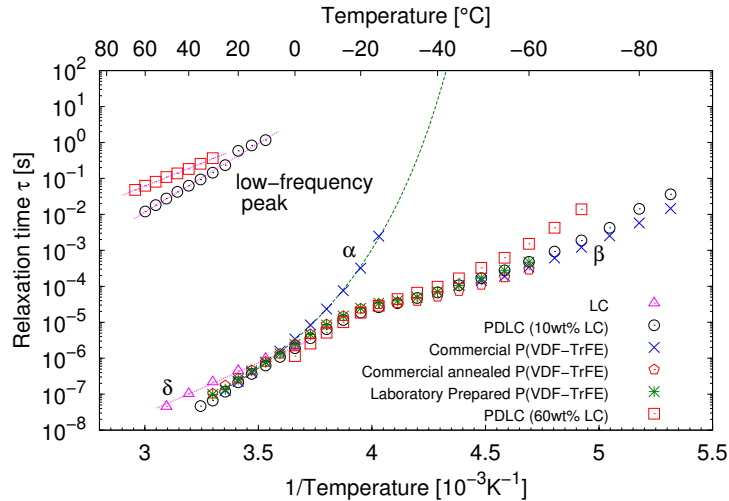


Figure 10.20: *Arrhenius plot for the commercial, annealed commercial, and laboratory-prepared P(VDF-TrFE) films, the LC and the PDLC films containing 10 and 60 wt% LC. The dashed and dotted lines correspond to VFT and Arrhenius fits, respectively.*

| Samples | $T_{\mathbf{A}}$, K | $T_0$, K | $E_{\mathbf{A}}$, eV |
|---|---|---|---|
| LC | - | - | 0.56 |
| PDLC (10 wt% LC) - $\boldsymbol{\beta}$ | - | - | 0.48 |
| PDLC (10 wt% LC) - $\boldsymbol{\alpha}$ | - | - | 0.72 |
| PDLC (10 wt% LC) - LF | - | - | 0.76 |
| PDLC (60 wt% LC) - LF | - | - | 0.50 |
| Commercial P(VDF-TrFE) - $\boldsymbol{\beta}$ | - | - | 0.39 |
| Commercial P(VDF-TrFE) - $\boldsymbol{\alpha}$ | 873.7 | 201.4 | - |

Table 10.1: *Fit parameters for the $\boldsymbol{\alpha}$ (obeys VFT behavior) and the $\boldsymbol{\beta}$ relaxation processes (obeys Arrhenius behavior). The abbrevation "LF" means low-frequency peak.*

### 10.4.8 Influence of bias field on the PDLC film

To determine the electric field required for the homeotropic alignment of LC in a PDLC film, PDLC films containing 10 and 60 wt% LC were subjected to a bias field of 2.4 and 1.6 MV/m, respectively. When these bias fields were applied to the PDLC film containing 10 wt% LC at 20 °C and the PDLC film with 60 wt% LC at 40 °C, no significant change in the dielectric loss was observed. Therefore, a high-voltage dielectric spectrometer was used to study the influence of the bias field on the PDLC film. For the PDLC film with 10 wt% LC, the bias field was varied from 0 to 27 MV/m at an AC amplitude of 1.4 MV/m at 10 °C (Fig. 10.21) whereas for the PDLC film containing 60 wt% LC, the bias field was varied from 0 to 18 MV/m at an AC amplitude of 1 MV/m at 40 °C(Fig. 10.22). The low-frequency relaxation peak is shifted to lower frequences, as the bias field is increased (Fig. 10.21). When a bias field is applied to the PDLC film the director tends to orient towards the field direction, thereby the movement of LC molecules is hindered, i.e. the relaxation process slows down.
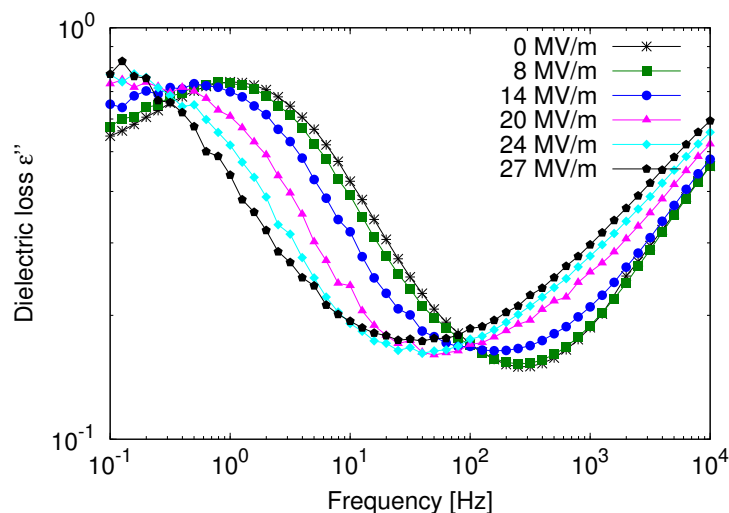
Figure 10.21: *Imaginary part of the permittivity($\epsilon''$) versus frequency at $10°C$ for the PDLC film containing 10 wt% LC with several bias fields as indicated.*
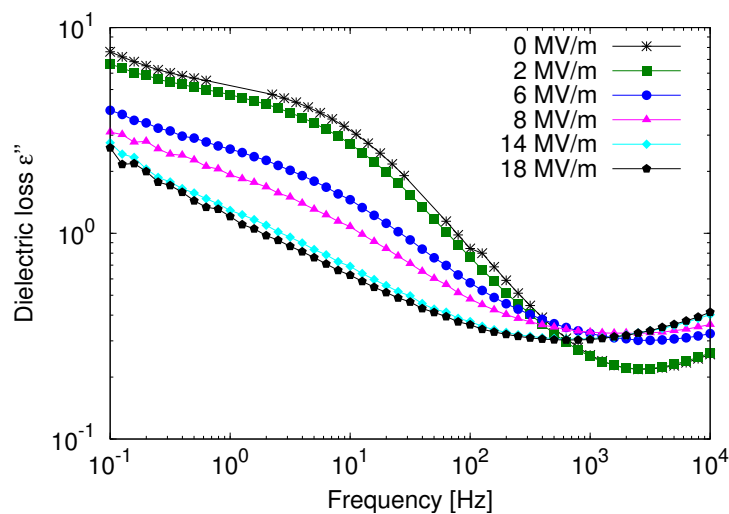


Figure 10.22: *Imaginary part of the permittivity($\epsilon''$) versus frequency at $40°C$ for the PDLC film containing 60 wt% LC with several bias fields as indicated.*

## 10.5 Fourier-transform infrared-spectroscopy

Fig. 10.23(a) presents the Fourier-transformed infrared spectrum of the pure P(VDF-TrFE) film. The bands at 840 cm$^{-1}$ and 510 cm$^{-1}$ are characteristic of the long all-trans (T) sequences and the trans sequences longer than three units, respectively [61]. The FTIR

spectrum of the LC is shown in Fig. 10.23(b). The strong band at 2915 cm$^{-1}$ may correspond to the carboxyl group of the LC. Since the composition of the LCs is unknown, the origin and the vibrational mode of the transmittance peak cannot be determined. Therefore the FTIR spectrum of the LC can be used only as a reference. The FTIR spectra of the PDLC film containing 10 and 60 wt% LCs are compared with the FTIR spectra of the pure LC and the pure P(VDF-TrFE) film. With the decrease in the P(VDF-TrFE) content the characteristic peak intensities of the trans sequences (Fig. 10.23(c)) are reduced, whereas the band intensity of the carboxyl group of the LC are increased with the increase in LC content (Fig. 10.23(d)). From the peak intensities, the phase composition cannot be estimated directly but it is confirmed that the PDLC film containing 60 wt% LC contains a higher amount of LC than the PDLC film with 10 wt% of LC.



Figure 10.23: *(a) FTIR spectrum of pure P(VDF-TrFE) film. (b) FTIR spectrum of the LC. (c) and (d) Comparison of FTIR spectra of the pure P(VDF-TrFE), the PDLC films containing 10 and 60 wt% LCs and the LC.*
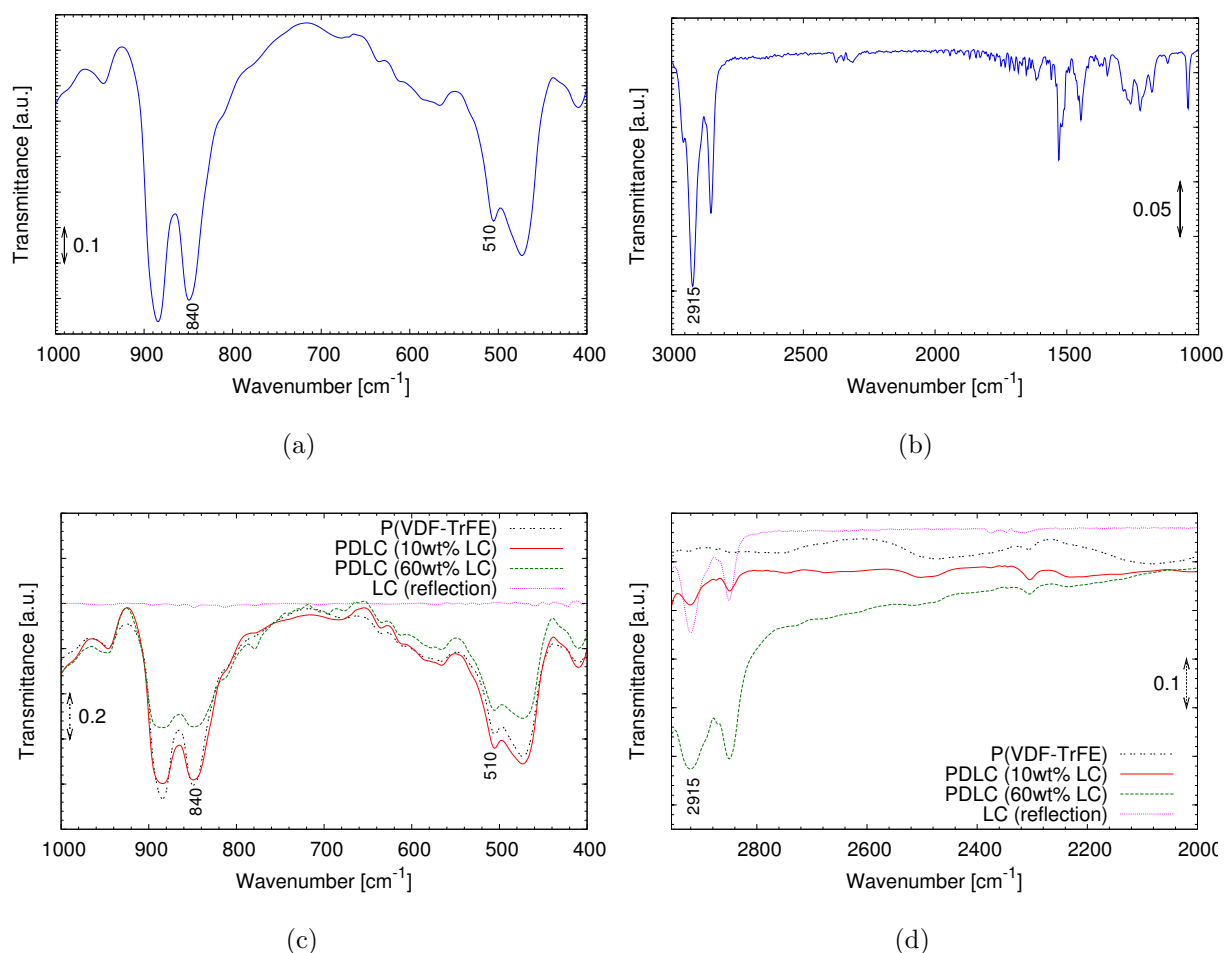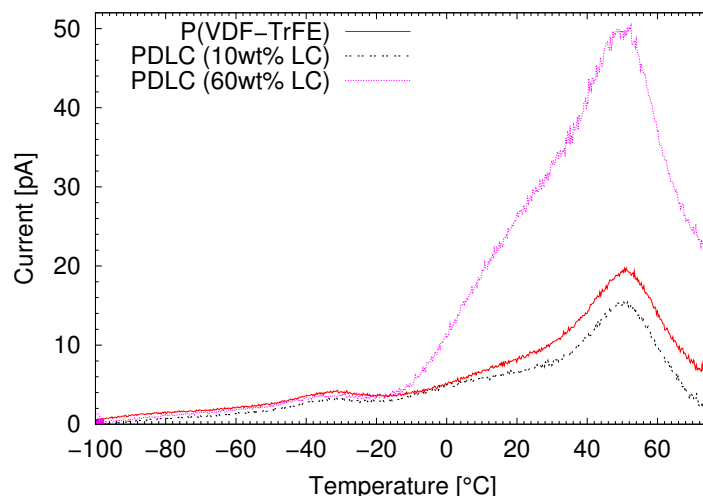
Figure 10.24: *TSC spectra of pure P(VDF-TrFE) film and the PDLC film containing 10 and 60 wt% LCs polarized at 0.5 MV/m.*

## 10.6    Thermally stimulated current behavior

Fig. 10.24 represents the thermally-stimulated-current (TSC) spectra of the pure P(VDF-TrFE) film and the PDLC film containing 10 and 60 wt% LCs. The peak at $-33\,°$C corresponds to the glass transition of P(VDF-TrFE). The step at $10\,°$C arises from the solid-crystalline to nematic transition of the LC and it is seen only in the PDLC films. When the liquid-crystal content is introduced and increased up to 60 wt%, there is no shift in the glass transition peak. This implies that the LC molecules are not dissolved in the polymer matrix but segregated to form a droplet morphology. The result is in good agreement with the DSC result. When an electric field is applied, space charges are created around the heterogenous structures of the P(VDF-TrFE) and on the boundaries between the LC and the polymer matrix (Maxwell-Wagner effect). Rollik *et al.* explained that the depolarization of Maxwell-Wagner interface polarization arises from the mutual recombination of the trapped charges at the amorphous-crystalline interfaces in the polymer or the trapped charges move towards the electrodes and their neutralization in the vicinity of the electrodes [62]. The current resulting from the movement of space charges is seen at $50\,°$C. With the increase in the LC content both the space charge peak intensity and the intensity of the solid crystalline to nematic transition increase. The PDLC film with 60 wt% LCs has more and relatively bigger droplets than the PDLC film with 10 wt% LCs. This results in an increase in the interfacial area which in turn leads to an increase in the number of space charge carriers.

When the PDLC film containing 60 wt% LC is polarized at or below $0\,°$C, only the glass transition peak and the Maxwell-Wagner peak are seen in Fig. 10.25. The solid-crystalline to nematic transition peak is not seen in the global TSC curve. During polarization the

LC molecules are not oriented, therefore they are not contributing to the depolarization current. The position of the space charge peak depends on the polarization temperature, as can be seen in Fig. 10.25.
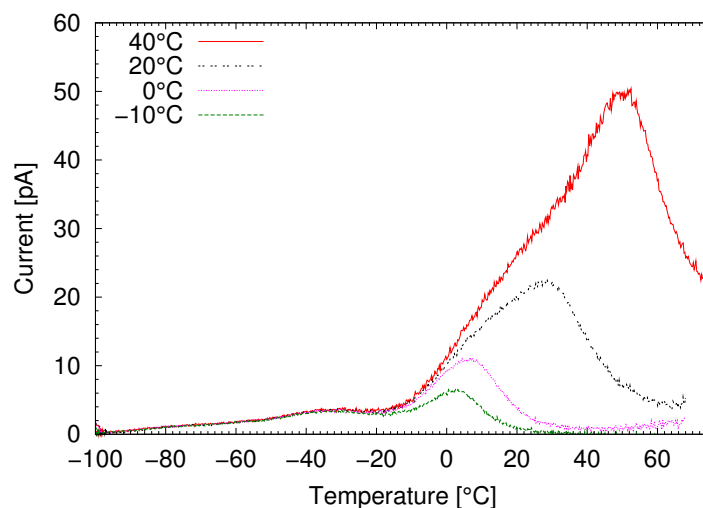


Figure 10.25: *TSC spectra of the PDLC film containing 60 wt% LCs polarized at 0.5 MV/m and at various polarization temperatures.*

The PDLC film containing 60 wt% LC was treated at various polarization voltages and their resultant TSC spectra are shown in Fig. 10.26. The intensities of the glass transition, solid-crystalline to nematic transition and the space charge peak are increased with the polarization voltage. The intensity of the glass transition increases linearly (slope is $0.91 \pm 0.04$) with the polarization voltage, whereas the intensity of the space charge increases non-linearly (slope is $1.24 \pm 0.08$), as shown in Fig. 10.27, as is expected for space charge peak [63].
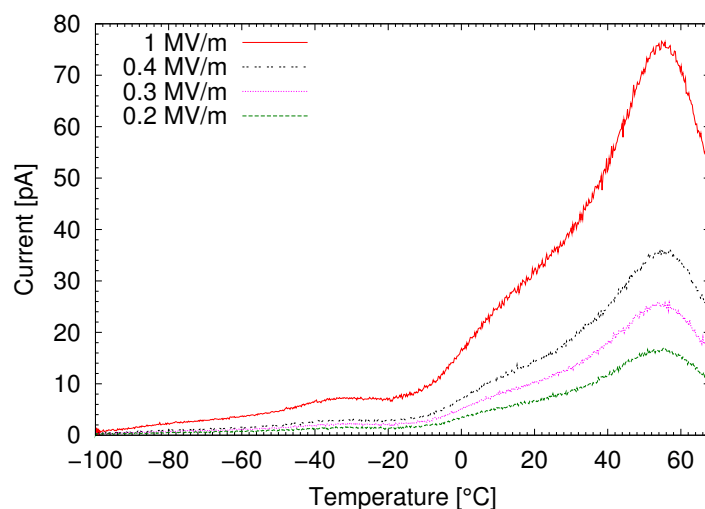
Figure 10.26: *TSC spectra of the PDLC film containing 60 wt% LCs polarized at 40°C at various electric fields.*
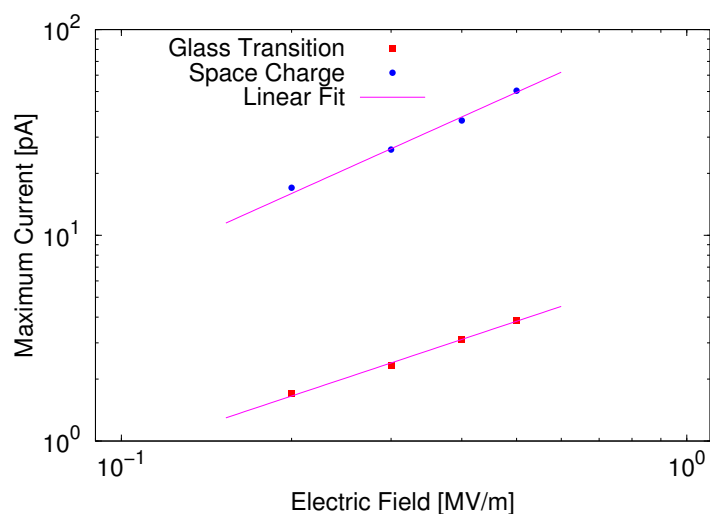


Figure 10.27: *TSC peak intensities versus polarization voltage for the PDLC film with 60 wt% LC.*

## 10.7 Electrical hysteresis behavior

The hysteresis between the electric displacement and the electric field of both pure P(VDF-TrFE) and the PDLC films was measured at room temperature. At high electric field the polarization saturated. The intersection of the loop with the abscissa defines the coercive

field. The coercive field is the field required to reduce the polarization to zero. The intersection of the loop with the ordinate gives the remanent polarization of the samples.

For both P(VDF-TrFE) film and the PDLC film containing 10 wt% LC, a unipolar/bipolar electric field having an amplitude of 70 MV/m and a frequency of 3 mHz was applied for the hysteresis measurement. The coercive field of the P(VDF-TrFE) and the PDLC film with 10 wt% LC is found to be 42 MV/m and 40 MV/m, respectively, as shown in Fig. 10.28. The remanent polarization of the P(VDF-TrFE) and the PDLC film containing 10 wt% LC is 58 mC/m$^2$ and 50 mC/m$^2$, respectively. When the liquid crystal is introduced to the polymer matrix, or in other terms when the ferroelectric polymer matrix content was decreased, the remanent polarization of the PDLC film is decreased, as expected. Koda *et al.* [20] observed a very similar behavior in the system where an antiferroelectric LC was dispersed in a P(VDF-TrFE) matrix.

A unipolar/bipolar electric field having an amplitude of 32 MV/m and a frequency of 3 mHz was applied to the PDLC film containing 60 wt% LCs. As already mentioned in section 10.6, the PDLC film with 60 wt% LC contains a higher amount of space charges. The polymer matrix appears only in the interfaces whose thickness varies between submicron to few µm ($1 - 2$ µm), as shown in Fig. 10.7. The dielectric constant of the polymer in the interface region is lower than the bulk copolymer [64]. The movement of ions in the PDLC film can set up depolarization fields acting in the opposite direction of the applied field [43]. The charge build-up at the polymer/LC interface may result in the increase of the polarization field across the polymer matrix and the coercive field dependency on the thickness of the film ($\sim d^{-2/3}$) [65] results in the decrease of the coercive field of the PDLC film. The coercive field of the PDLC film dropped to 20 MV/m and the remanent polarization decreased to 8 mC/m$^2$. At higher electric field, the conductivity increases and the film starts to behave like a paraelectric material.

## 10.8   Electro-optic behavior of PDLC

The pure P(VDF-TrFE) film is more transparent than the PDLC film. Due to the mismatch in the refractive indices of the liquid crystal and the matrix material, the PDLC composite materials scattered light ("OFF" state) and thus the film is opaque/less transparent. When an electric field is applied, the director of the liquid crystal aligns along the electric field. If the perpendicular refractive index of the liquid crystal matches the refractive index of the polymer matrix material, the PDLC film becomes transparent ("ON" state), as shown in Fig. 1.3.

For the electro-optic measurement, thin (semi-transparent) gold electrodes were evaporated on both sides of the free standing PDLC film. The transmittance of the gold electrode at 785 nm is 63%. Therefore the observed photodiode current was only in µA range. To increase the photodiode currents to be in the range of mA, the gold electrodes
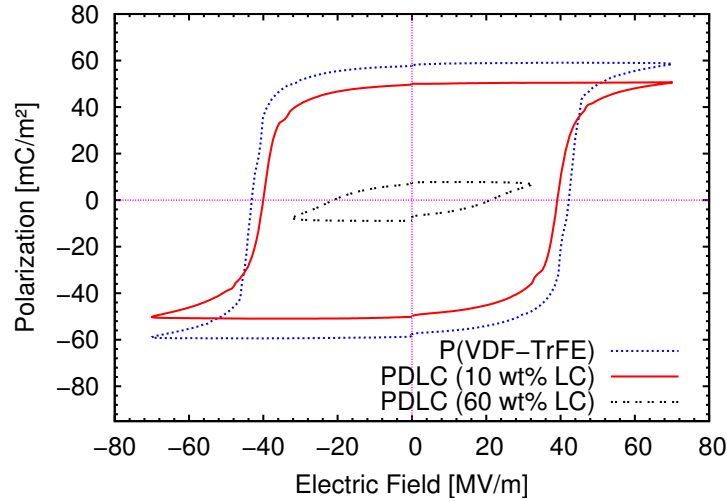
Figure 10.28: *Room-temperature P-E hysteresis curves of the pure P(VDF-TrFE) and the PDLC film containing 10 wt% and 60 wt% of LCs.*

were replaced by ITO electrodes. In this case, the sample is not a free standing film. The solution was drop cast on an ITO coated glass substrate. The PDLC film containing 20 wt% LC was prepared. Using a UV-curable adhesive, another ITO coated glass substrate was adhered to the polymer film. The sample is shown in Fig. B.1 (see Appendix B). A unipolar/bipolar electric-field was applied to the sample, and the field-dependent optical transmission of the sample is shown in Fig. 10.29. As expected, the magnitude of the observed photodiode current was in the range of mA. The electric field applied to the PDLC film, $E_P$ was different from the electric field applied to the adhesive layer, $E_{Ad}$. Since the dielectric constant of the adhesive layer ($\epsilon_A = 4$) is less than that of the composite layer ($\epsilon_P \approx 10$) the electric field applied to the adhesive layer is higher than that of the field applied to the PDLC layer i.e. $E_{Ad} \approx 2.5\ E_P$. The dielectric breakdown strength of the adhesive is 32.3 MV/m. Before poling the PDLC layer, the adhesive layer undergoes a break down. Therefore the sample was modified. The solution was drop casted on an ITO coated glass substrate. Instead of using a second ITO coated glass plate on top of the film, 15 nm gold was evaporated onto the PDLC film.

A unipolar/bipolar electric field having an amplitude of 70 MV/m and a frequency of 3 mHz was applied to the PDLC film containing 10 wt% of LC. The field-dependent optical transmission measurement is shown in Fig. 10.30. The dotted line indicates the first unipolar cycle and the solid line indicates the second unipolar cycle. A small trough is seen only in the first unipolar cycle; it appears at approx. 42 MV/m which is the coercive field of P(VDF-TrFE). This trough most likely arises from the switching of the matrix crystalline domains, as shown by a similar electro-optical transmission measurement of a pure P(VDF-TrFE) film (Fig. 10.31). A similar kind of behavior is observed when the
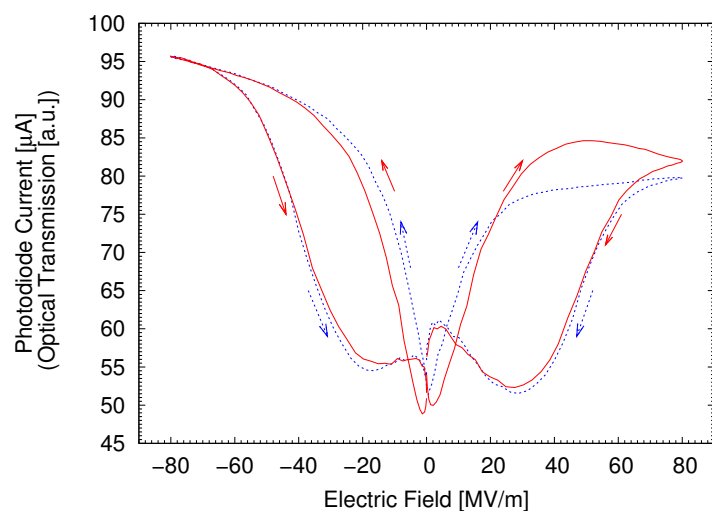
Figure 10.29: *The field dependent optical transmission of PDLC film containing 20 wt%*
*LC sandwiched between the two ITO-coated glass substrates. The dotted line and the solid*
*line represent the first and the second unipolar cycle, respectively.*

electric field is reversed.



Figure 10.30: *Field-dependent optical transmission of PDLC film containing 10 wt% liquid*
*crystals. The dotted line and the solid line represent the first and the second unipolar cycle,*
*respectively.*

67

Figure 10.31: *Field-dependent optical transmission of pure P(VDF-TrFE) film. The dotted line and the solid line represent the first and the second unipolar cycle, respectively.*

A unipolar/bipolar electric field having an amplitude of 26 MV/m and a frequency of 3 mHz was applied to the PDLC film containing 60 wt% of LC. The field-dependent optical transmission measurement is shown in Fig. 10.32.
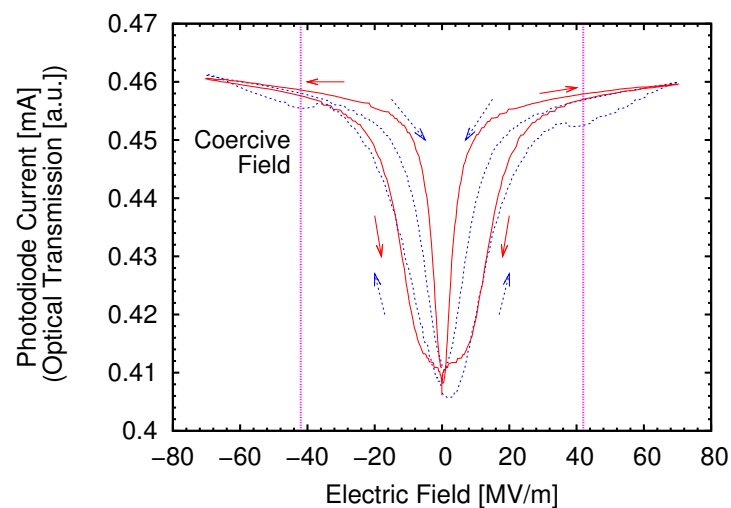


Figure 10.32: *Field-dependent optical transmission of PDLC film containing 60 wt% liquid crystals. The dotted line and the solid line represent the first and the second unipolar cycle, respectively.*
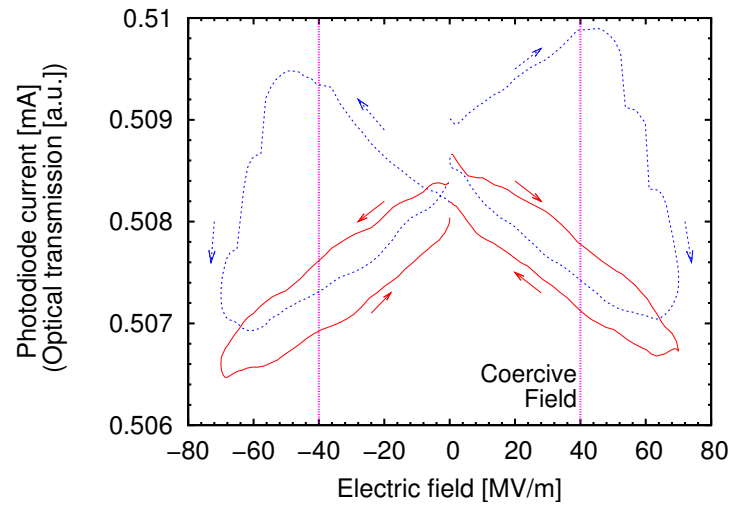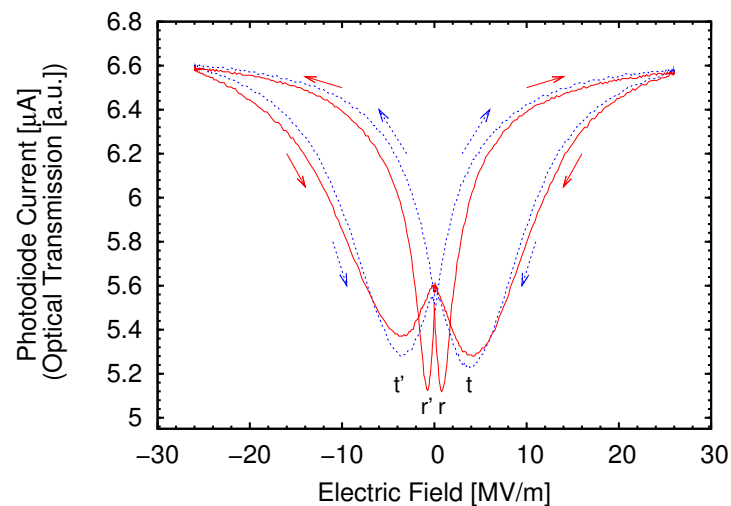
The photodiode output current $I_{pd}$ is a function of the internal electric field $\overline{E}_{int}$.

$$I_{pd} = f(\overline{E}_{int}). \tag{10.3}$$

$f(\overline{E}_{int})$ can be defined as [66]

$$f(\overline{E}_{int}) = f(\overline{E}_{ext} + \overline{E}_{P}). \tag{10.4}$$

where $\overline{E}_{ext}$ is the external electric field and $\overline{E}_{P}$ is the electric field induced by the polarization and the space charges in the film. The field-dependent optical transmission was measured while poling the sample. At $\overline{E}_{ext} = \overline{E}_{t}$, the internal electric field becomes zero. Therefore,

$$\overline{E}_{P} = -\overline{E}_{ext}. \tag{10.5}$$

Here, the field induced by the polarization and charges is in the opposite direction of the polarization of the matrix polymer which might have arised from the non-uniform spontaneous polarization in the PDLC film. The non-uniform spontaneous polarization of the PDLC film is due to the inhomogeneous permittivity of the PDLC film. When the internal electric field drops to zero, the photodiode current reaches the minimum value/trough (t). When an electric field of the same polarity is increased, the trough (r) is shifted to lower field. A similar kind of behavior is observed when the electric field is reversed (t' and r'). Compared to the PDLC film with 10 wt% LC, the PDLC film with 60 wt% LC has a lot more space charges, therefore the effect is well-pronounced in the PDLC film with 60 wt% LC.

The extraordinary $n_e$ (or parallel) and ordinary $n_o$ (or perpendicular) refractive indices of the liquid crystal are 1.5488 and 1.4758, respectively. The refractive index of the polymer matrix $n_P$ is 1.42. While applying an electric-field, the nematic directors tend to align parallel to the electric-field. If the perpendicular refractive index of the liquid crystal matches the refractive index of the polymer matrix i.e. when $n_o \approx n_P$, the PDLC film becomes transparent. In this work, $n_P < n_o$ which limits the increase in transmission. For the PDLC systems where $n_P/n_o < 1$ and the polarization of light is perpendicular to the plane of incidence, Wu *et al.* found that the maximum transmission occurs at normal incidence [48], which is the geometry used in the present experiments. At 70 MV/m, the transmission of the PDLC film with 10 wt% increased by approx. 14%. With a relatively low electric field (26 MV/m) the transmission of the PDLC film containing 60 wt% LC increased by approx. 20%. While this increase is less than that of non-ferroelectric PDLCs, it is still substantially larger than the 0.7% transmission increase observed in the pure P(VDF-TrFE) film, thus corroborating the switching of the LC phase.

As shown in Fig. 10.33, the oblate spheroidal droplets favor the orientation of LC molecules along the major axis of the droplet, as the LC director is "anchored" to the
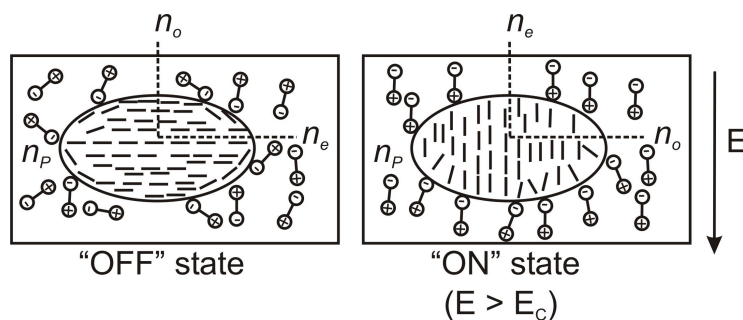
Figure 10.33: *Illustration of an alignment of nematic molecules inside a droplet in the absence and the presence of an electric field, where $n_e$ and $n_o$ are the refractive indices of the LC molecules parallel and perpendicular to the direction of molecular alignment. $n_P$ is the refractive index of the polymer matrix. In the "ON" state the electric field applied is higher than the coercive field, $E_C$ of the polymer matrix.*

interfacial surface [60]. When an electric-field is applied, the electric-field has to overcome this preferred orientation. Compared to the PDLC film containing spherical droplets, the PDLC film containing oblate spheroidal droplets needs a higher voltage to switch the LC molecules. The polymer matrix used in this work is a ferroelectric polymer which contains dipoles. The movement of the LC molecules at the interface is hindered by the polymer-matrix dipoles, which is also seen in the dielectric relaxation spectroscopy measurements [60]. Therefore, the LC molecules at the interface need higher activation energy which means higher voltage, for switching. Due to the interfacial effect, the fully homeotropic alignment of the LC molecules inside the droplet is difficult in the "ON" state [67]. The polymer boundary separating the LC droplets in the PDLC film containing 10 wt% LCs is in the order of supramicron which generates a refractive index gradient between the two neighbouring droplets. This could be another reason (in addition to the poor refractive index matching) for the relatively low percentage of increase in transmission. The PDLC film with 60 wt% LCs has a high droplet density which allows the electric field scattered from one droplet to be scattered by another droplet. The light transmission is dominated by the refractive index difference between neighboring droplets rather than the refractive index mismatch between the LC and the polymer matrix. The possible electrostatic interaction between the hydrogen atoms of the LC molecules and the fluorine atoms of the polymer matrix [68] might be the reason for the low percentage of increase in transmission. Here, $kR_d \gg 1$ ($\lambda \approx 680$ nm and $R_d \sim 2$ µm) and the refractive index of the LC is greater than the refractive index of the polymer matrix i.e. $(n_{LC}/n_P) \gg 1$), therefore Anomalous diffraction (AD) scattering theory can be used to describe the scattering property of the PDLC film.

The PDLC film containing 10 wt% LC shows a hysteresis effect. The transmittance measured with decreasing voltage is higher than the transmittance measured with increasing voltage. With increasing the field, the LC molecules at the interface lag the orientation

of the LC molecules at the center of the droplet. The elastic-free energy of the oblate spheroid microdroplets in the aligned state provides the restoring force to allow the LC molecules to relax to its OFF state rapidly [47]. The PDLC film containing 60 wt% LC does not show hysteresis effect. Neither of them show the memory effect [6,13,69], as once the electric field has been switched off the transmittance goes back to the initial value, as shown in Fig. 10.34 and 10.35.
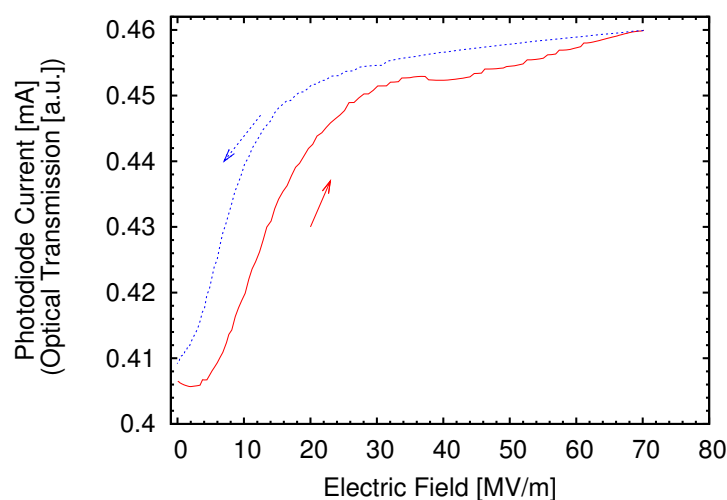


Figure 10.34: *Transmission properties of the PDLC film containing 10 wt% liquid crystals as a function of applied voltage.*
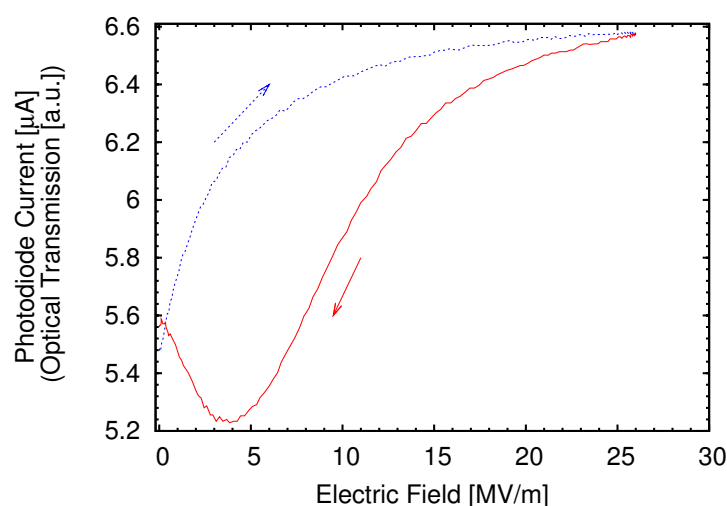


Figure 10.35: *Transmission properties of the PDLC film containing 60 wt% liquid crystals as a function of applied voltage.*

71

## 10.9 Piezo-optical behavior

The PDLC films clearly show a change in the transmittance as the dynamic force changes. The electric-field generated in the sample by the application of mechanical stress, can be calculated as

$$E = \frac{d_{33}F_{\text{dyn}}}{Cd} \tag{10.6}$$

where $d_{33}$ is the piezoelectric coefficient, $F_{\text{dyn}}$ is the dynamic force applied on the sample, $C$ is the capacitance of the sample and $d$ is the thickness of the sample. The piezo-electric coefficient of the copolymer of vinylidene fluoride and trifluoroethylene depends on the trifluoroethylene content and the sample's preparation conditions. The piezoelectric coefficient $d_{33}$ of a single crystalline film of P(VDF-TrFE) (75/25) was found to be $-38$ pC/N [70], whereas Neese *et al.* measured $-33.5$ pm/V for the copolymer containing 25% trifluoroethylene [71]. For P(VDF-TrFE) containing 80/20 molar composition Or *et al.* and Tang *et al.* determined $d_{33} = 20$ pC/N [72, 73]. The piezoelectric coefficients $d_{33}$ of pure P(VDF-TrFE) and the PDLC film containing 10 wt% LC are determined dynamically (using a technique described elsewhere [74]), and the values are 3.8 pC/N and 2.1 pC/N, respectively. The capacitances of the pure polymer matrix and the composite film at 25 °C and 1 Hz were found to be 521 pF and 549 pF, respectively. The thickness of the samples is approximately 20 µm. The dynamic force applied to the sample is around 7 N. Using the eq. 10.6, the electric-field generated in the pure P(VDF-TrFE) film is calculated as 2.5 kV/m, whereas the electric field generated in the PDLC film containing 10 wt% LC is calculated as 1.3 kV/m. As mentioned earlier the PDLC film containing oblate spheroidal droplets needs a higher electric-field to switch the LC molecules in the droplet, therefore only an increase of few percent in transmission is expected.

The sample is loaded with a force

$$F(t) = F_{\text{stat}} + F_{\text{dyn}}\sin(2\pi f_0 t), \tag{10.7}$$

where $F_{\text{stat}}$ is a static force of $5 - 7$ N and $F_{\text{dyn}}$ is the dynamic force amplitude (up to 7 N). Both $F(t)$ and the transmitted light intensity are measured in the time domain. In order to isolate transmission changes occurring at the excitation frequency $f_0$, a fast Fourier transformation of the data is done. The increase in transmission, $T_{\text{incr}}$ is then calculated as

$$T_{\text{incr}} = \left| \frac{\text{FFT}(I_t, f_0)}{I_0} \right|, \tag{10.8}$$

where $I_t$ is the transmitted light intensity, $\text{FFT}(I_t, f_0)$ is the Fourier-transformed light intensity at $f_0 = 1$ Hz and $I_0$ is the initial transmitted light intensity (without dynamic force). The increase in transmission is plotted against the dynamic force, as shown in Fig. 10.36. All samples exhibit some increase in optical transmission with increasing dynamic force, but the largest transmission changes were found in the PDLC samples. The modulation

in the transmission of the glass plates without any sample is due to the interference of the transmitted and the refracted light intensities of the glass plates. The modulation in the transmission of the pure P(VDF-TrFE) film comes from both interference and the change in the symmetry refractive index of the polymer film, whereas the piezo-optic response of the PDLC film containing 10 wt% LC arises from a combination of interference, changes in the refractive index of the polymer matrix and the switching of the LC molecules in the droplet. At a given dynamic force amplitude, the change in optical transmission for the 10 wt% PDLC film is approx. 60% higher than for the pure P(VDF-TrFE) material. Even higher transmission changes are possible if the LC concentration is increased. In a PDLC film containing 60 wt% LC, the $d_{33}$ coefficient and the capacitance are 0.88 pC/N and 648 pF, respectively. In this case, according to eq. 10.6, the electric field generated via the piezoelectric effect is only 0.47 kV/m, substantially less than the electric field generated by both pure P(VDF-TrFE) and 10 wt% PDLC films. The PDLC film containing 60 wt% LC contains relatively bigger and more droplets than the PDLC film with 10 wt% LC, reducing the refractive index gradient between the two neighbouring droplets which resulted in a 2% increase in transmission of the piezo-optical measurement.
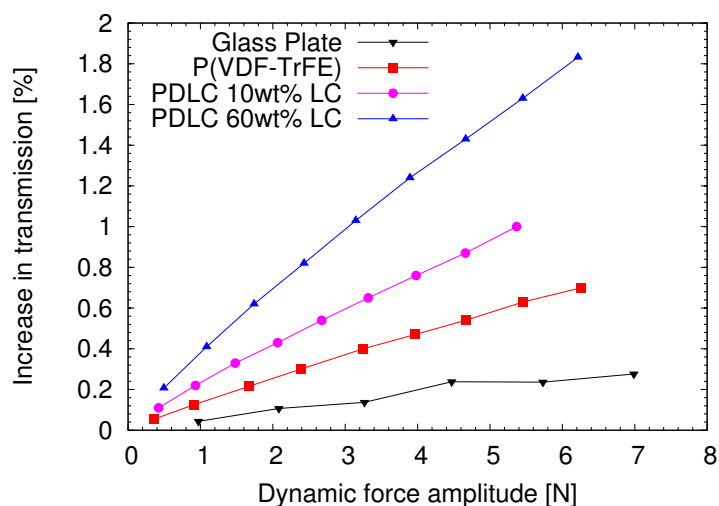


Figure 10.36: *Transmission change vs. dynamic force amplitude for a single glass plate, pure P(VDF-TrFE), and PDLC films containing 10 and 60 wt% LC.*

# Chapter 11

# PDLC system using PMMA

For the nematic liquid crystal (MDA-03-1767) dispersed in poly(vinylidene fluoride-trifluoroethylene), the refractive index of the polymer matrix is less than the ordinary refractive index of the LC, which prevented the increase in transmission, shown in section 10.8. In order to achieve a higher percentage of change in transmission ($> 20\%$), a polymer having a higher refractive index ($n_P > 1.4758$) is selected as the polymer matrix. Poly(methyl methacrylate) (PMMA) (catalogue number 445746, Aldrich, Germany) is used as the polymer matrix, whose refractive index is 1.489 [75].

## 11.1 Sample preparation

The PDLC film with PMMA is prepared similarly to the PDLC film prepared with P(VDF-TrFE). The composite films were prepared by solvent-induced phase separation (SIPS) from a nematic liquid crystal (MDA-03-1767 from Merck Chemicals, Germany) and PMMA. Both the liquid crystal and the PMMA were dissolved in DMF and toluene (2:1) solvents. The solvent was evaporated at $70\,°C$ for 150 min and the film was annealed at $120\,°C$ for 4 h. A PDLC film containing 60 wt% LC was prepared and for comparison a pure PMMA film was prepared in the same way.

## 11.2 Optical micrograph images

Optical micrographs of the PMMA film and the PDLC film containing 60 weight percent of liquid crystals are shown in Fig. 11.1. The PDLC with 60 wt% LCs contains droplets of a few micrometer in size. Unlike the PDLC film with P(VDF-TrFE), the PDLC film prepared using PMMA contains well-dispersed smaller droplets. The mean diameter and the morphology of the droplets can be found from the SEM (Scanning electron microscope) micrographs.
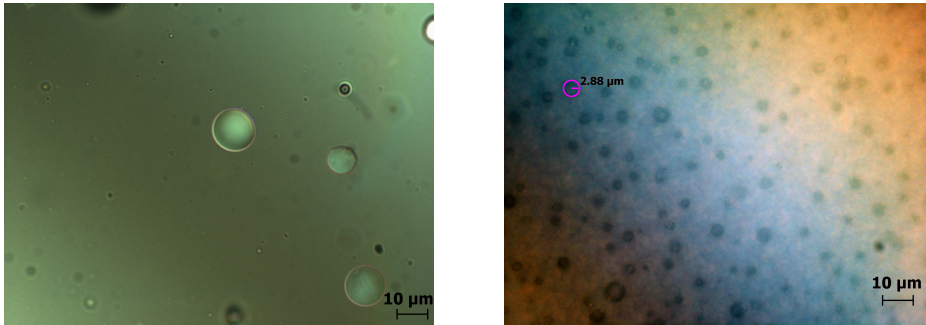
Figure 11.1: *Optical micrograph images of the PMMA film (left) and the PDLC film containing 60 wt% (right) liquid crystal.*

## 11.3    Scanning electron microscope images

A Scanning electron microscopy image of the PMMA film and the PDLC film containing 60 wt% LC is shown in Fig. 11.2. For the PDLC film containing 60 wt% LC, the LC droplets mostly appear as distinct droplets. Like the PDLC films prepared using P(VDF-TrFE), the PDLC films prepared using PMMA have the oblate spheroidal droplet morphology. The major axis of the droplet is parallel to the film surface. The major and minor radii of the PDLC film containing 60 wt% LCs are approx. 5.4 µm and 2.5 µm, respectively, shown in Fig. 11.2. The oblate spheroidal droplets favor the orientation of LC molecules along the major axis of the droplet.
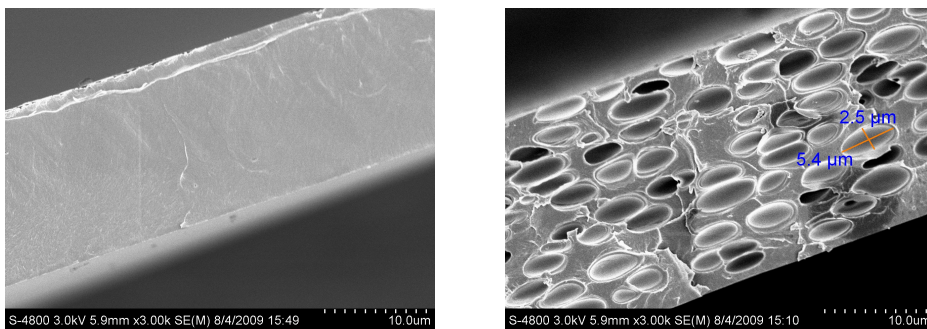


Figure 11.2: *SEM images of the PMMA film (left) and the PDLC film containing 60 wt% (right) liquid crystal.*
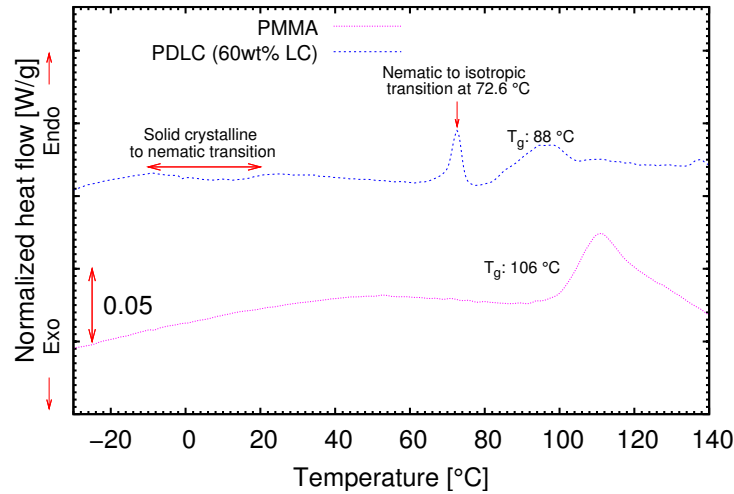
Figure 11.3: *DSC thermogram of the PMMA film and the PDLC film containing 60 wt% LCs during the second heating.*

## 11.4   DSC

Due to the bulky nature of the pendant group and the absence of stereoregularity, poly(methyl methacrylate) is an amorphous polymer [76]. The glass transition of PMMA powder is 122 °C. At about 106 °C a glass transition is observed in the DSC thermogram of the PMMA film. Between $-10$ °C and 20 °C a flat heat flow peak is visible in the DSC thermogram of the PDLC film containing 60 wt% LC (Fig. 11.3) which could be attributed to the solid crystalline to nematic transition of the LC. At 72.6 °C, an endothermic peak is seen in the PDLC film, where the LC undergoes a transition from the anisotropic nematic phase to isotropic liquid phase. In the PDLC film containing 60 wt% LC, the glass transition of the polymer matrix is shifted to lower temperature (88 °C). Both the $T_g$ and the nematic to isotropic transition is lowered by the plasticizing effect of the dissolved LC in the matrix polymer. This has been reported by several authors [43, 77].

## 11.5   Electro-optical behavior

A unipolar/bipolar electric field having an amplitude of 6 MV/m and a frequency of 10 mHz was applied to the PDLC film containing 60 wt% of LC. The field-dependent optical transmission measurement is shown in Fig. 11.4. Compared to the PDLC film prepared using P(VDF-TrFE), the PDLC film fabricated using PMMA is characterized by small threshold fields ($1.5 - 2$ MV/m). The transmission of the PDLC film containing 60 wt% LC increase by approx. 83% with an electric field of 6 MV/m (Fig. 11.4). The electrostatic interaction between the hydrogen atoms of the LC molecules and the fluorine atoms of the polymer matrix (P(VDF-TrFE)) at the polymer/LC interface might be the reason for the

high threshold fields $(4-10$ MV/m) of the PDLC films fabricated using P(VDF-TrFE) and 60 wt% MDA-03-1767. Poly(methyl methacrylate) is a non-polar material which should not have a strong interaction with the LC molecules at the polymer/liquid crystal interface and the refractive index of the polymer matrix is higher than the refractive index of the LC molecules.

The PDLC film does not show either a hysteresis or memory effect, as can be seen in Fig. 11.5. With increasing electric field, the transmission shows a sharper OFF-ON transition. When the electric field starts to decrease, the transmission falls rapidly to the scattering OFF state.
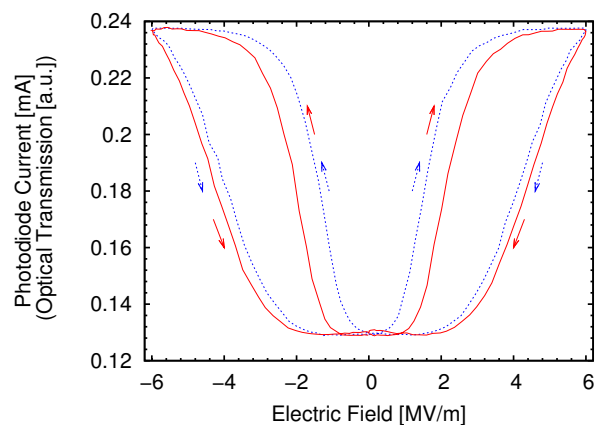


Figure 11.4: *Field-dependent optical transmission of PDLC film containing 60 wt% liquid crystals. The dotted line and the thick line represents the first and the second unipolar cycle, respectively.*
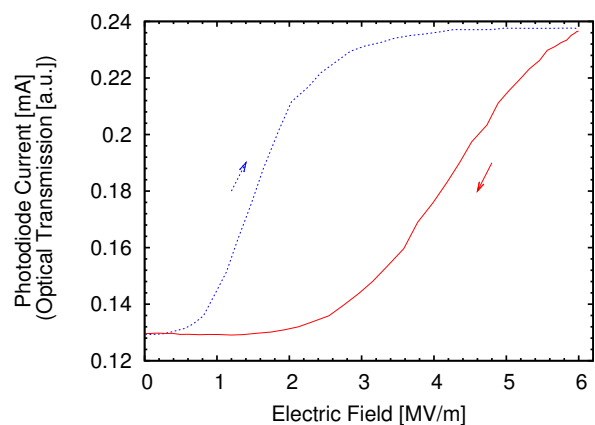


Figure 11.5: *Transmission properties of the PDLC film containing 60 wt% liquid crystals as a function of applied voltage.*

# Chapter 12

# Summary and conclusions

Using a nematic liquid crystal (MDA-03-1767) and a copolymer of vinylidene fluoride and trifluoroethylene, PDLC composite films were prepared by a solvent-induced phase-separation technique. Since the morphology of the PDLC films strongly depends on the preparation conditions, the preparation conditions were optimized to obtain well-dispersed LC droplets within the polymer matrix. The morphology of the PDLC films was determined by means of optical and scanning electron microscopy. The PDLC films have oblate spheroidal droplet morphology.

The thermal behavior of the PDLC film and the influence of LC content on phase transitions of the polymer matrix were studied with DSC. The glass-transition temperature of the PDLC film containing 10 wt% LCs was found to be $-37.1\,^{\circ}$C which is close to the value ($-37.8\,^{\circ}$C) obtained on pure P(VDF-TrFE) film. Consequently, the LC molecules are not dissolved in the polymer matrix, but only dispersed as LC droplets. With the decrease in P(VDF-TrFE) content in the PDLC films, small changes in melting enthalpy and melting temperature of P(VDF-TrFE) were observed. A small change in the melting enthalpy means that the LC acts as a nucleator for the polymer matrix, and the interaction between the LC and the polymer matrix is weak.

The anchoring effect of the LCs was studied by means of dielectric relaxation spectroscopy. To find out the electric field required to orient the LC molecules along the field direction, the electric field across the LC was varied from 0 to 0.4 MV/m at $10\,^{\circ}$C. In the absence of a bias field, the LC molecules are pinned on the substrate, i.e. the molecules are aligned parallel to the substrate. When a bias field is applied, the LC molecules tend to orient along the field direction forming a homeotropic alignment. As a result, all LC molecules are aligned parallel to the electric field and perpendicular to the substrate. The homeotropic alignment of the LC occurs at 0.24 MV/m.

In the Arrhenius plot, two well-separated relaxation processes were seen in the commercial P(VDF-TrFE) film denoted by $\boldsymbol{\alpha}$ and $\boldsymbol{\beta}$. In case of both the annealed commercial P(VDF-TrFE) and the laboratory-prepared P(VDF-TrFE) films, these relaxation processes merge at a temperature above $T_\mathrm{g}$. The low-frequency dispersion of the PDLC films appears

in the same temperature range as the $\boldsymbol{\delta}$ relaxation process of the LC which is attributed to the movement of the LC molecules in the PDLC. Since the movement of the LC molecules in the polymer matrix is hindered by anchoring, the low-frequency peak of the PDLC film with 10 wt% LCs appears at much lower frequencies (six orders of magnitude). The PDLC films with 60 wt% LC contain more droplets, i.e. also a higher number of LC molecules at interfaces. Therefore, the low-frequency peak is shifted further to lower frequencies (one order of magnitude). Furthermore, the PDLC film containing 60 wt% LCs has a higher percentage of LC molecules in the bulk of the LC droplets. Therefore, the low-frequency relaxation requires an activation energy (0.5 eV) close to the activation energy of the $\boldsymbol{\delta}$ relaxation in the pure LC (0.56 eV).

The influence of the LC content on the ferroelectric properties of the polymer matrix was investigated. The remanent polarization and the coercive field of pure P(VDF-TrFE) were found to be 58 mC/m² and 42 MV/m, respectively. When the ferroelectric-polymer content decreases in the PDLC films containing 10 and 60 wt% LCs, the remanent polarization is reduced to 50 mC/m² and 8 mC/m², respectively.

In order to study the electro-optical behavior of the PDLC films, the optical transmission was measured. In the absence of an electric field, the LC molecules are oriented at random in the polymer matrix which results in a mismatch between the refractive indices of the LC and of the polymer. Therefore, the PDLC film scatters light. When an electric field is applied to the PDLC film, the LC molecules tend to orient along the electric field, the mismatch of the refractive indices decreases, and the transmission increases. With an electric field of 70 MV/m, the transmission of the PDLC film with 10 wt% LC is increased by 14% and the threshold field is 10 - 20 MV/m. With a relatively low electric field (26 MV/m), the transmission of the PDLC film containing 60 wt% LC is increased by 20% and the threshold field is 4 - 10 MV/m. In addition to the poor refractive index matching ($n_P < n_o$), the possible electrostatic interaction between the hydrogen atoms of the LC molecules and the fluorine atoms of the polymer matrix might be the reason for the relatively low increase in transmission.

The main aim of this thesis was to investigate the optical response of PDLC films when subjected to pressure variations. The PDLC films clearly show a change in the transmittance as the dynamic force changes. At a given dynamic-force amplitude, the change in optical transmission for the 10 wt% PDLC film is about 60% higher than for the pure P(VDF-TrFE). In the piezo-optical measurement, a PDLC film containing 60 wt% LC shows a 2% increase in transmission.

As a consequence of the low increase of transmission with a P(VDF-TrFE) matrix, a polymer with a higher refractive index was employed as the polymer matrix. PDLC films with poly(methly methacrylate) and 60 wt% LC were prepared similarly to the PDLC films with P(VDF-TrFE). PMMA is a non-polar material which should not have a strong interaction with the LC molecules at the polymer/LC interface. The refractive index of the PMMA is higher than the refractive index of the LC molecules. Due to the above reasons,

the PDLC film fabricated with PMMA achieves a higher change in transmission (83%) already with a low electric field (6 MV/m) and is also characterized by a small threshold field (1.5 - 2 MV/m).

# Outlook

In order to develop a piezo-optical switch having a higher increase in transmission, the following options may be considered:

- To increase the piezoelectric coefficient of the P(VDF-TrFE), the annealing conditions have to be optimized.

- A nematic liquid crystal having an ordinary refractive index equal to or lower than the refractive index of the polymer matrix has to be selected.

- The LCs should not have any electrostatic interaction with the polymer matrix.

# Bibliography

[1] P. S. Drzaic. Polymer dispersed nematic liquid-crystal for large area displays and light valves. *Journal of Applied Physics*, 60:2142–2148, 1986.

[2] H. Kitzerow. Polymer-dispersed liquid crystals from the nematic curvilinear aligned phase to ferroelectric films. *Liquid Crystals*, 16:1–31, 1994.

[3] P. S. Drzaic. Recent progress in dichroic polymer-dispersed liquid crystal materials. *Pure and Applied Chemistry*, 68:1435–1440, 1996.

[4] B. Jérôme. Surface effects and anchoring in liquid crystals. *Reports on Progress in Physics*, 54:391–451, 1991.

[5] J. W. Han. Temperature dependence of electro-optical characteristics of polymer dispersed liquid crystal films. *Liquid Crystals*, 28:1487–1493, 2001.

[6] R. Yamaguchi and S. Sato. Highly transparent memory states in polymer dispersed liquid crystal films. *Liquid Crystals*, 14:929–935, 1993.

[7] D. A. Higgins. Probing the mesoscopic chemical and physical properties of polymer-dispersed liquid crystals. *Advanced Materials*, 12:251–264, 2000.

[8] R. A. Weiss and C. K. Ober. *Liquid crystalline polymers*. American Chemical Society, United States of America, 1990.

[9] D. Demus, J. Goodby, G. W. Gray, H. W. Spiess, and V. Vill. *Handbook of liquid crystals, vol. 1*. Wiley-VCH, Germany, 1998.

[10] G. H. Brown and W. G. Shaw. The mesomorphic state. *Chemical Reviews*, 57:1049–1157, 1957.

[11] Fergason Patent Properties LLC. Dr. James Fergason - full biograpy, 2005-2009. http://fergasonpatents.com/company/jlfbio.php.

[12] The Ohio Academy of Science. Ohio's legacy of discovery and innovation, 2005. http://www.heartlandscience.org/comm/pdf/lcd.pdf.

[13] D. Cupelli, F. P. Nicolettal, G. A. Filpo, and G. Chidichimo. Persistence effects and memory states in charged polymer dispersed liquid crystals. *Molecular Crystals and Liquid Crystals*, 372:255–261, 2001.

[14] C. E. Hoppe, M. J. Galante, P. A. Oyanguren, and R. J. J. Williams. Polymer-dispersed liquid crystals based on polystyrene and EBBA: Analysis of phase diagrams and morphologies generated. *Macromolecular Chemistry and Physics*, 204:928–935, 2003.

[15] H. K. Lee, A. Kanazawa, T. Shiono, T. Ikeda, T. Fujisawa, M. Aizawa, and B. Lee. Reversible optical control of transmittance in polymer/liquid crystal composite films by photoinduced phase transition. *Journal of Applied Physics*, 86:5927–5934, 1999.

[16] R. C. Kell. Modern applications of ferroelectricity. *British Journal of Applied Physics*, 14:249–255, 1963.

[17] T. Furukawa. Structural and functional properties of ferroelectric polymers. *Advances in Colloid and Interface Science*, 71-72:183–208, 1997.

[18] K. Tashiro, H. Tadokoro, and M. Kobayashi. Structure and piezoelectricity of poly(vinylidene fluoride). *Ferroelectrics*, 321:167–175, 1981.

[19] J. C. Dubois. Advanced polymers for electrooptics. *Polymers for Advanced Technologies*, 6:10–14, 1995.

[20] T. Koda, Y. Morito, and S. Ikeda. Liquid crystal droplets dispersed in ferroelectric copolymer of vinylidene fluoride and trifluoroethlyene. *Polymer Journal*, 33:475–480, 2001.

[21] H. J. Shah, D. Delaine, and A. K. Fontecchio. Tailored liquid-crystal switching on ferroelectric polymer films. *Journal of the Society for Information Display*, 15:579–584, 2007.

[22] A. Andreau, R. Farhi, J. M. Tarascon, and P. Gisse. Elaboration and electro-optic study of a new type of open porosity PDLC. *Liquid Crystals*, 27:1–4, 2000.

[23] M. C. Christie, J. I. Scheinbeim, and B. A. Newmann. Ferroelectric and piezoelectric properties of a quenched poly(vinylidene fluoride-trifluoroethylene) copolymer. *Journal of Polymer Science: Part B: Polymer Physics*, 35:2671–2679, 1997.

[24] G. Höhne, W. Hemminger, and H. J. Flammersheim. *Differential scanning calorimetry An introduction for practitioners.* Springer, Germany, 1996.

[25] E Verdonck, K. Schaap, and L. C. Thomas. A discussion of the principles and applications of modulated temperature DSC (MTDSC). *International Journal of Pharmaceutics*, 192:3–20, 1999.

[26] A. Miyamoto, H. Kikuchi, S. Kobayashi, Y. Morimura, and T. Kajiyama. Dielectric property-electrooptical effect relationships of polymer/liquid crystal composite films. *Macromolecules*, 24:3915–3920, 1991.

[27] F. Kremer and A. Schönhals. *Broadband dielectric spectroscopy*. Springer, Germany, 2003.

[28] Y. González, B. Palacios, M. A. P. Jubindo, M. R. Fuente, and J. L. Serrano. Dielectric relaxation study in a glassy low-molecular-weight ferroelectric liquid crystal. *Physical Review E*, 52:R5764–R5767, 1995.

[29] R. Richert and M. Yang. Solvation dynamics of molecular glass-forming liquids in confinement. *Journal of Physics: Condensed Matter*, 15:S1041–S1050, 2003.

[30] P. R. Griffiths and J. A. de Haseth. *Fourier transform infrared spectometry*. Wiley Interscienc Publication, New York, 1986.

[31] Y. Bormashenko, R. Pogreb, O. Stanevsky, and Ed. Bormashenko. Vibrational spectrum of pvdf and its interpretation. *Polymer Testing*, 23:791–796, 2004.

[32] H. Frei and G. Groetzinger. Über das Freiwerden elektrischer Energie beim Aufschmelzen des Elektreten. *Physik Zeitschrift*, 37:720–724, 1936.

[33] G. Groetzinger and H. Kretsch. Über die permanente Polarisation des Elektreten. *Zeitschrift für Physik A Hadrons and Nuclei*, 103:337–349, 1936.

[34] C. Bucci and R. Fieschi. Ionic thermoconductivity. method for the investigation of polarization in insulators. *Physical Review Letters*, 12:16–19, 1964.

[35] G. Collins and B. Long. A thermally stimulated current/relaxation map analysis of the relaxation processes in aromatic polyester liquid crystal polymer film. *Journal of Applied Polymer Science*, 53:587–608, 1994.

[36] C. Bucci and R. Fieschi. Ionic thermocurrents in dielectrics. *Physical Review*, 148:816–823, 1966.

[37] J. A. Giacometti, S. Fedosov, and M. M. Costa. Corona charging of polymers: Recent advances on constant current charging. *Brazilian Journal of Physics*, 29:269–279, 1999.

[38] W. Künstler, Z. Xia, T.Weinhold, A. Pucher, and R. Gerhard-Multhaupt. Piezoelectricity of porous polytetrafluoroethylene single- and multiple-film electrets containing high charge densities of both polarities. *Applied Physics A: Materials Science and Processing*, 70:5–8, 2000.

[39] B. Dickens, E. Balizer, A. S. DeReggi, and S. C. Roth. Hysteresis measurements of remanent polarization and coercive field in polymers. *Journal of Applied Physics*, 72:4258–4264, 1992.

[40] M. Wegener. Electrical poling of polymers, 2002. http://www.uni-potsdam.de/u/physik/fprakti/ANLEIF10.pdf.

[41] S. C. Jain and R. S. Thakur. Thermo-electro-optic switch based on polymer dispersed liquid crystal composite. *Applied Physics Letters*, 61:1641–1642, 1992.

[42] H. C. van de Hulst. *Light scattering by small particles*. Dover, New York, 1981.

[43] P. S. Drzaic. *Liquid crystal dispersions*. World Scientific, Singapore, 1995.

[44] J. V. Champion, A. Killey, and G. H. Meeten. Small-angle polarized light scattering by spherulites. *Journal of Polymer Science: Part B: Polymer Physics*, 23:1467–1476, 1985.

[45] G. H. Meeten and P. Navard. Small-angle scattering of polarized light. I comparison of theoretical predictions for isotropic and anisotropic spheres. *Journal of Polymer Science: Part B: Polymer Physics*, 27:2023–2035, 1989.

[46] O. Biganska, T. Budtova, E. P.-Disdier, and P. Navard. Small-angle scattering of polarized light. V: liquid crystalline droplets in an isotropic polymer. *Molecular Crystals and Liquid Crystals*, 261:167–175, 1995.

[47] P. S. Drzaic and A. Muller. Droplet shape and reorientation fields in nematic droplet/polymer films. *Liquid Crystals*, 5:1467–1475, 1989.

[48] B. G. Wu, J. L. West, and J. W. Doane. Angular discrimination of light transmission through polymer-dispersed liquid-crystal films. *Journal of Applied Physics*, 62:3925–3931, 1987.

[49] A. Yariv. *Optical electronics in modern communications*. Oxford University Press, New York, 1997.

[50] P. S. Drzaic and A. M. Gonzales. Phenomenological scattering models for nematic droplet/polymer films: refractive index and droplet correlation effects. *Molecular Crystals and Liquid Crystals*, 222:11–20, 1992.

[51] G. P. Montgomery, J. L. West, and W. T. Lis. Droplet size effects in light scattering from polymer-dispersed liquid crystal films. *Proc. SPIE*, 1445:45–53, 1991.

[52] S. A. Carter, J. D. LeGrange, W. White, J. Boo, and P. Wiltzius. Dependence of the morphology of polymer dispersed liquid crystal on the uv polymerization process. *Journal of Applied Physics*, 81:5992–5999, 1997.

[53] F. Zhang, W. Qiu, L. Yang, T. Endo, and T. Hirotsu. Crystallization and melting behaviors of maleated polyethylene and its compostie with fibrous cellulose. *Journal of Applied Polymer Science*, 89:3292–3300, 2003.

[54] J. Menegotto, L. Ibos, A. Bernes, P. Demont, and C. Lacabanne. Dielectric relaxation spectra in ferroelectric P(VDF-TrFE) copolymers. *Ferroelectrics*, 228:1–22, 1999.

[55] J. Ding, J. Zhu, H. Fang, and Y. Yang. Compensation effects of crystals and liquid crystals in polarizing optical microscope. *Japanese Journal of Applied Physics*, 35:4427–4433, 1996.

[56] M. J. Weber. *Handbook of laser science and technology supplement 2: optical materials*. CRC press, USA, 1995.

[57] A. Daoudi, F. Dubois, C. Legerand, V. Laux, and J. M. Buisine. Static and dynamic electro-optic properties of a smc* phase in surface stabilized geometry and dispersed in the polymer matrix. *The European Physical Journal E*, 12:573–580, 2003.

[58] G. Williams, S. E. Shinton, and G. A. Aldridge. Dielectric relaxation spectroscopy and alignment behavior of a polymer-dispersed liquid crystal and its component materials. *Journal of Polymer Science: Part B: Polymer Physics*, 39:1173–1194, 2001.

[59] A. Boersma, J. V. Turnhout, and M. Wübbenhorst. Dielectric characterization of a thermotropic liquid crystalline copolyesteramide: 1. relaxation peak assignment. *Macromolecules*, 31:7453–7460, 1998.

[60] L. M. Ganesan, P. Frübing, A. Mellinger, and R. Gerhard. Dielectric relaxation behaviour of nematic liquid crystals dispersed in a poly(vinylidene fluoride-trifluoroethylene). *Journal of Physics: D: Applied Physics*, 42:092006, 2009.

[61] H. Smogór, B. Hilczer, and S. Warchol. Relaxor-like behaviour of P(VDF/TrFE) film irradiated with 1 mev electrons. *Ferroelectrics*, 258:291–296, 2001.

[62] D. Rollik, S. Bauer, and R. Gerhard-Multhaupt. Separate contributions to the pyroelectricity in poly(vinylidene fluoride) from the amorphous and crystalline phases, as well as from their interface. *Journal of Applied Physics*, 85:3282–3288, 1999.

[63] L. P. Hsin and W. K. Chin. Tsc study and electro-optical properties of epoxy/acrylic polymer-dispersed liquid-crystal film in dicy thermal cure. *Journal of Polymer Science: Part B: Polymer Physics*, 39:507–514, 2001.

[64] H. Xu. Dielectric properties and ferroelectric behavior of poly(vinylidene fluoride-trifluoroethylene) 50/50 copolymer ultrathin films. *Journal of Applied Polymer Science*, 80:2259–2266, 2001.

[65] C. Björmander, K. Sreenivas, M. Duan, A. M. Grishin, and K. V. Rao. Thickness dependence of the coercive electric field of laser ablated niobium-doped lead-zirconium-titanate films. *Applied Physics Letters*, 66:2493–2495, 1995.

[66] T. Koda, T. Shimizu, S. Imai, T. Takahahi, A. Nishioka, and S. Ikeda. Nematic liquid crystals dispersed in a ferroelectric copolymer of vinylidene fluoride and trifluoroethylene. *Japanese Journal of Applied Physics*, 42:4426–4430, 2003.

[67] E. Büyüktanir, N. Gheorghiu, J. L. West, M. Mitrokhin, B. Holter, and A. Glushchenko. Field-induced polymer wall formation in a bistable smectic-a liquid crystal display. *Applied Physics Letters*, 89:031101, 2006.

[68] R. Flores Súarez, L. M. Ganesan, W. Wirges, A. Mellinger, and R. Gerhard. Imaging liquid crystals dispersed in a ferroelectric polymer matrix by means of Thermal-Pulse Tomography. submitted to *Applied Physics Letters*, 2009.

[69] J. Han. Study of memory effects in polymer dispersed liquid crystal films. *Journal of the Korean Physical Society*, 49:1482–1487, 2006.

[70] K. Omote, H. Ohigashi, and K. Koga. Temperature dependence of elastic, dielectric, and piezoelectric properties of single crystalline films of vinylidene fluoride trifluoroethylene copolymer. *Journal of Applied Physics*, 81:2760–2769, 1997.

[71] B. Neese, Y. Wang, B. Chu, K. Ren, S. Liu, and Q. M. Zhang. Piezoelectric responses in poly(vinylidene fluoride/hexafluoropropylene) copolymers. *Applied Physics Letters*, 90:242917, 2007.

[72] S. W. Or, H. L. W. Chan, and C. L. Choy. P(VDF-TrFE) copolymer acoustic emission sensors. *Sensors and Actuators*, 80:237–241, 2000.

[73] Y. W. Tang, X. Z. Zhao, H. L. W. Chan, and C. L. Choy. Electron irradiation effects in electrostrictive p(vdf-trfe) copolymers. *Proceedings of the 12th IEEE international symposium on Applications of Ferroelectrics*, 2:793–796, 2001.

[74] A. Kremmer. *Untersuchungen der Struktur von Polyamid 11 - Filmen und ihres Einflusses auf deren piezo- und ferroelektrische Eigenschaften*. PhD thesis, Institute of Physics, University of Potsdam, Germany, 2008.

[75] K. B. Yoon. Fabrication of multimode polymeric waveguides by hot embossing process: Effect of sidewall roughness on insertion loss. *Macromolecular Research*, 12:437–442, 2004.

[76] R. O. Ebewele. *Polymer science and technology*. CRC press, United States of America, 2000.

[77] B. G. Wu, J. H. Erdmann, and J. W. Doane. Response times and voltages for PDLC light shutters. *Liquid Crystals*, 5:1453–1465, 1989.

# Appendix A

# *Relationship between the impedance and the capacitance*

When a sinsoidal electric field $E(\omega)$ is applied to the dielectric material, the frequency dependence of the alternating current density is

$$J(\omega) = i\omega\epsilon_0\epsilon_r E(\omega) \tag{A.1}$$

where $\omega$ is the angular frequency, $\epsilon_0$ is the permittivity of free space and $\epsilon_r$ is the relative permittvity of the dielectric material. Eq. A.1 can be re-written as

$$I(\omega) = i\omega\epsilon_0\epsilon_r V(\omega)\frac{A}{d} \tag{A.2}$$

where $A$ and $d$ are the area and thickness of the material, respectively. The current in an AC circuit is given as

$$I(\omega) = \frac{V(\omega)}{Z(\omega)} \tag{A.3}$$

$$I(\omega) = V(\omega)Y(\omega) \tag{A.4}$$

where $V(\omega)$ is the voltage applied, $Z(\omega)$ and $Y(\omega) = 1/Z(\omega)$ are the impedance and admittance of the material, respectively. Comparing eq. A.2 and A.4, the impedance of the dielectric material is obtained

$$Y(\omega) = i\omega\epsilon_0\epsilon_r\frac{A}{d} \tag{A.5}$$

Thus, the relationship between admittance and the capacitance is given by

$$Y(\omega) = i\omega C(\omega) \tag{A.6}$$

# Appendix B

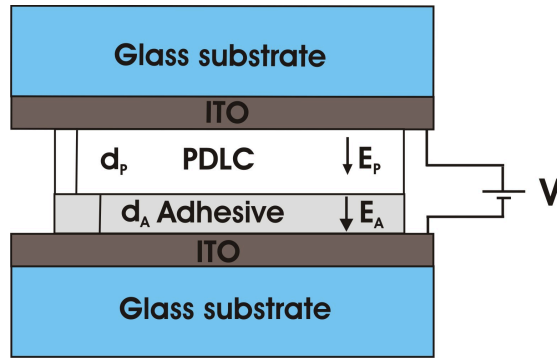# *Electric Field across the adhesive and the PDLC layer*



Figure B.1: *A schematic representation of the sample and the electric field applied across the relevant layers.*

The sample consists of two parallel plate capacitors, one is a PDLC layer and the other one is an adhesive layer. The voltage $V$ applied to the sample is

$$V = V_P + V_{Ad}$$
$$V = E_P d_P + E_{Ad} d_{Ad}$$

(B.1)

$V_P$ and $V_{Ad}$ are the voltage across the PDLC and the adhesive layer, respectively. $E_P$ is the electric-field across the PDLC layer and $d_P$ is the thickness of the PDLC layer. Similarly, $E_{Ad}$ and $d_{Ad}$ are the electric-field across the adhesive layer and the thickness of the adhesive layer. The total voltage applied to the sample can be re-written as a function of the charge stored ($Q$) in the capacitor and the capacitance ($C$) of the capacitor.

$$V = \frac{Q_P}{C_P} + \frac{Q_{Ad}}{C_{Ad}}$$

(B.2)

where $Q_P$ and $C_P$ are the charge stored in the PDLC layer and the capacitance of the PDLC layer and $Q_{Ad}$ and $C_{Ad}$ are the charge stored in the adhesive layer and the capacitance of the adhesive layer. Since, $Q = Q_P = Q_{Ad}$ eq. B.2 can be written as

$$V = Q \left( \frac{1}{C_P} + \frac{1}{C_{Ad}} \right) \tag{B.3}$$

$$V = \frac{Q}{\epsilon_0 A} \left( \frac{d_P}{\epsilon_{rP}} + \frac{d_{Ad}}{\epsilon_{rAd}} \right) \tag{B.4}$$

$$Q = V \epsilon_0 A \left( \frac{\epsilon_{rP} \epsilon_{rAd}}{\epsilon_{rAd} d_P + \epsilon_{rP} d_{Ad}} \right) \tag{B.5}$$

The charge stored in the PDLC layer is given by

$$Q_P = E_P d_P C_P \tag{B.6}$$

Using eq. B.5 and B.6, the electric-field applied to the PDLC layer can be calculated using the following equation

$$E_P = V \left( \frac{\epsilon_{rAd}}{\epsilon_{rAd} d_P + \epsilon_{rP} d_{Ad}} \right) \tag{B.7}$$

Similarly the electric-field applied to the adhesive layer is given by

$$E_{Ad} = V \left( \frac{\epsilon_{rP}}{\epsilon_{rAd} d_P + \epsilon_{rP} d_{Ad}} \right) \tag{B.8}$$

# Appendix C

# *The relaxation time at which the maximum loss occurs*

To find the relaxation time, $\tau$ at which the maximum loss occurs, an explicit equation (eq. C.1) was suggested by Turnhout et al. [59].

$$\omega\tau_{HN} = \left(\frac{\sin\left(\frac{\pi\beta}{2(1+\gamma)}\right)}{\sin\left(\frac{\pi\beta\gamma}{2(1+\beta)}\right)}\right)^{1/\gamma} \tag{C.1}$$

where $\omega$ is the frequency at which the maximum loss occurs, $\tau_{HN}$, $\beta$ and $\gamma$ are the relaxation time, the symmetric and the asymmetric shape parameters obtained by fitting the Havriliak and Negami function (eq. 4.14) to the dielectric loss curves. Since $\omega\tau = 1$ and $1/\tau_{HN} = \omega_{HN}$. Eq. C.1 can be re-written as

$$\left(\frac{1}{\omega\tau_{HN}}\right)^{\gamma} = \left(\frac{\sin\left(\frac{\pi\beta}{2(1+\gamma)}\right)}{\sin\left(\frac{\pi\beta\gamma}{2(1+\beta)}\right)}\right)^{-1}$$

$$(\tau\omega_{HN})^{\gamma} = \left(\frac{\sin\left(\frac{\pi\gamma\beta}{2(1+\beta)}\right)}{\sin\left(\frac{\pi\beta}{2(1+\gamma)}\right)}\right) \tag{C.2}$$

Using the fitting parameters obtained from the HN fit, the relaxation time at which maximum loss occurs can be calculated.

$$\tau = \tau_{HN}\left(\frac{\sin\left(\frac{\pi\gamma\beta}{2(1+\beta)}\right)}{\sin\left(\frac{\pi\beta}{2(1+\gamma)}\right)}\right)^{1/\gamma} \tag{C.3}$$

# Appendix D

# *Electric field generated in the sample by applying mechanical stress*

When a force $F$ is applied to the sample having a piezoelectric coefficient $d_{33}$, the charge generated $Q$ is given by

$$Q = d_{33}F \tag{D.1}$$

Knowing the capacitance of the sample $C$, the voltage generated in the sample can be found

$$V = \frac{Q}{C} \tag{D.2}$$

Using eq. D.1 and D.2, the electric-field generated in the sample by the application of mechanical stress, can be calculated as

$$E = \frac{d_{33}F}{Cd}, \tag{D.3}$$

where $d$ is the thickness of the film.

# Publications

Parts of this work have been published in the following journals and conference proceedings as well as presented in the listed conferences as oral presentation or poster.

## Journal

**Dielectric relaxation behavior of nematic liquid crystals dispersed in poly(vinylidene fluoride-trifluoroethylene)**
> L. M. Ganesan; P. Frübing; A. Mellinger and R. Gerhard
> Journal of Physics D: Applied Physics,
> Vol. 42, 092006 (2009)

**Piezo-optical and electro-optical behaviour of nematic liquid crystals dispersed in a ferroelectric copolymer matrix**
> L. M. Ganesan; W. Wirges; A. Mellinger and R. Gerhard
> submitted to Journal of Physics D: Applied Physics,
> Vol. 43, 015401 (2010)

**Electro-optical behavior of a nematic liquid crystal dispersed in a polar copolymer or in a non-polar polymer**
> L. M. Ganesan; W. Wirges; and R. Gerhard
> in preparation

**Imaging liquid crystals dispersed in a ferroelectric polymer matrix using Thermal-Pulse Tomography**
> R. Flores Suarez; L. M. Ganesan; W. Wirges; A. Mellinger and R. Gerhard
> submitted (2009)

# Conference contributions

**Optical switching and dielectric response of nematic liquid crystals dispersed in a ferroelectric poly(vinylidene fluoride/trifluoroethylene) matrix**
    L. M. Ganesan; A. Mellinger; M. Wegener; W. Wirges and R. Gerhard-Multhaupt
    DPG-Spring Meeting 2006, Dresden, Germany, March 27-31, 2006

**Electro-optical switching and dielectric response of nematic liquid crystals dispersed in a ferroelectric poly(vinylidene fluoride-trifluoroethylene) matrix**
    L. M. Ganesan; A. Mellinger; M. Wegener; W. Wirges and R. Gerhard-Multhaupt
    Polydays 2006, Berlin, Germany, October 4-6, 2006

**Electro-optical switching and dielectric response of nematic liquid crystals dispersed in a ferroelectric copolymer matrix**
    A. Mellinger; L. M. Ganesan; M. Wegener; W. Wirges and R. Gerhard-Multhaupt
    9th International Conference on Dielectric and Related Phenomena, Poznan, Poland, September 3-7, 2006

**Towards multifunctional composites: preparation and characterization of polymer-dispersed liquid crystals**
    L. M. Ganesan; A. Mellinger; M. Wegener; W. Wirges and R. Gerhard
    DPG-Spring Meeting 2007, Regensburg, Germany, March 26-30, 2007

**Dielectric relaxation behavior of nematic liquid crystals dispersed in ferrolectric polymer**
    L. M. Ganesan; A. Mellinger; P. Frübing; W. Wirges and R. Gerhard
    DPG-Spring Meeting 2008, Berlin, Germany, February 25-29, 2008

**Electro-optical and opto-mechanical behavior of nematic liquid crystals dispersed in ferrolectric polymer matrix**
    L. M. Ganesan; A. Mellinger; W. Wirges and R. Gerhard
    9th European Conference on Applicatiions of Polar Dielectrics, Rome, Italy, August 26-29, 2008

**Thermal and electrical characterization of nematic liquid crystal dispersed in ferrolectric polymer matrix**
    L. M. Ganesan; W. Wirges; P. Frübing and R. Gerhard
    18th Conference on Liquid Crystals, Augustow, Poland, September 14-18, 2009

# Curriculum Vitae

## Lakshmi Meena Ganesan

---

### Personal Details

| | |
|---|---|
| Date of birth | 9$^{\text{th}}$ March 1981 |
| Place of birth | Chennai, India |
| Marital status | Single |

---

### Schooling

| | |
|---|---|
| 1987 - 1997 | Northwick Girls' Higher Secondary School, Chennai, India |
| 1997 - 1999 | Muruga Dhanushkodi Girls' Higher Secondary School, Chennai, India |

---

### University

| | |
|---|---|
| 1989 - 2003 | Bachelor of Technology in Polymer Technology at Crescent Engineering College, University of Madras, Chennai, India |
| | Bachelor Thesis "Development of high performance synthetic acrylic latex based construction sealant" at Anabond Limited, Research and Development, Perungudi, Chennai, India |
| 2004 - 2006 | Master of Science in Polymer Science at Free University Berlin, Humboldt University Berlin, Technical University Berlin, University of Potsdam |
| | Master Thesis "Optical switching and dielectric response of nematic liquid crystals dispersed in a ferroelectric poly(vinylidene fluoride-trifluoroethylene) matrix" at Universiy of Potsdam |

---

### Doctoral Study

| | |
|---|---|
| since 2006 | Ph.D. thesis at the University of Potsdam, Germany. Research done as scientific employee of the Institute of Physics and Astronomy, Applied Condensed-Matter Physics group |

---

### Job and Teaching

| | |
|---|---|
| 2004 - 2006 | Student Assistant at University of Potsdam, Applied Condensed-Matter Physics group |

| | |
|---|---|
| since 2006 | Research Associate at University of Potsdam, Applied Condensed-Matter Physics group |

## Languages known

| | |
|---|---|
| Tamil | Mother tongue |
| English | fluent spoken and written |
| Hindi | can write and speak |
| German | Basic knowledge |